ELECTRON PARAMAGNETIC RESONANCE STUDIES OF SPIN-LABELLED ETHIDIUM BROMIDE DNA INTERACTIONS

by

David James Keeble, BSc, MInstP

A Thesis submitted for the Degree of
Doctor in Philosophy at the 1986
University of Keele,
Staffordshire.

ABSTRACT

Spin-Labelled Ethidium Bromide (SLEB) was prepared in order to study its interactions with natural DNA in the form of fibres . The technique of electron paramagnetic resonance was used in this thesis. Knowledge of the conformational transition pathway of natural DNA for given counterion concentration as a function of relative humidity was utilised in the study of effect DNA confomation on the binding of SLEB. To aid interpretation of the results the relevant background material was reviewed.

In order to attempt to extract geometric information on binding computer EPR lineshape simulations were used. To facilitate this a microcomputer spectrometer control system was designed and implemented. This allowed spectra to be acquired in digital form and transfered to the mainframe computer. Two schemes for magnetic field control were investigated, one based on a commercial NMR magnetometer, and a superior pulsed NMR field locking magnetometer developed in this laboratory.

In order to obtain lineshapes undistorted by dipolar broadening it is advantageous to use fibres with a high phosphate to drug ratio (P/D), however spectrometer sensitivity becomes a limiting factor. A review of noise in spectrometer systems is included. The use of a microwave low-noise preamplifer to reduce the system noise figure was investigated. An attempt to construct a loop-gap resonator was made and justified theoretically.

A 35GHz spectrometer was constructed and a cavity designed and built to allow the humidity to be varied. The system was made compatible with the control system. Spectra recorded and simulated at this frequency should help confirm those obtained at 9GHz.

The results obtained from P/D=70 fibres with a 0.5mM NaCl

concentration show the SLEB is in a disordered state from 33% to 75% relative humidity. Spectral changes occur in the range 75% to 98% consistant with intercalation. In this humidity range a transition to the B-form is expected.

Dedicated to my *Mother and Grandmother*

ACKNOWLEDGEMENTS

I wish to express my gratitude to the following:

Professor Watson Fuller, Head of the Department of Physics, University of Keele, for providing the facilities for this research and for his encouragement thought my stay within the department.

Dr. E.F. Slade for supervising and correcting this thesis. Dr. P.K. Grannel for his guidance on instrumentation and Dr. D.V. Griffiths for his assistance in the spin-labelling experiments.

Dr. A. Mahendrasingham and Dr. R.W. Strange for many illuminating and friendly discussions. Dr. D.G. Holloway and Dr. D.C. Laine for their interest and support. Dr. D.E. Dugdale for his helpful discussions on theory.

Mr. Fred Rowerth, Laboratory Superintendant, who was ever helpful. Mr. Jim Minshall for his invaluable technical support in the laboratory. Mr Geoff Dudley, Mr Graham Marsh and Mr Ted Greasley for their excellent work in the workshop. All the Technical staff of the Department of Physics for making my stay so entertianing and enlightening.

The Keele Research Association for providing social facilities. Friends Debbie, Rachel and Nigel, Rachel, John, Len, Janet and Jon, Kay and Martin, Kala and George, David, Steve, Ruquia, Margy, Berni and Pete, and Becca.

Mrs Helen Moors for typing this thesis.

CONTENTS

CHAPTER ONE

INTRODUCTION

It is known that many small molecules exert some physiological effects through interaction with nucleic acids. As a consequence these interactions have been thoroughly investigated. Many of the classes of molecule able to interact have been identified as have the major modes of interaction. These have been found to be covalent or electrostatic bonding to exposed groups of the nucleic acid or interaction with its secondary structure. However, it is known that a single molecule may show different binding modes dependent on local environment. Molecules sharing a common mode have been found to exhibit substantial differences in their physiological action. The drugs daunomycin and proflavine are both known to favour intercalation yet daunomycin is thought to be an anti-cancer drug while proflavine is a mutagen. One of the major aims of molecular biology is to deduce a molecular theory of drug action capable of explaining such diverse effects.

Substantial progress has been achieved by the application of x-ray diffraction techniques to nucleic acids and nucleic acid drug complexes. Preferences for certain nucleic acid base-pair sequences has been observed and combined with recent identification of sequence dependent nucleic acid local structure indicate a potential for future advances.

The technique of electron paramagnetic resonance spectroscopy (EPR) has been used in nucleic acid drug studies of a restricted class of drug molecules to yield information on the ability to bind, the degree of mobility of the bound species, and occasionally geometric information. The restricted class consists of those molecules that are stable paramagnets or those labelled by a magnetic reporter molecule.

In general these studies are carried out in solution and binding is inferred from spectral changes consistent with immobilisation. Oliniskiu and McConnel[1] extended the scope of the technique by applying it to oriented samples. The resultant spectra possess a higher information content and hence allow conclusions on binding geometry to be made. Similar studies were performed in this laboratory. Oriented fibres of the type used in fibre x-ray diffraction were studied and a theoretical model for the fibre developed. This formed the basis of a computer program for lineshape simulation. These methods were applied to the chlorpromazine nucleic acid interaction[2].

Recently Strange[3] has extended the techniques to a study on the interaction of nitroxide spin-labelled proflavine with deoxyribose nucleic acid (DNA). It was found that not only did the technique indicate possible binding geometries, but that induced nucleic acid conformational changes were paralleled by changes in the EPR spectra. Such affects have not previously been reported in these systems and hence were considered worthy of further investigation. The intercalator ethidium bromide was chosen for this study and a nitroxide spin-labelled derivative synthesised. Evidence for the ethidium bromide DNA interaction has been obtained from a number of physical techniques, x-ray diffraction, nuclear magnetic resonance (NMR) and various optical methods. EPR studies have also been carried out Hong and Piette[4] studied spin-labelled ethidium bound to oriented films of DNA, Robinson[5] and co-workers have used it as a probe of nucleic acid internal motion. It was therefore considered that ethidium bromide was a suitable well characterised probe for the study of conformational influence.

The conformation of the nucleic acid may be altered experimentally by changing the humidity within the EPR spectrometer

cavity. The proflavine studies were carried out on a 10GHz-band spectrometer it was decided to extend observations to the 35GHz-band to take advantage of the increased g-value anisotropy and to impose a further test on the lineshape simulations. A 35GHz-band spectrometer suitable for these studies was constructed.

The EPR spectra from nucleic acid drug hydrated fibres have been, in general, found to be in the region where the motion of the spin-label is highly hindered. On the EPR time scale this represents the motional range $\tau_c > 10^{-8}$sec. Robinson[5] has observed a rotational correlation time of the order of 30nsecs. Recently Shino[6] has studied nucleic acid fibres by phosphorous NMR and deduced that in the high humidity state the nucleic acid molecules are undergoing rotational diffusion with a correlation time of the order of 10^{-5}sec. In order to further investigate the motions occurring in the fibre state and how they are affected by conformation the 10GHz-band spectrometer was adapted and calibrated to allow the saturation transfer EPR (ST-EPR) experiment to be carried out. The saturation transfer technique extends sensitivity to motion over the range 10^{-3} to 10^{-7} sec.

The ability to extract geometric information from nucleic acid drug fibre studies is directly related to the degree of order present. Nucleic acids are known to possess an induced dipole moment coincident with the helix axis but to have a negligible permanent dipole moment[7]. A study was instigated into the possible orientating influence of high electrostatic fields applied during fibre formation.

The work of Strange[3] showed the advantage of using high phosphate to drug ratio (P/D) fibres. It was found that the influence of exchange broadening was negligible for P/D=50 and hence true powder lineshapes were obtainable. From fibre x-ray diffraction studies it has been found that thinner fibres yield a higher degree of order and hence are preferable. The ability to satisfy these two conditions is,

however, limited by spectrometer sensitivity.

Spectrometer sensitivity is related to the noise factor for the system. A review of spectrometer noise contributions was undertaken and noise measurements on the 10GHz-band spectrometer carried out. In order to improve the performance the use of low noise microwave preamplifiers and low Q factor high filling factor loop-gap resonators were investigated.

In order to carry out lineshape simulations a direct comparison between calculated and observed spectra is required. Previously this was achieved by digitizing the experimental spectrum on a digitizing bed. This is unsatisfactory due to the addition of noise in the digitizing process and may be overcome by recording the original spectrum digitally. To this end a computer control and data acquisition system was designed and constructed. This had the additional advantages of simplifying the operation of the spectrometer and allowing multiple sweep averaging and data manipulation. The system involved the control of the magnetic field sweep and the acquisition of data from a high sensitivity lock-in amplifier. Both were common to the 9GHz and 35GHz spectrometers allowing either to be controlled. The system was made compatable with the GPIB bus hence any computer with this facility may act as a controller.

In order to allow multiple sweep averaging the frequency source must be highly stable and the sweep range reproducible. The former condition is often met, however, the ability to reproduce accurate absolute magnetic field sweep ranges is more problematic. Two methods of magnetic field sweep were investigated one based on a Bruker field regulation unit and NMR magnetometer the other was a pulsed NMR field locking magnetometer designed and constructed in this laboratory.

It was considered appropriate to begin this thesis with a review of previous related work. Although EPR theory related to nitroxide

spin-labels is well known those aspects required for an analysis of drug-nucleic acid systems are detailed in Chapter 2. In order to aid in interpretation of the results and to guide design of future experiments a review of drug-nucleic acid interactions is given in Chapter 3.

The experimental procedure adopted to obtain spin-labelled ethidium bromide and for forming the drug-nucleic acid solutions and fibres are described in Chapter 5. The results obtained by the application of EPR, ST-EPR and computer simulations to these systems are given in Chapter 6.

The instrumentational aspects of the project are discussed in Chapter 4. This chapter has been sub-divided into three parts. The first reviews the contributions to spectrometer noise and contains the results of noise measurements carried out on the 10GHZ band spectrometer. A description of both spectrometers is also given. Part two covers the modifications and calibration of the 9GHz spectrometer for ST-EPR and details the experimental procedure adopted. The final part describes the computer control and data acquisition system and the two methods of magnetic field control used.

The concluding remarks and suggestions for further work are contained in Chapter 7.

REFERENCES

1. Oniski, S., McConnel, H., (1965), J.Amer.Chem.Soc., 87, 2293.
2. Porumb, T., and Slade, E.F., (1976), Euro.J.Biochem., 65, 21.
3. Strange, R.W. (1985), Ph.d. Thesis, University of Keele.
4. Hong, S.J. and Piette, L.H. (1976), Cancer Res., 30, 1159.
5. Robinson, B.H., Lerman, L.S., Bethe, A.H., Frisch, H.L.,

Dalton, L.R. and Auer, C., (1980), J.Mol.Biol., 139, 13.

6. Fujiwara, T. and Shino, H., (1985), Biochemistry, 24, 896.

7. Jennings, B.R. and Rindler, P.J. (1977), Chem.Phys.Letts., 45 550.

CHAPTER TWO

THE THEORY OF ELECTRON PARAMAGNETIC RESONANCE

2.1 Introduction

This chapter has been divided into three parts. The first outlines basic EPR theory, emphasising those results pertinent to an understanding of nitroxide spin-labelling. Part two details the theoretical background to the EPR lineshape simulations used in this study. The final section describes the saturation transfer EPR experiment. The reader is referred too to the excellent books by Pake[1] and Atherton[2] for a more detailed discussion of many of the theoretical aspects dealt with in this chapter.

PART 1

2.1.1 The Zeeman Interaction

The Zeeman interaction is the interaction between a magnetic moment μ and a magnetic field B_o. The hamiltonian is given by

$$H = -\mu.B_o \qquad -(2.1)$$

The magnetic resonance phenomenon exists because many atomic and molecular systems possess a non zero angular momentum. This arises from the presence of unpaired electrons and/or nuclei with non-zero spin. The magnetic moment and the angular momentum are related by the equation

$$\mu = -\gamma J \qquad -(2.2)$$

where γ is the gyromagnetic ratio and is given by

$$\gamma = g(e/2m) \qquad -(2.3)$$

where e is electronic charge, m is the mass of the electron (or proton) and g is a dimensionless constant. From this it is seen that the magnetic moment associated with nuclei is less, by the ratio of the masses, than that due to electrons.

If the only contribution to the total angular momentum is from the electronic spin angular momentum **S** (where S is the electronic spin vector $\mathbf{S} = [S(S+1)]$, and $\hbar$ is Plank's constant divided by 2π) and B_0 is in the z-direction then the interaction Hamiltonian has the form

$$H = g(e/m)\hbar\, B_z S_z \qquad -(2.4)$$

where S_z is the z component of the spin vector. The term $(e\hbar/2m)$ is referred to as the Bohr magenton denoted β_e. The vector **S** may have 2S+1 values projected against the field direction hence in the case of S=1/2 there are two possible spin states (m_s =1/2 , m_s = -1/2 the quantum number for the z component of the spin angular momentum). The energy level of an electron is split in the static magnetic field into two levels.

The application of time dependent perturbation theory shows that transitions can be induced between the two Zeeman energy levels (Δm_s = ±1) by applying an oscillating magnetic field at right angles to the static magnetic field of a frequency

$$h\upsilon = g\beta_e B_z \qquad -(2.5)$$

In thermal equilibrium the energy levels are unequally populated consistent with Boltzmann's law. The probabilities of a stimulated transitions for absorption and emission are equal and the rate of population change of each level is proportional to the population itself. For a two level system absorption would cease on the equalisation of the populations, the transition would saturate. Magnetic resonance is made observable because non-radiative relaxation processes exist to return higher energy electrons back to the ground state. Such spin-lattice relaxation pathways will be considered further in section 2.1.3.

The EPR experiment is conducted at a fixed frequency, the energy absorbed from the radiation field is monitored as a function of magnetic field strength. The frequencies used in the study are in the 10GHz band and the 35GHz band hence the free electron resonance position for these frequencies are approximately represented by magnetic field strengths of 0.33T and 1.2T respectively.

Thus far only the situation of an unpaired free electron at g=2.002322 has been considered, this is a unique resonance position for any magnetic moment derived purely from the electronic spin vector. In general, however, a contribution from orbital angular momentum may be present. In the case of a free atom obeying LS coupling the resultant angular momentum is associated with the quantum number J where J = L + S. The g-factor is then identical with the Lande g-factor. For intermediate and heavy atoms as well as atoms contributing to molecular bonding the situation is more complex. The convention adopted in EPR is to use the electronic spin vector and associate any orbital contribution to a deviation from the free spin g-value. The presence of an orbital contribution may be due to a mixing of excited states through a bonding orbital. In many cases the g-value may no longer be isotropic and should be treated as a tensor whose elements are

$$\begin{bmatrix} g_{xx} & g_{xy} & g_{xz} \\ g_{yx} & g_{yy} & g_{yz} \\ g_{zx} & g_{zy} & g_{zz} \end{bmatrix}$$

The diagonal elements, g_{xx}, g_{yy}, g_{zz}, of which are termed the principle g-values. The Hamiltonian for the Zeeman interaction must in general, be written in tensor form.

$$H = \beta_e \, B.g.S \qquad -(2.6)$$

In general, the g-tensor is symmetric and as such it may be diagonalised in the correct coordinate system transformation. The diagonal matrix reduces the Hamiltonian to terms involving the three principle values.

$$H = \beta_e \, (g_{xx}S_x + g_{yy}S_yB_y + g_{zz}S_zB_z) \qquad -(2.7)$$

The consequence of this discussion is that the position of resonance may be dependent on the orientation of the magnetic field to the spin system.

2.1.2 The Nuclear Hyperfine Interaction

The other major interaction influencing the energy level scheme pertinent to EPR is the nuclear hyperfine interaction. As was discussed in the previous section those nuclei with a none zero spin possess a magnetic moment, the nuclear spin vector is denoted I and the associated magnetic quantum number by m_I. Their interaction with unpaired electrons may be composed of two parts. An isotropic part arising from the "Fermi contact interaction" which can only occur if the electron has a finite probability density at the nucleus, that is

it possesses some s-orbital character and an anisotropic part. This latter contribution arising from the electron-nuclear dipolar interaction may be written as

$$g\beta_e g_n \beta_n [(I.S/r^3) - (3/r^5)(I.r)(S.r)] \qquad -(2.8)$$

The complete nuclear hyperfine interaction Hamiltonian is given by

$$H = aS.I + S.T.I \qquad -(2.10)$$

where a is the isotropic coupling constant and T the dipole hyperfine tensor. This may be rewritten in the form

$$H = S.A.I \qquad -(2.11)$$

where A is termed the hyperfine tensor. The principal hyperfine terms are given by $A_{xx} = T_{xx} + a$, $A_{yy} = T_{yy} + a$ and $A_{zz} = T_{zz} + a$.

The dipolar term eq (2.8) is required to be averaged over the probability distribution $\psi^2(r)$ of the electronic orbital. In the case of s-orbitals spherical symmetry reduces the term to zero. For none zero angular momentum orbitals reduced symmetry exists and the dipolar has a $\langle(1-3\cos^3\theta)/r^3\rangle$ a dependence, where θ is the angle between the applied field and the vector joining the electron and nucleus.

The isotropic term is determined by the unpaired spin density at the nucleus $\psi(0)$, the coupling constant is given by

$$a = -(8\pi/3)g\beta_e g_n \beta_n \psi^2(0) \qquad -(2.12)$$

2.1.3 The Spin Hamiltonian

The complete spin Hamiltonian in the absence of exchange affects zero field splitting and crystal field affects may be given by

$$H = \beta_e B.g.S + S.A.I - g_n\beta_n B.I + I.Q.I$$

The first two terms have been introduced, the third is the nuclear zeeman term and the final interaction is the nuclear quadrapole affect. These latter two interactions have negligible effects in the system considered in this study hence no further comment will be made.

For The nitroxide free radicals used in this study the principal g- and A-tensor axes coincide, this axes system along which both tensors are diagonal is termed the molecular coordinate system $\sum(x,y,z)$. The form of the spin-Hamiltonian is invariant under coordinate system transformation and in the laboratory coordinate frame $\sum(X,Y,Z)$ is defined as

$$H = \beta_e B'.g.S' + S'.A'.I' \qquad -(2.13)$$

where $g' = L.g.L$ and $A' = L.A.L$ are the g- and A-tensors in the laboratory system and L is the molecular to laboratory frame transformation matrix. An expansion of the A'-tensor term is given below

$$\begin{bmatrix} A_{XX} & A_{XY} & A_{XZ} \\ A_{YX} & A_{YY} & A_{YZ} \\ A_{ZX} & A_{ZY} & A_{ZZ} \end{bmatrix} = \begin{bmatrix} l_{Xx} & l_{Xy} & l_{Xz} \\ m_{Yx} & m_{Yy} & m_{Yz} \\ n_{Zx} & n_{Zy} & n_{Zz} \end{bmatrix} \begin{bmatrix} A_{xx} & 0 & 0 \\ 0 & A_{yy} & 0 \\ 0 & 0 & A_{zz} \end{bmatrix} \begin{bmatrix} l_{Xx} & m_{Yx} & n_{Zx} \\ l_{Xy} & m_{Yy} & n_{Zy} \\ l_{Xz} & m_{Yz} & n_{Zz} \end{bmatrix}$$

where l_{Xx}, m_{Xx}, n_{Zx} ... are the directional cosines relating the coordinate systems.

If the applied magnetic field direction is defined as the z-direction and those terms involving off diagonal elements in S_x and S_y are neglected then eq (2.13) may be rewritten as

$$H = \beta_e g_{ZZ} B_z S_z + S_z A_{ZZ} I_z + S_z A_{XZ} I_x + S_z A_{YZ} I_y \qquad -(2.14)$$

with

$$g_{ZZ} = g_{xx} l^2_{Zx} + g_{yy} m^2_{Zy} + g_{zz} n^2_{Zz}$$
$$A_{ZZ} = A_{xx} l^2_{Zx} + A_{yy} m^2_{Zy} + A_{zz} n^2_{Zz}$$
$$A_{XZ} = A_{xx} l_{Xx} l_{Zx} + A_{yy} m_{Xy} m_{Zy} + A_{zz} n_{Xz} n_{Zz}$$
$$A_{YZ} = A_{xx} l_{Yx} l_{Zx} + A_{yy} m_{Yy} m_{Zy} + A_{zz} n_{Yz} n_{Zz}$$

The approximation of the spin-Hamiltonian is called the "intermediate field treatment" in which the electron spin is quantised along the external field while the nuclear spins quantize along the vector sum between the external field and that due to the electron at the nucleus. Under this approximation g'=g and

$$A' = (A^2_{XZ} + A^2_{YZ} + A^2_{ZZ})^{1/2} \qquad -(2.15)$$

A further approximation is the "high field treatment" in which the terms I_x and I_y of eq (2.14) are neglected. This corresponds to complete decoupling of spin vectors I and S. Again $g'=g_{zz}$, however, the expression for the hyperfine tensor is further simplified $A'=A_{zz}$.

Libertini and Griffiths[3] have shown that the intermediate field approach adequately accounts for the anisotropy of the **g**- and **A**-tensors in nitroxide free radicals. The matrix elements, eigenfunctions and eigenvalues of the Hamiltonian eq (2.14) may be evaluated from the basis set of spin functions $|m_s m_I\rangle$. In the case of limited **g**- and

A-tensors anisotropy, as for example in free radicals in solution the high field approximation is, in general, found adequate.

2.1.4 Spin Relaxation and EPR Lineshape

The correct form of the spin-Hamiltonian has been developed hence by applying the basis functions the transition probabilities could be obtained and a spectrum of delta functions obtained. Further comment is now required on the characteristics of magnetic resonance transitions.

The Boltzman distribution within the Zeeman levels results in a net excess of spins aligned parallel to the external field this is equivalent to the sample possessing a bulk magnetisation M_0. This is related to the field intensity through $M_0 = \chi_0 B_0$ where

$$\chi_0 = g^2\beta^2_e N\, S(S+1)/3kT \qquad -(2.17)$$

The equation of motion for a magnetisation M_0 interacting with a magnetic field B_0 is given by

$$dM_0/dt = M_0 \times B_0 \qquad -(2.18)$$

which leads to the precession of M_0 about B_0 at the Larmor frequency $\omega_0 = \gamma B_0$.

This classical approach was successfully applied to magnetic resonance by Bloch, the magnetic field is replaced by the vector sum of the external and microwave fields and an energy loss term added. The resulting equations are

$$dM_z/dt = (M_0-M_z)/T_1 + \gamma(MxB)_z \qquad -(2.19)$$

$$dM_{x,y}/dt = \gamma(MxB)_{x,y} - M_{x,y}/T_2 \qquad -(2.20)$$

The energy of the spin system is dependent on M_z the loss term represents energy dissipated via degrees of freedom other than the spin system. The characteristic time for this decay is termed longitudinal or spin-lattice relaxation T_1. Decay of the M_x and M_y components do not contribute to the spin energy they account for the possibility of loss of coherence of the precessing spins. This is equivalent to a spread of Larmor frequency and may be due to local field variations caused by dipolar field fluctuations. The time T_2 is called "transverse" or "spin-spin" relaxation.

It should be noted that solution of the Bloch equations is dependent on the experimental situation, in particular the relationship between the rate of change of B_0 with respect to the relaxation times. Two conditions have been identified called slow and rapid passage.

In rapid passage the size of the microwave field is such that the nutation imposed on the rapid lamor precession by this field is faster than the inverse relaxation time $\gamma B_1 >> T_1^{-1}$. This results in the magnetisation precessing several times around B_1 and out of alignment with B_0 before decaying. In slow passage $\gamma B_1 << T_1^{-1}$ and the magnetisation remains aligned in the field direction. The steady state condition is fulfilled by slow passage and rates of sweep of the order of $(dB_0/dt) << \gamma B_1$.

The solutions to the Bloch equations under steady state conditions are as follows

$$M_x = M_0 \Gamma \gamma B_1 T^2_2 (\omega_0 - \omega) \qquad -(2.21a)$$

$$M_y = M_0 \Gamma \gamma B_1 T_2 \qquad -(2.21b)$$

$$M_z = M_0 \Gamma \, (1 + T^2_2 (\omega_0 - \omega)^2) \qquad -(2.21c)$$

where $\Gamma = (1 + T^2_2(\omega_0 - \omega)^2 + \gamma^2 B_1 T_1 T_2)^{-1}$

The component M_x is in-phase with B_1 while M_y is $\pi/2$ out of phase. The concept of complex susceptibility was introduced $\chi = \chi' - j\chi''$ where $\chi' = (M'_x/2B_1)$ and $\chi'' = (M_y/2B_1)$ this gives

$$\chi' = 1/2\chi_o\omega_o\Gamma T_2(\omega-\omega_o) \qquad -(2.22a)$$

$$\chi'' = 1/2\chi_o\omega_o\Gamma T_2 \qquad -(2.22b)$$

These are termed the dispersive component (χ') and the absorptive component (χ "). The average power absorbed by a sample is given by

$$P = B^2_1\Gamma\omega_o\omega\chi_o T_2 \qquad -(2.23)$$

In the case of an unsaturated spin system, in general small B_1, then Γ reduces to $(1 + T_2(\omega_o - \omega^2))^{-1}$ these yields a Lorentzian shape function

$$g(\omega) = T_2 / \pi[1+ T^2_2(\omega_o-\omega)^2] \qquad -(2.24)$$

The other shape function observed in EPR is the Gaussian given by

$$g(\omega) = T_2(2\pi)^{-1/2} \exp[1/2T^2_2(\omega_o - \omega)^2] \qquad -(2.25)$$

This occurs under conditions of inhomogeneous broadening for example when dipolar interactions are involved or unresolved structure is present in the spectrum. The lineshapes are shown in Figures 2.1a and b.

2.1.5 EPR Linewidths

It may be seen from eq (2.24) that the line width of a normal Lorentzian line is related to the relaxation time T_2, this is equivalent to the half width at half height. It should be noted that

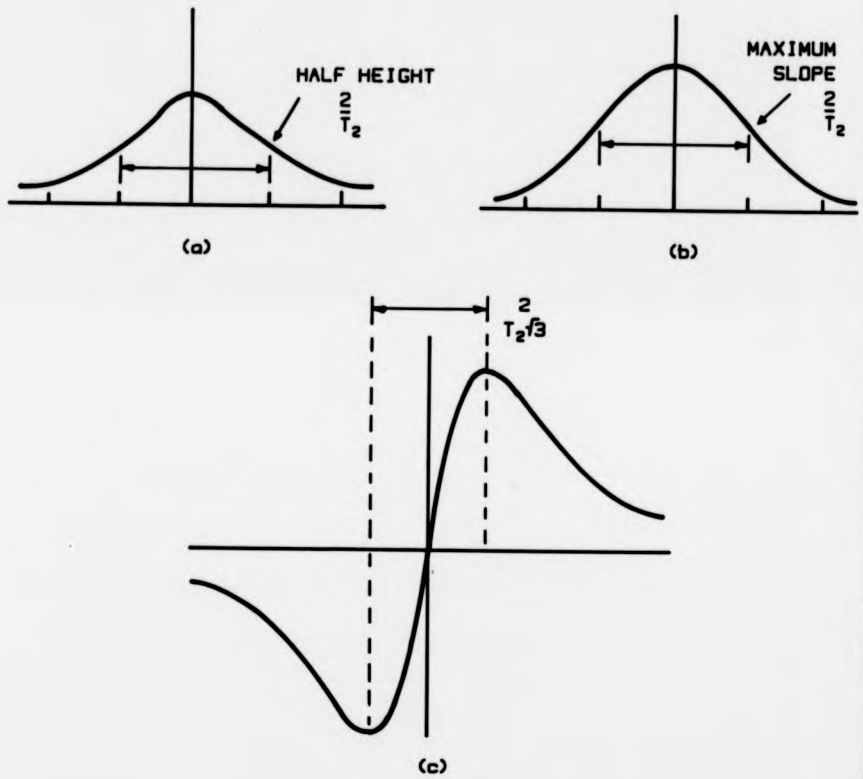

FIG. 2.1. EPR LINESHAPES (a) LORENTZIAN, (b) GAUSSIAN, (c) DERIVATIVE OF THE LORENTZIAN.

in fact the spin-lattice relaxation may affect linewidth through the Uncertainty Principle ($\Delta\nu \sim 1/T_1$). The T_2 of eq (2.24) is composed of a pure spin-spin term and a lifetime broadening term from the spin-lattice relaxation. In general $T_1 >> T_2$ hence has negligible affect, however, this is not the situation in transition metal ions.

The major sources of broadening are instrumental broadening, exchange interactions, spin-spin dipolar interactions and motional modulation. The latter two mechanisms will be considered further.

(a) The Dipolar Interactions - This is the most important source of line broadening in a rigid lattice of magnetic dipoles assuming separation of $\geq$ 10A hence no exchange effects. Van Vleck[4] showed that average of the local magnetic fields at one ion due to its neighbours was related to the linewidth by

$$\langle B^2_d \rangle = (3/5)g^2\beta^2_e(1/n)S(S+1)\Sigma(1/r_{ij}) \qquad -(2.26)$$

where n is the number of dipoles per unit volume and r_{ij} is the distance between two nearest neighbour spins (i,j). The resultant lineshape is Gaussian.

(b) Motional Modulation - This is the dominant affect in solutions of medium and low concentrations. The observed linewidth is dependent upon the relationship between the frequency of random motion, the inverse of the correlation time τ_c and the size of the g- or A-tensor anisotropy in frequency units. If $\tau_c << h[(g_{zz}-g_{xx})\beta B]^{-1}$ or $\tau_c << (A_{zz} - A_{xx})^{-1}$ where the difference term is assumed to be the largest present then the effects of this anisotropy are averaged and a motional narrowed spectrum results. This occurs for $\tau_c \simeq 10^{-8}$ sec.

The modulation of the anisotropic terms does result in modulation

of the energy levels hence an increase in lifetime broadening.

In the case of nitroxide spin-labels where an unpaired electron is interacting with a nucleus of I=1 the linewidths vary as a function of m_I.

$$T_2^{-2} = A + Bm_I + Cm_I^2 \qquad -(2.28)$$

This may be rewritten as

$$T_2(0)/T_2(M) = 1 - BM - CM^2 \qquad -(2.29)$$

where $M = \pm 1$

$$B = -(4\tau_c/15h)\beta_e\,[g_{zz} - 1/2(g_{xx}+g_{yy})]\; bB_oT_2(0)$$
$$C = (\tau_c/8)\; b^2T_2(0)$$
$$b = (4\pi/3)\;(A_{\parallel} - A')$$

and B_o is the field centre and $T_2^{-1}(M)$ and $T_2^{-1}(0)$ are the widths of the $m_I = \pm 1$ and $m_I = 0$ hyperfine lines.

2.1.6 Experimental Detection of EPR

This subject is dealt with in detail in Chapter 4, Part 1, however, a brief description is required at this point. From eq. (2.23) an EPR signal is monitored as an absorption of power from a microwave field set perpendicular to a slowly swept static field. A fixed frequency swept field measurement. It should be noted, however, in order to increase sensitivity it is required to move the detailed signal away from DC in order that phase-sensitive signal recovery techniques may be used. This is achieved by modulating the slowly swept magnetic field with a high frequency (100 kHz) alternating

magnetic field - the Zeeman modulation. This has several effects: (1) the response is now proportional to the gradient of the absorption hence the derivative of the absorption is observed, (2) if the amplitude of the modulation is $\geq \Delta B/10$ where ΔB is the linewidth then broadening may occur, (3) there is a fixed broadening equivalent to the modulation frequency in field units (100 kHz = 0.036 mT).

2.1.7 Free Radical Solution Spectra

In the situation where anisotropic g- and A-tensors are averaged to their isotropic values the Hamiltonian is given by

$$H = \beta_e g B_z S_z + a I_z S_z \qquad -(2.30)$$

Consider the case of a single electron interacting with a ^{14}N nucleus (as in the nitroxide case) I=1. The Zeeman interaction gives rise to two levels each of which is split into three by the hyperfine interaction see Fig. 2.2.

$$|1/2,\ 1\rangle = 1/2\beta_e g B_z + 1/2a \qquad |-1/2,-1\rangle = -1/2\beta_e g B_z + 1/2a$$
$$|1/2,\ 0\rangle = 1/2\beta_e g B_z \qquad |-1/2,\ 0\rangle = -1/2\beta_e g B_z$$
$$|1/2,-1\rangle = 1/2\beta_e b B_z - 1/2a \qquad |-1/2,\ 1\rangle = -1/2\beta_e g B_z - 1/2a$$

Application of the selection rules $\Delta m_s = \pm 1$, $\Delta m_I = 0$ results in the spectrum shown in Fig. 2.3. The treatment may easily be extended to interactions with more than one nucleus through a term $\sum a_n S_z I_{zn}$ where a_n is the coupling constant of the n^{th} nucleus of spin I_{zn}.

2.1.8 Single Crystal Free Radical Spectra

A single crystal represents an ordered symmetric array of radicals hence by recording EPR spectra as a function angle

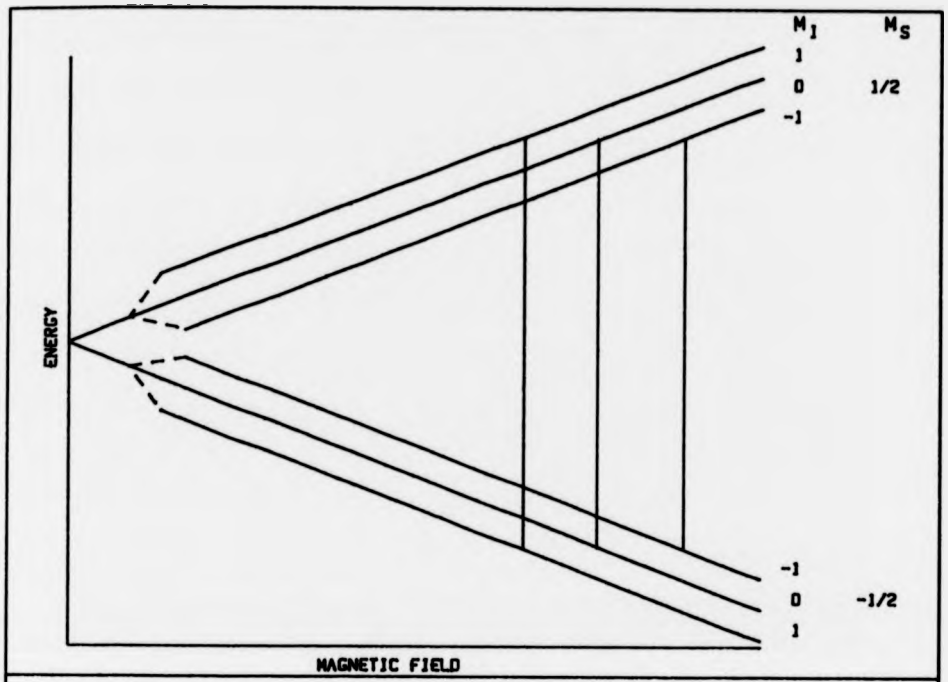

FIG. 2.2 HYPERFINE ENERGY LEVELS AND TRANSISTIONS FOR A SPIN S=1/2 INTERACTING WITH A SINGLE NUCLEUS I=1.

FIG. 2.3 NITROXIDE RADICAL SOLUTION SPECTRUM.

between the crystal axes and magnetic field the g- and A-tensor elements may be determined from eq.(2.14). In the particular case of a nitroxide both tensors have the same principal axis system. The g_{zz} and A_{zz} elements are the largest and coincide with the $2p\pi$ -orbital of the ^{14}N atom which contains the greatest spin density, the x-axis is orientated along the N-O bond direction. The resultant principal axis spectra are shown in Fig. 2.4, it may be seen that the A_{xx} and A_{yy} components are approximately equal, $A_{yy} = A_{xx} = 0.6$ mT while $A_{zz} = 3.2$mT.

2.1.9 Power EPR spectra

These are representative of an immobilised random array of radicals despite this it is often possible to obtain certain components of the g- and A-tensors from the turning points. The exact information available is dependent on reactive anisotropy and size of the two tensors. Intensity builds up abruptly at the extrema of the spectrum corresponding to the largest anisotropic tensor component, in the nitroxide case A_{zz}. This spectrum is shown in Fig. 2.4. For a more detailed account of powder spectra see the account by Kneabahl[5]

PART TWO

2.2.1 Synthesis of EPR spectra of Systems with One Axis of symmetry

The theoretical model used to simulate the EPR spectra of cylindrical samples with one axis of symmetry will be expanded. The formalism developed by Jost and Griffiths[6] and Porumb and Slade[7] is adopted. The model will be illustrated by the case of a nitroxide labelled drug molecule bound to large molecular weight helical molecular deoxyribose nuclei acid (DNA) orientated into a cylindrical fibre sample.

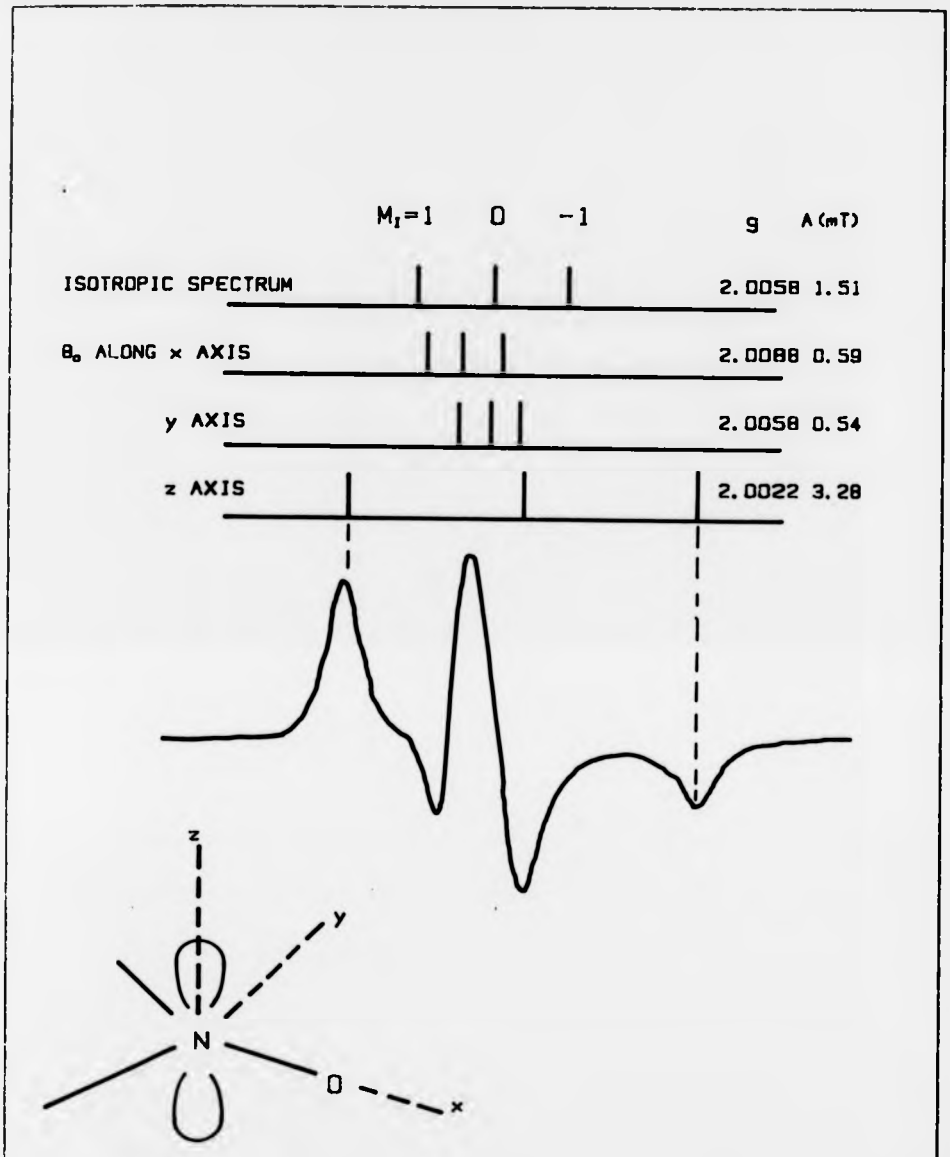

FIG. 2.4. THE NITROXIDE RADICAL POWDER SPECTRUM.

In the nitroxide reference frame the nitrogen 2pπ orbital is defined as the z-axis. Within this reference frame the **g**- and **A**-tensors are diagonal with principal values g_{xx}, g_{xy}, g_{zz} and A_{xx}, A_{yy}, A_{zz}. In the laboratory XYZ frame, in general, this will not be the case. The Hamiltonian is a scalar and hence invariant to an orthogonal coordinate transformation (L). The Hamiltonian may be in the form

$$H = \beta_e H'^{T}.g'.S' + S'^{T}.A'.I' \qquad -(2.31)$$

where

$$g' = L.g.L^{T} \qquad -(2.32)$$

and

$$A' = L.A.L^{T} \qquad -(2.33)$$

The primes denote quantities in the laboratory frame and **g**- and **A**- are the diagonal tensors. The matrix **L** rotates the nitroxide x, y, z axes into the laboratory X,Y, Z axes.

$$\begin{bmatrix} A'_{XX} & A'_{XY} & A'_{XZ} \\ A'_{YX} & A'_{YY} & A'_{YZ} \\ A'_{ZX} & A'_{ZY} & A'_{ZZ} \end{bmatrix} = \begin{bmatrix} l_{Xx} & l_{Xy} & l_{Xz} \\ l_{Yx} & l_{Yy} & l_{Yz} \\ l_{Zx} & l_{Zy} & l_{Zz} \end{bmatrix} \begin{bmatrix} A_{xx} & 0 & 0 \\ 0 & A_{yy} & 0 \\ 0 & 0 & A_{zz} \end{bmatrix} \begin{bmatrix} l_{Xx} & l_{Yx} & l_{Zx} \\ l_{Xy} & l_{Yy} & l_{Zy} \\ l_{Xz} & l_{Yz} & l_{Zz} \end{bmatrix}$$

A similar expression for **g'**- may be written where the l's represent the directional cosines of the rotation **L**. Applying the intermediate field approximation the Hamiltonian may be rewritten as

$$H = \beta_e g_{ZZ} B_o S_Z I_Z + A_{XZ} S_Z I_X + A_{YZ} S_Z I_Z + A_{ZZ} S_Z I_Z \qquad -(2.34)$$

The tensors **g'**- and **A'**- are reduced to

$$g' = g_{xx}l^2_{Zx} + g_{yy}l^2_{Zy} + g_{zz}l^2_{Zz}$$

and

$$A' = (A^2_{xx}l^2_{Zx} + A^2_{yy}l^2_{Zy} + A^2_{zz}l^2_{zz})^{1/2}$$

Transformation between two right handed orthogonal coordinate systems may be accomplished by three successive rotations represented by $L^{\theta}\ L^{\phi}\ L^{\psi}$ expressed in terms of the three Eulerian angles θ,ϕ,ψ and defined in Fig. 2.4.

In transforming from the nitroxide to the laboratory two intermediate coordinate systems may be identified. The frame associated with the DNA molecule x_2, y_2, z_2 and the fibre and sample frame X,Y,Z.

X Y Z	LABORATORY	L_o	L
X_1 Y_1 Z_1	FIBRE	L_1	
x_2 y_2 z_2	DNA	L_2	
x y z	NITROXIDE		

The relationships between the coordinate systems are illustrated in Fig. 2.5.

The transformation from the nitroxide to the DNA

$$L_2 = L^{\psi}_2\ L^{\phi}_2\ L^{\theta}_2 \qquad -(2.35)$$

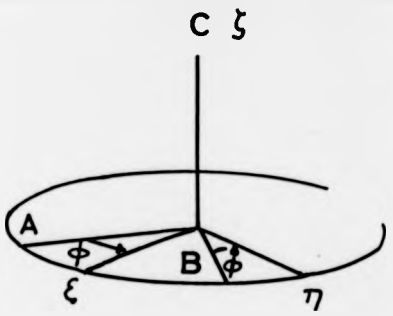

$$L^{\phi} = \begin{pmatrix} \cos\phi & \sin\phi & 0 \\ -\sin\phi & \cos\phi & 0 \\ 0 & 0 & 1 \end{pmatrix}$$

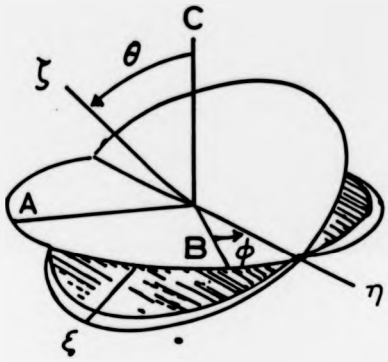

$$L^{\theta} = \begin{pmatrix} \cos\theta & 0 & -\sin\theta \\ 0 & 1 & 0 \\ \sin\theta & 0 & \cos\theta \end{pmatrix}$$

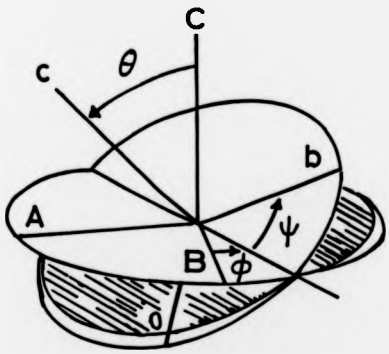

$$L^{\psi} = \begin{pmatrix} \cos\psi & \sin\psi & 0 \\ -\sin\psi & \cos\psi & 0 \\ 0 & 0 & 1 \end{pmatrix}$$

TRANSFORMATION MATRIX OF DIRECTION COSINES

FIG. 2.5. COORINATE AXES AND EULERIAN ANGLES.

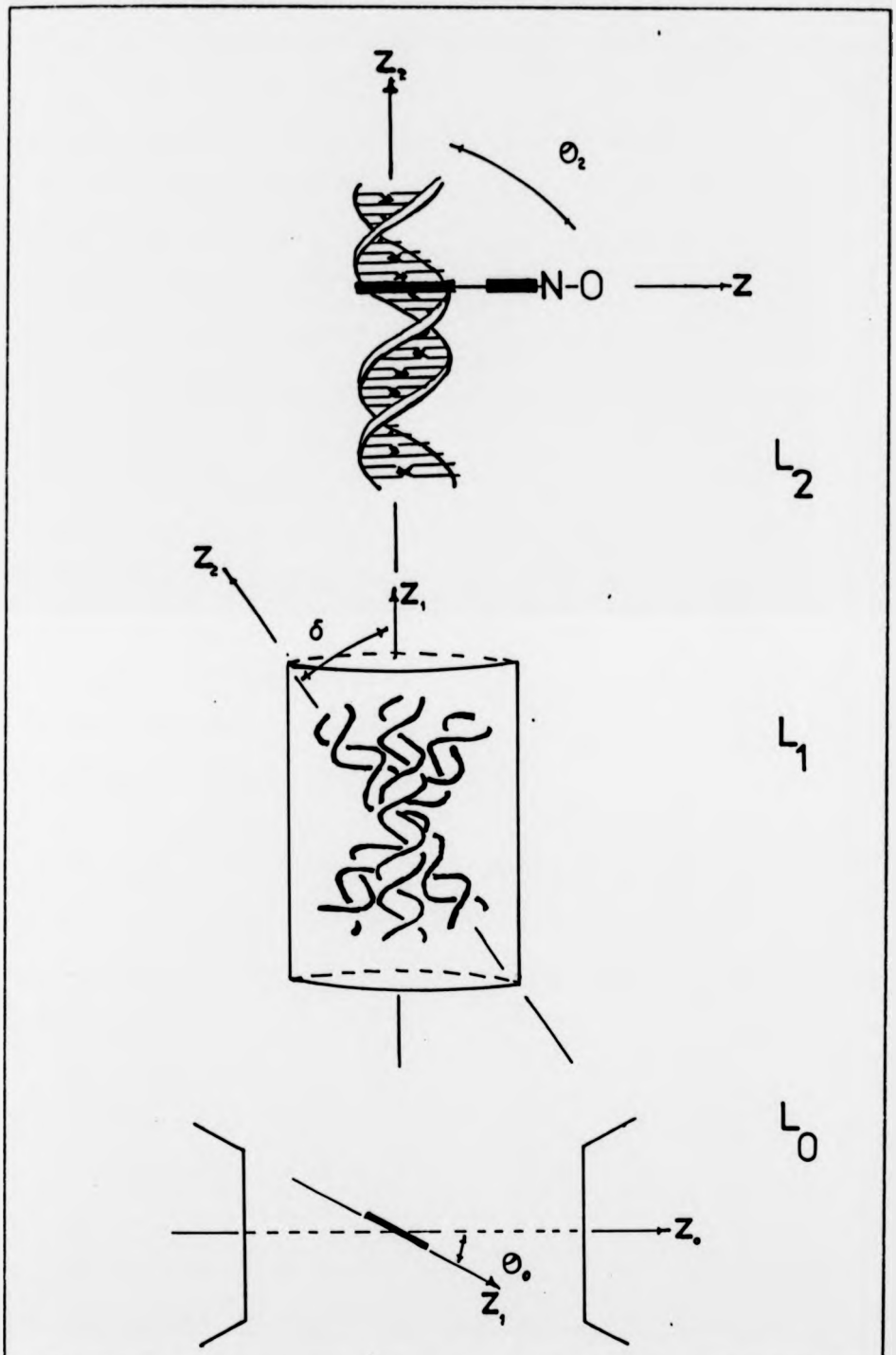

FIG. 2.6. NITROXIDE TO LABORATORY TRANSFORMATION.

involves a rotation of the nitroxide about the DNA z_2 axis by angle ϕ_2; θ_2 represents the tilt of the nitroxide z axis to the DNA z_2 axis and ψ_2 is a rotation of the nitroxide about its own z-axis.

In the DNA to fibre transformation ϕ_1, represents a rotation of the DNA about the fibre Z_1 axis; θ_1 represents the tilt of the DNA z_2 axis to the fibre Z_1 axis and ψ_1 is a rotation of the DNA about its own z_2 axis. This final rotation is redundant as it is similar to the rotation ϕ_2 hence the transformation may be written as

$$L_1 = L^{\theta}_1 L^{\phi}_1 \qquad -(2.36)$$

The final transformation from the fibre to the laboratory involves ϕ_o, θ_o and ψ_o. The rotation ψ_o is similar to ϕ_1. The Hamiltonian is invariant to rotations about the laboratory z-axis hence ϕ_o is also redundant. The angle θ_o represents the angle of rotation of the fibre to the magnetic field.

$$L_o = L^{\theta}_o \qquad -(2.37)$$

The transformation from the nitroxide to the laboratory may thus be represented by

$$\begin{bmatrix} X \\ Y \\ Z \end{bmatrix} = L^{\tau}_o L^{\tau}_1 L^{\tau}_2 \begin{bmatrix} x \\ y \\ z \end{bmatrix} \qquad -(2.38)$$

In the case of a perfect fibre the angle θ_1 representing the deviation of the DNA z_2 axis from the fibre z_1 axis should be set to zero however a degree of misalignment is always present[8]. If this is assumed to be Gaussian then the distribution function

$$P(\theta_1) = N^{-1} \sin(\theta_1) \exp[-(\theta_1)^2/2\delta^2] \qquad -(2.39)$$

may be applied where N is a normalising constant and δ the half width of the distribution.

2.2.2 The Computer Program

A computer program based on the above model developed by Porumb and Slade[7] similar to that of Libertini[3] and modified by Strange[8] was used. The program was written in Fortran IV and run interactively on the Keele Computer Centre GEC 4190 from a tectronix compatible graphics terminal. The input parameters are listed below.

1. The microwave frequency
2. The principal A- and g-values
3. The nuclear spin quantum number
4. The linewidths
5. The lineshape
6. The initial magnetic field value and sweep range
7. The tilt of the nitroxide z-axis to the DNA z_2 axis (θ_2)
8. The twist of the nitroxide about its own z-axis (ψ_2)
9. The orientation of the fibre z_1 axis to the magnetic field (ψ_o)
10. The angular stepsize for (ψ_1)
11. The angular stepsize for (ϕ_2)
12. The angular stepsize for (ϕ_1)
13. The degree of misalignment of DNA in the fibre (ϕ)

The geometry of the nitroxide to DNA is defined by the tilt and twist all possible orientations of the nitroxide are then generated by averaging ϕ_2 and ϕ_1 over the range 0^o to 360^o and θ_1 from 0_o to 180^o by the given step interval. The direction cosines for each orientation are calculated and hence g- and A-values evaluated. The line positions are found from

$$B_I = h\nu/g\beta - \sum m_I A \qquad -(2.40)$$

Each absorption is convolved with either a gaussian or lorentzian lineshape function and weighted by the function $P(\psi_1)$. The accumulated spectrum is normalised by dividing by the sum of weights. The derivative is then calculated.

The program may also be used to calculate the powder spectrum. This may be achieved by redefining ψ_1 and ϕ_1 as the polar angles of the nitroxide within the laboratory reference frame hence setting ψ_0, ψ_2, ψ_2 and δ to zero. The angles are stepped over their appropriate ranges $0<\psi_1<90$ and $0<\phi_1<180$ (if g- and A- are symmetric $\phi_1=0$) and the calculated spectrum weighted by $P(\psi_1) = \sin \psi_1$.

PART THREE

2.3 The Saturation-Transfer EPR Experiment

The growth in the use for biological application of the nitroxide spin-label method over the last decade has been largely due to the technique's sensitivity to motion. The expression for spin quantum number dependent linewidths eq(2.29) allows the molecular rotational correlation time τ_c to be determined from the spectrum if the motion falls in the range 10^{-12} to 10^{-8}s. Through the use of computer lineshape simulation this maybe extended to 10^{-7}s[9].

Interest in studying the dynamics of biological macromolecules and supramolecular complexes such as protein and lipids has motivated the development of techniques sensitive in the 10^{-7} to 10^{-3}s region. Following the pioneering work of Hyde, Dalton and Thomas[10,11] the saturation transfer EPR experiment was conceived. The experiment requires that the rapid passage condition $\gamma B_1 >> T_1$ be fulfilled (see section 2.1.4) hence a saturating microwave field is applied. The field

sweep employed is slow to meet the adiabatic condition ($dB/dt \ll \gamma B_1$) yet fast compared to T_1. This occurs when high frequency Zeeman modulation is applied. Under these conditions the magnetisation vector will follow the effective field throughout the sweep. Saturation transfer spectra rely on the breakdown of the rapid passage condition due to competition between rotational motion and spin-lattice relaxation. This occurs over the range $100T_1 > \tau_c > 0.01T_1$. Within the period τ_c the spin-label axis will rotate at an angle θ say, hence the resonant frequency of that spin packet will change. As the time period is comparable to that for relaxation spectral intensity will be transferred through the spectrum. The degree of spectral diffusion varies across the spectrum according to anisotropy. The extent of spectral diffusion for a nitroxide spectrum is given by

$$\sin\theta \frac{dB_r(\theta)}{d\theta} = \frac{\sin^2\theta \cos\theta \, (B^2_\perp - B^2_\parallel)}{(B^2_\perp \sin^2\theta + B^2_\parallel \cos^2\theta)^{1/2}}$$

It may be seen from this expression that no spectral diffusion occurs at the extrema $\theta=0, \pi/2$ despite angular diffusion
The effect is illustrated in Fig. 2.6a.

The breakdown of the rapid passage condition in a component of the magnetisation contributing to spectral intensity with the zeeman modulation reference phase set $\pi/2$ out of phase. For non-saturating fields there would be zero intensity in this position.

A systematic study of possible saturation transfer sensitive displays was carried out by Thomas[11] out of phase first and second harmonic absorption and dispersion were investigated. The out of phase first harmonic dispersion and the second harmonic out of phase absorption were found to be most sensitive. A series of calibration spectra against isotropic rotational correlation time for the two displays were given using spin-labelled haemoglobin under

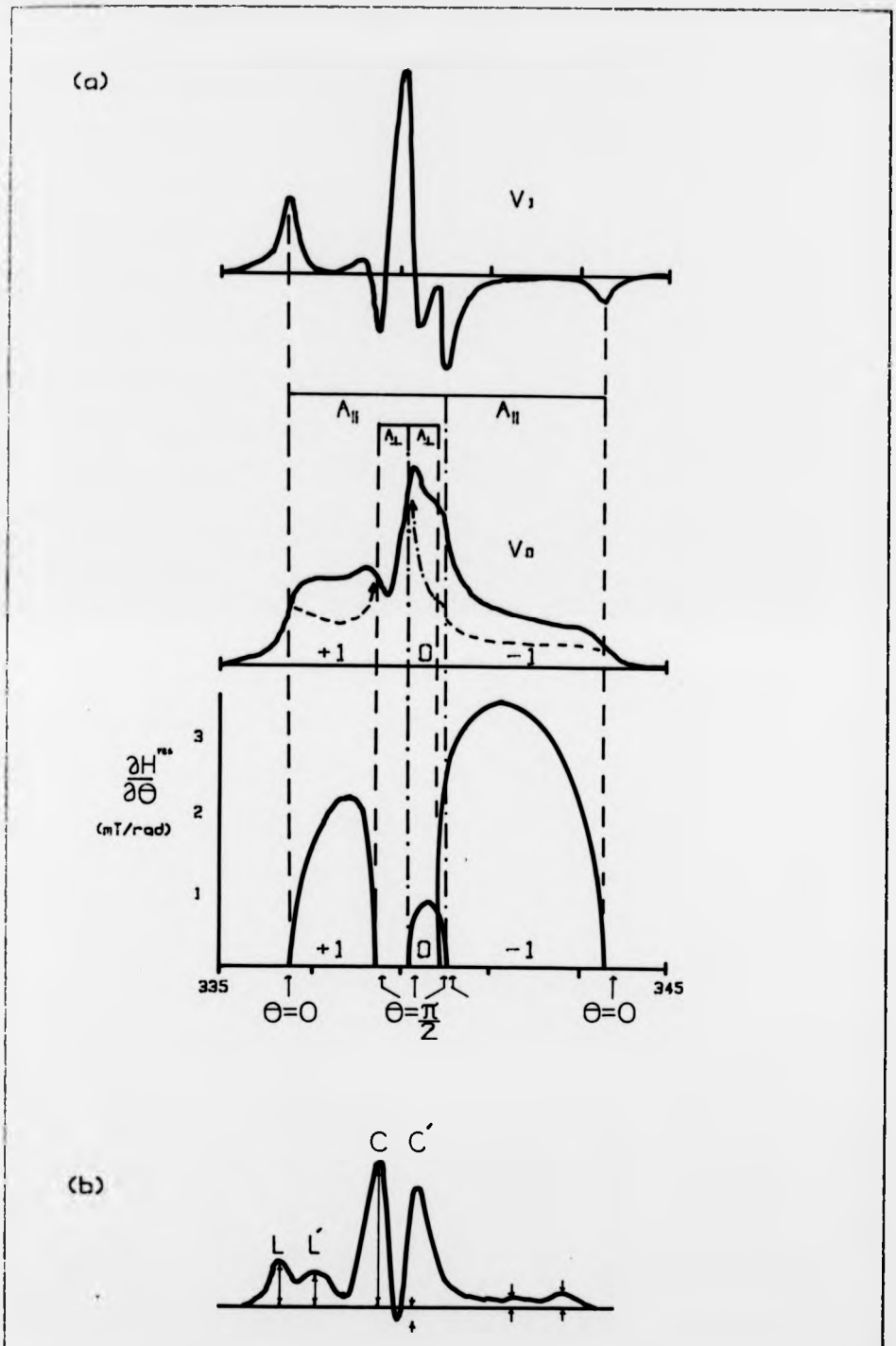

FIG. 2.7. (a) THE FIRST HARMONIC DERIVATIVE (V_1) AND ABSORPTION (V_a) (CENTER) SPECTRA FROM A RIGID ISOTROPIC POPULATION OF NITROXIDE SPIN-LABELS. THE CONTRIBUTIONS FROM THE THREE NUCLEAR SPIN STATES. THE RESONANCE FIELD θ^{RES} A FUNCTION OF ANGLE OF THE NITROXIDE AXIS TO THE EXTERNAL FIELD AND NUCLEAR SPIN STATE IS SHOWN AGAINST MAGNETIC FIELD (LOWER). (b) A SECOND HARMONIC DERIVATIVE (V_2) SPECTRUM.

varying viscosity temperature conditions. The spectra were characterised through comparison of spectral intensity ratios taken from the motionally sensitive regions of the spectrum as shown in Fig. 2.6b.

Quantitative calibration of ST-EPR spectra relies on the validity for the Debye equation for rotational diffusion hence the restriction of isotropic motion is imposed. In many biological situations, however, anisotropic motion occurs. The problem of anisotropic motion and ST-EPR has been studied by Robinson and Dalton[12], Gaffney[13], and Hemminga and Faber[14]. Gaffney studied the motion of a spin-labelled derivative of cholestanone undergoing slow reorientation about the nitroxide axis in the anisotropic environment of a powder of crystalline adduct of thiourea.

Accurate simulation of ST-EPR spectra has proved difficult. The methods of coupled Bloch equations and the stochastic Liouville equation have been applied but with limited success. At the present no complete theory of magnetic resonance in the slow motion regime exists.

REFERENCES

1. Pake,G.E., **Paramagnetic Resonance**, Benjamin, 1962.

2. Atherton,N.M., **Electron Spin Resonance**, Halstead Press, London, 1973.

3. Libertini,L.J.,and Griffith,O.H., (1970), J. Chem. Phys., 53, 1359.

4. Van Vleck,J.H., (1948), Phys. Rev., 74, 1168.

5. Kneubuhl,F.K., (1960), J. Chem. Phys., 33, 1074.

6. Jost,P.C.,and Griffith,O.H., in**Spin-Labelling I: Theory** and

Practice, Berliner,L.J, (ed), Academic Press, New York, (1976).

7. Porumb,T.,and Slade,E.F, (1976), J. Magn. Res., 22, 219.

8. Strange,R.W., (1985), Ph.d. Thesis, University of Keele.

9. Freed,J.S., in **Spin Labelling I: Theory and Practice**, Berliner,L.J, (ed), Academic Press, New York, (1976).

10. Hyde, J.S,and Dalton,L.R., (1972), Chem. Phys. Lett., 16, 568.

11. Thomas,D.D., Dalton,L.R,and Hyde,J.S., (1976), J. Chem. Phys., 65, 3006.

12. Robinson,B.J.,and Dalton,L.R., (1980), J. Chem. Phys., 72, 1312.

13. Gaffney,B.J., (1979), J. Phys. Chem., 83, 3345.

14. Hemminga,M.A.,and Faber,A.J., (1986), J. Magn. Res., 66, 1.

CHAPTER THREE

A REVIEW OF NUCLEIC ACID STRUCTURE AND NUCLEIC ACID-DRUG COMPLEXES

3.1 Introduction

There exists a class of small molecule, mainly drugs and dyes, that show strong interactions with nucleic acids. The induced biological activity has been shown to vary markedly within this group. For example, members of the acridines cause insertions or deletions in the genetic code hence are mutagens[1] while molecules such as daunomycin and actionomycin are anti-cancer drugs and the quinoxaline family act as antibiotics. An understanding of the molecular basis for nucleic acid-drug interactions may help to account for such divergent affects.

To gain such an understanding the following must be addressed: How does a drug interact, is it bound externally or is it intercalated within the nucleic acid, what form of bonding occurs?

Is the drug interaction dependent on nucleic acid sequence through recognition of local structure?

What affect on local structure occurs on binding, does this affect the binding of other molecules, e.g. repressors, histones or drugs?

To obtain the answers to such questions many physical techniques have found application.

Much of our understanding of nucleic acid structure and nucleic acid-drug complexes has come from x-ray diffraction. This has been performed on two types of system, fibres of oriented polynucleotides, and single crystals of mono, di and oligonucleotides. The information from the former is often of high quality, however, it is incomplete due to cylindrical averaging. Structures are hence obtained from a model building and refinement procedure. In the case of single crystals data

processing results in a near atomic resolution electron density map.

Another technique capable of giving structural information is nuclear magnetic resonance (NMR)[2]. The introduction of high frequency machines has improved resolution allowing the multiple resonances obtained from large molecules to be separated. In the case of nucleic acids those resulting from protons on the backbone may be distinguished from those of the bases. The shifts and couplings of these resonances give valuable conformational information.

Optical spectroscopy is also important, the techniques of absorption, fluorescence polarisation, circular dichroism, film dichroism, electric birefringence and electric dichroism have found application. They have been of particular use in drug-nucleic acid studies. If the relationship between the transition dipole moment and the molecular axes is known then by using ordered samples the orientation of the drug to the nucleic acid may be inferred.[3] Raman spectroscopy[4] and circular dichroism[5] have been found to be sensitive to nucleic acid conformational change. Optical spectroscopy has also been used simply as a monitor of a nucleic acid-drug interaction in kinetic experiments[6]. The techniques of temperature-jump relaxation, pressure-jump chemical relaxation and equilibrium dialysis have given information on binding constants and allowed the existence of different modes of binding to be separated. The possibility of neighbouring site exclusion may also be tested by such experiments.

Finally, electron paramagnetic resonance (EPR) has also been used to probe nucleic acid structure and certain small molecule -nucleic acid interactions. Nucleic acids are non paramagnetic hence must be labelled with a magnetic reporter. This may be attached covalently to a portion of the nucleic acid or it may be a drug molecule whose interactions are to be studied.

The following sections describe nucleic acid structure, its

conformational flexibility and drug-nucleic acid interactions.

3.2 Nucleic Acid Structure

The following discussion is restricted to deoxyribonucleic acid (DNA) and double stranded forms of ribonucleic acid (RNA). Both molecules take the form of an unbranched polymer and may have a molecular weight of many millions. The repeating unit is the nucleotide (320 MW). This consists of a deoxyribose sugar in DNA or a ribose sugar in RNA covalently bonded to a phosphate group and a purine or pyrimidine base. There are four commonly occurring base molecules in DNA two purines, adenine (A) and guanine (G), and two pyrimidines, thymine (T) and cytosine (C). The repeating units are joined by phosphodiester bonding between the 3' hydroxyl group of the sugar of one unit to the 5' hydroxyl group of the next. The architecture proposed by Watson and Crick[7] was for two polynucleotide chains, running in opposite directions, to be wound helically about the same axis constrained by hydrogen bonding between the bases. A sugar and phosphate attached at one side of a base-pair is related by a two-fold rotation axis in the plane of the base, the helical symmetry generates a further set of diad axes disecting the base-pair planes. Base pairing occurs between a purine and pyrimidine as shown in Figure 3.1. The allowed combinations are A-T and G-C hence the ratio of (G,A) to (C,T) remains constant while the amount of G-C to A-T may vary dependent on the origin of the DNA.

The molecular structure may be described in terms of a set of conformational or torsion angles. These are the projected angles between two adjacent bonds when viewed along the central bond. The convention used here is presented in Fig. 3.2. The angle χ defines a rotation about the glycosidic bond it relates the sugar O1' to the purine C8 or pyrimidine C6. It has been observed to take

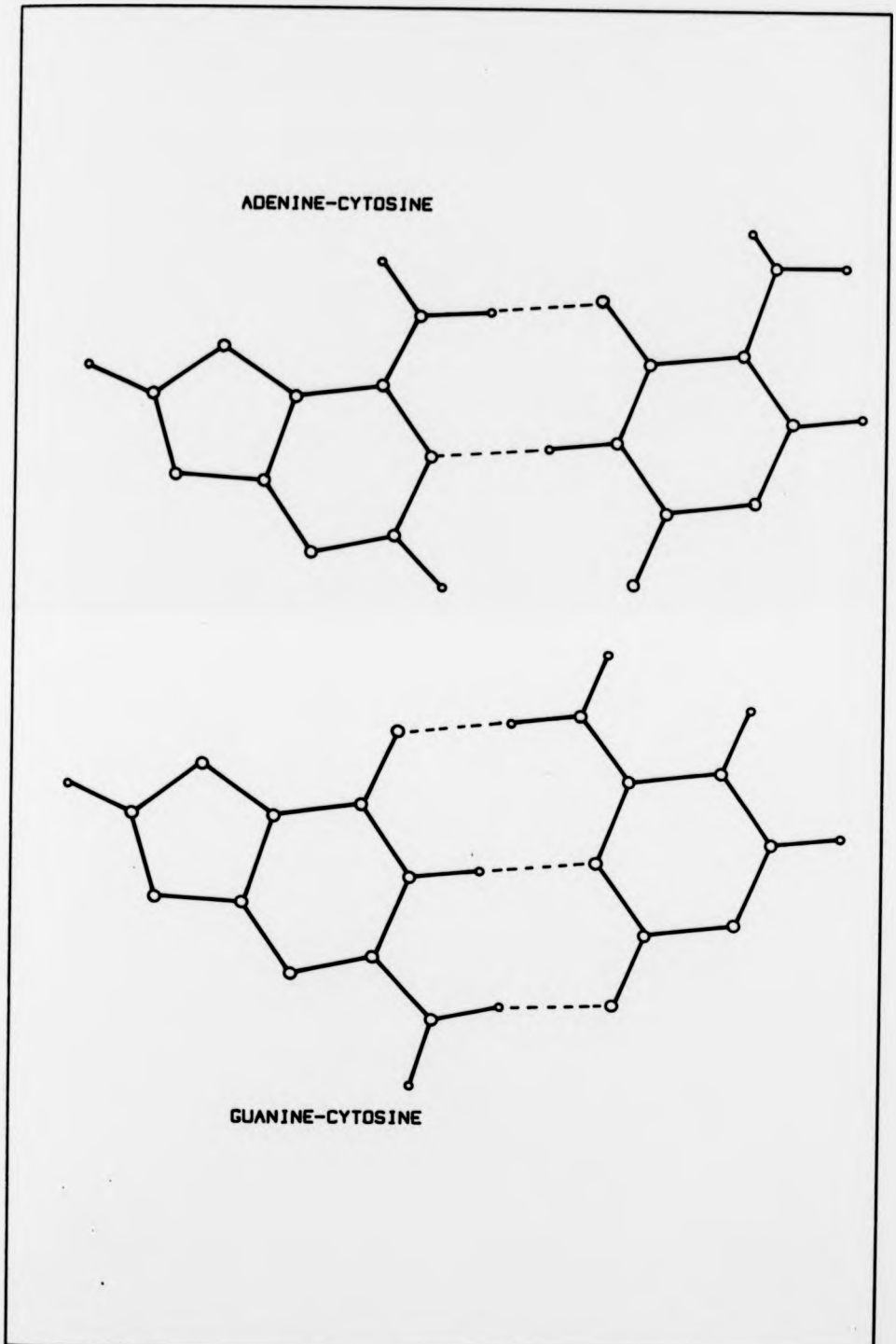

FIG. 3. 1. WATSON-CRICK BASE-PAIRING GEOMETRY

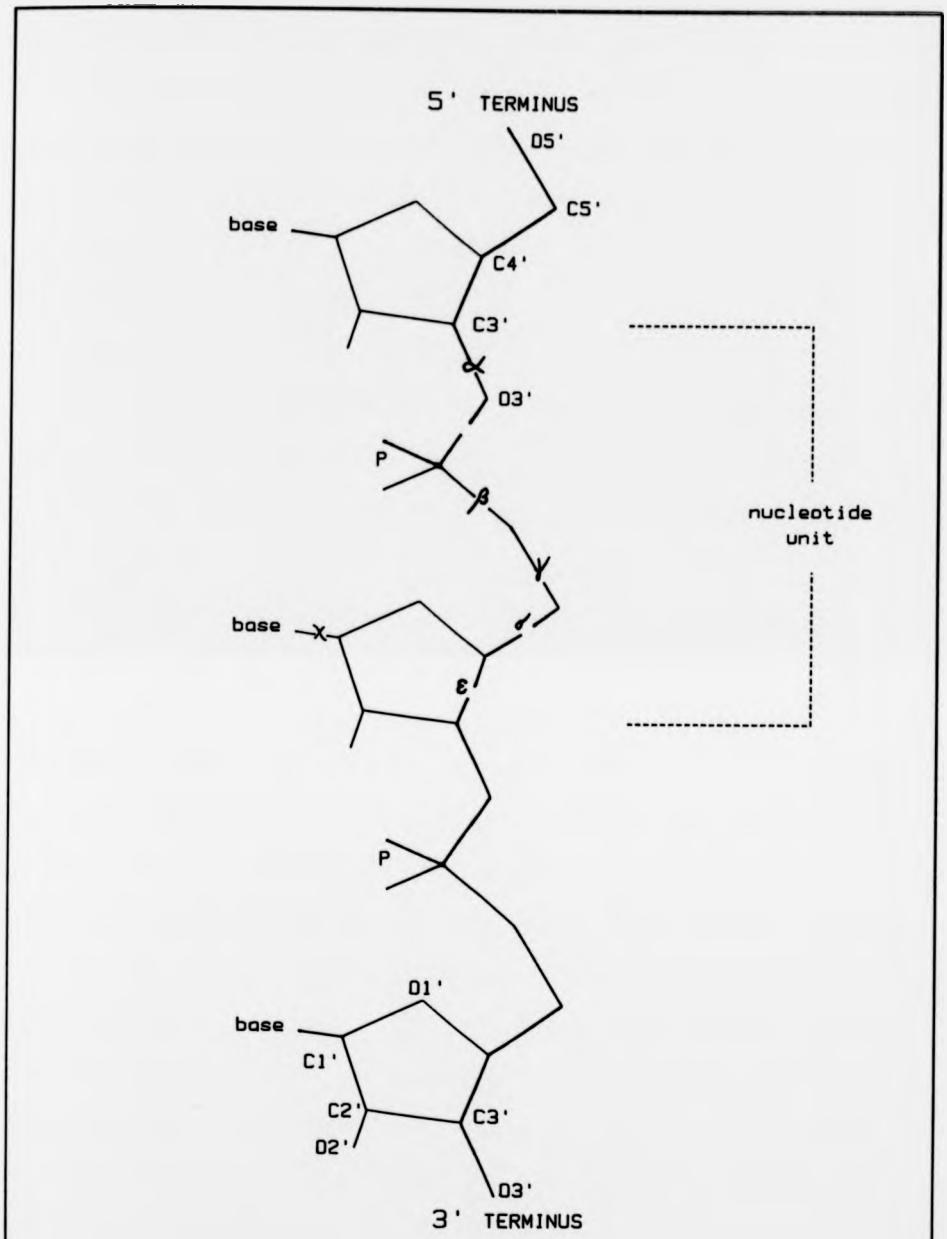

FIG. 3. 2. A SECTION OF THE NUCLEOTIDE BACKBONE DEFINING NOMENCLATURE.

values from slightly less than zero to more than 90^0 and again around 270^0. Those low value angles are termed anti, those in the 90^0 range as high anti while those around 270^0 are syn. The backbone torsion angles are divided into three regions, given below

a) gauche$^+$(g^+) $\quad 0^0 < \tau < 120^0$

b) gauche$^-$(g^-) $\quad -120^0 < \tau < 0^0$

c) trans (t) $\quad 120^0 < \tau < 240^0$

The molecular conformation is also influenced by the sugar pucker this describes the deviation of the sugar ring atoms from coplanar. The C2' or C3' atom may be displaced giving four possible puckers shown in Fig. 3.3.

In order to define the position and orientation of the base-pairs with respect to the helix axis the following parameters are commonly defined twist, tilt, roll, displacement and slide. The twist is the rotation per base-pair about the diad axis; roll is a rotation about a line connecting the purine C8 with the pyrimidine C6; displacement (D) is the distance from the helix axis to the base-pair; slide is defined as the translation of the base-pairs relative to one another down their long axis. The base-pairs themselves are also flexible. They are rarely perfectly coplanar, they can either be propeller-twisted or bent. A propeller twist is a rotation of the two bases with respect to each other about the C8-C6 link. A bend involves rotation about an axis parallel with the dyad axis passing through the centre of the base-pair hydrogen bonds. The base-pair degrees of freedom are shown in Fig. 3.4.

Examination of a model of DNA, for example Fig. 3.5c shows the presence of two grooves running the length of the structure. These are the major and minor grooves and may vary in depth and width dependent on molecular conformation. They are important as potential sites for interactions.

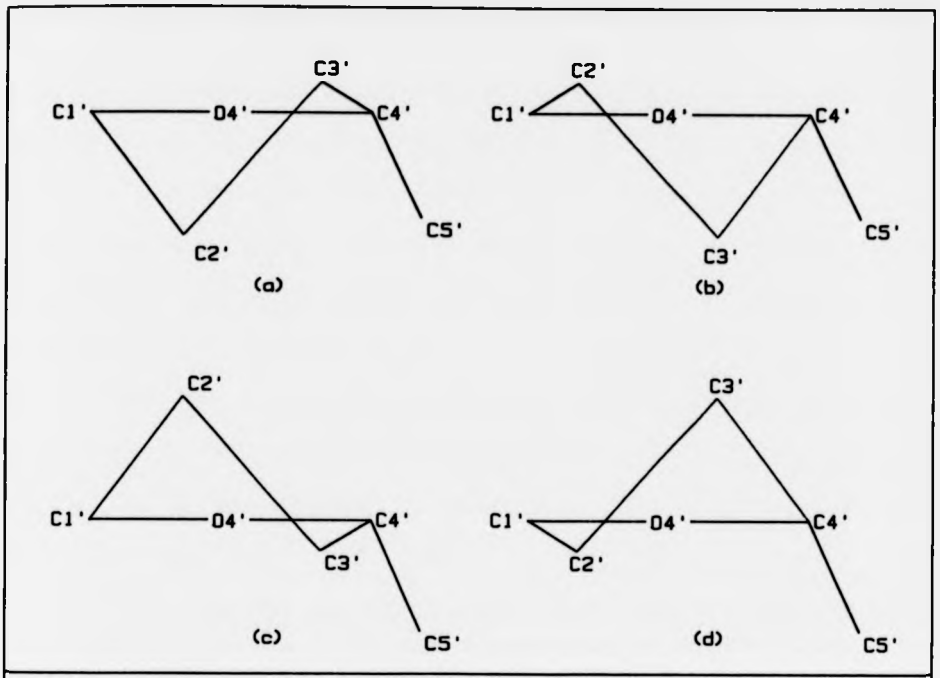

FIG. 3.3. THE FOUR POSSIBLE SUGAR PUCKERS: (a) C2'-ENDO (b) C3'-ENDO (c) C2'-EXO (d) C3'-EXO.

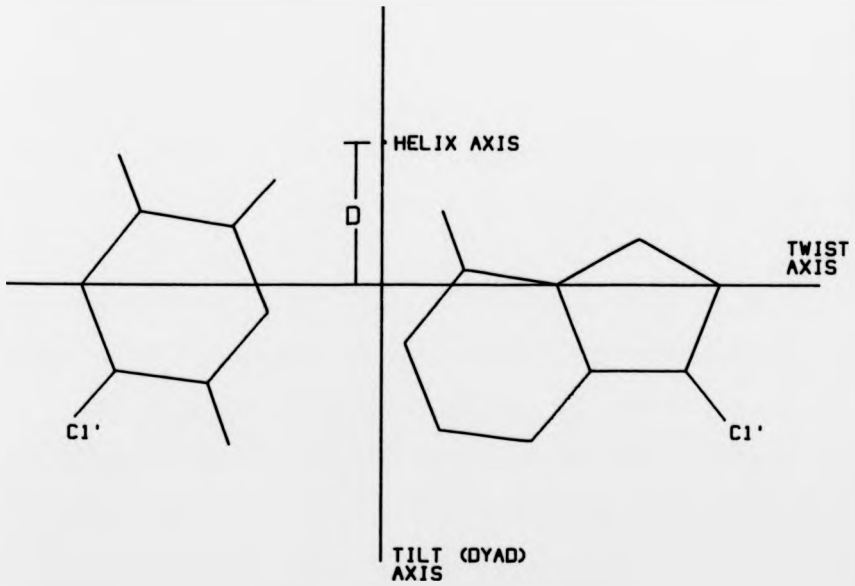

FIG. 3.4. THE PARAMETERS DEFINING THE POSITION OF A BASE-PAIR RELATIVE TO THE HELIX AXIS.

It should be noted that the stability of the double helix can not be accounted for by base-pair hydrogen bonding alone since the bond energy (~16 kT) is too small. In addition bases show a preference for stacking, the hydrogen bonds are instead taken up by water. The stacking mechanism arises from interactions between the π-electrons of the aromatic bases and accounts for the stability of single strand polynucleotides. Base-pair stacking in DNA results in the exclusion of water. Hydrogen bonding between the base-pairs is then a favourable interaction. The influence the negative phosphate groups of the backbone is counterbalanced by interactions with small, positively charged salt ions, such as Na^+ and K^+.

In this section we have examined the main features of the Watson-Crick model and have given the terminology necessary for an accurate description of molecular structure. Nucleic acids, however, do not exhibit a unique arrangement. A molecule may be induced into making transitions between several distinct forms.

3.3 Conformational Flexibility in DNA

From the first x-ray studies on DNA fibres carried out by Franklin[8] over 30 years ago it was discovered that the molecule was able to switch between two double-helical forms, A and B, on changing the state of hydration. Subsequent studies varying molarity and type of counterion under a range of hydration conditions have yielded further forms. Naturally occurring DNA in the fibre state are found to exhibit A[9], B[10] and C[11] forms see Fig. 3.5a,b,c while synthetic polymers such as poly (dA).poly (dT) and poly (dG-dC) have been found in D and S forms[12]. Single crystal DNA oligonucleotide segments have so far been observed in A, B and Z forms[13].

The B-form is observed under conditions of high humidity and or high salt.

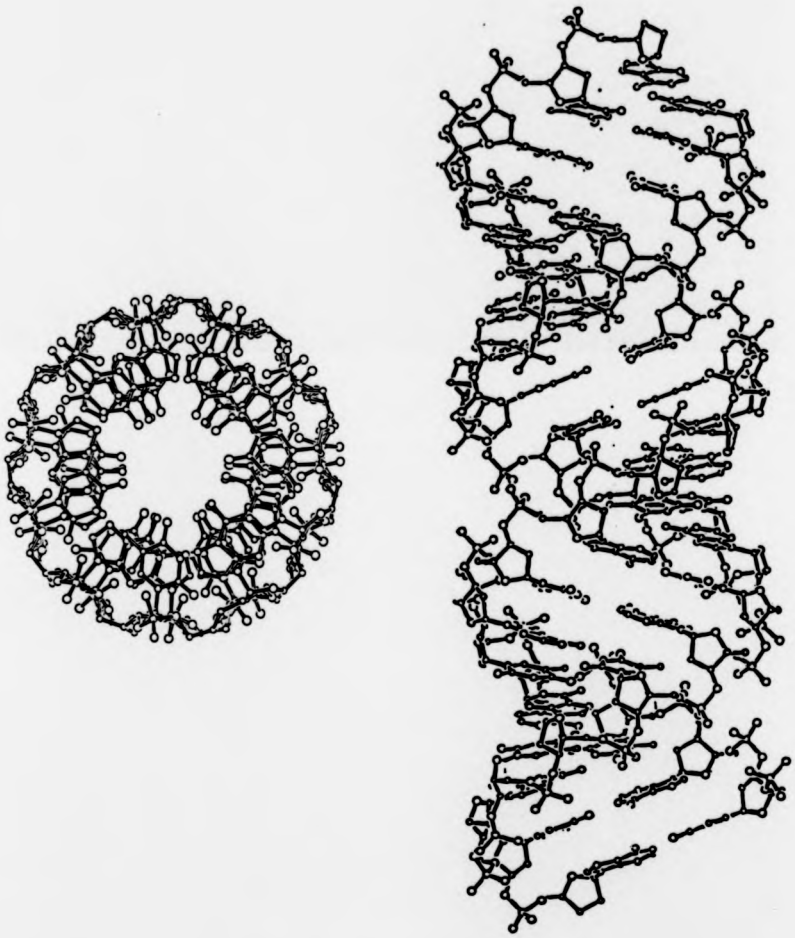

FIG. 3.5a A COMPUTER GENERATED LINE DRAWING OF A-DNA.

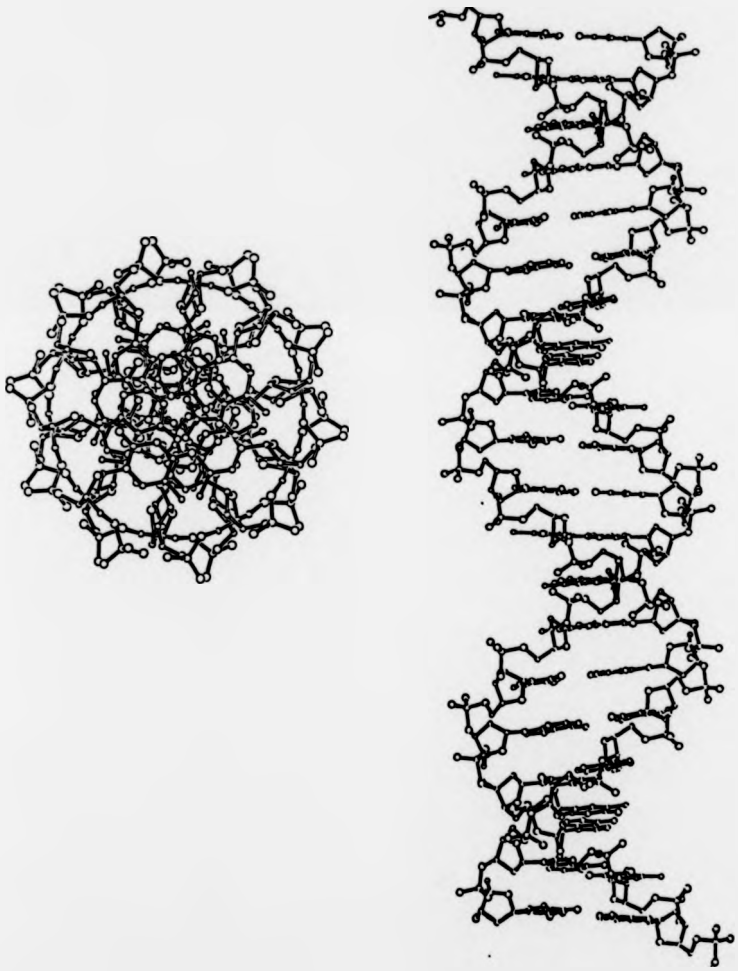

FIG. 3.5b A COMPUTER GENERATED LINE DRAWING OF B-DNA.

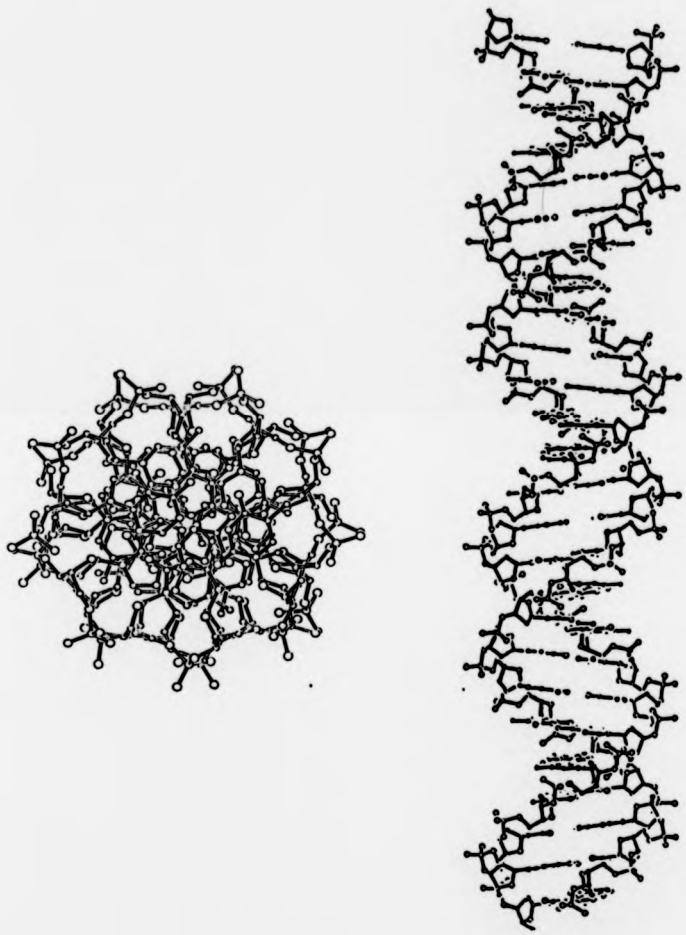

FIG. 3.5c A COMPUTER GENERATED LINE DRAWING OF C-DNA.

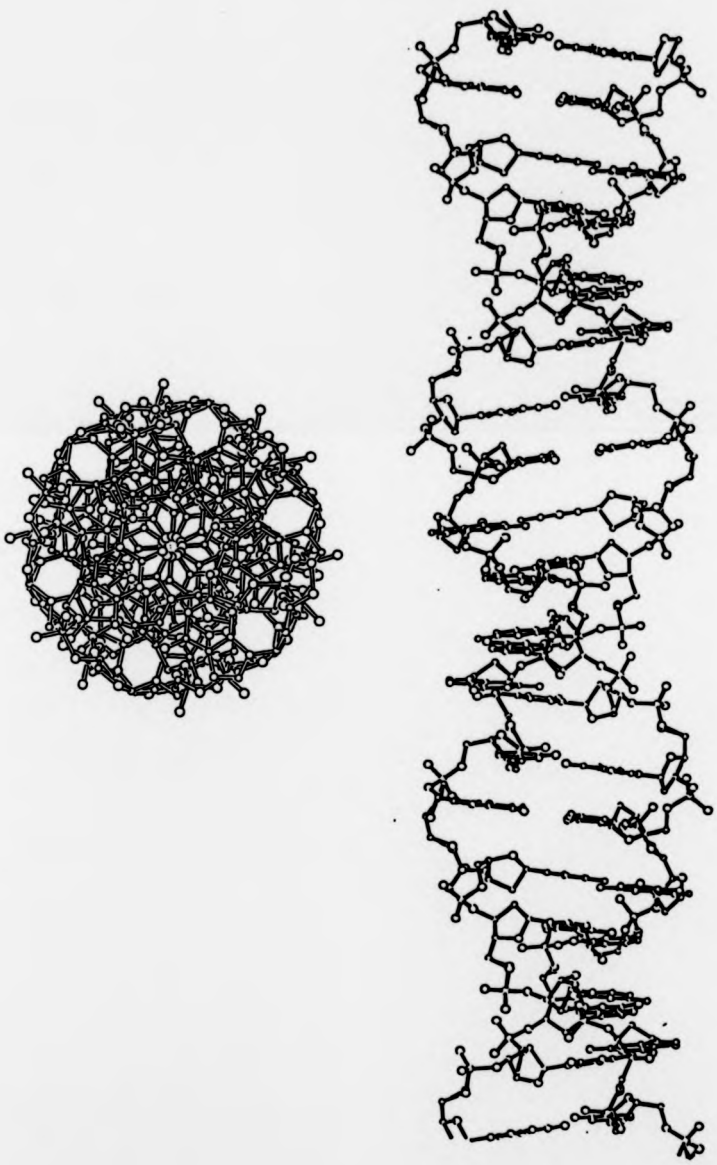

FIG. 3.5d A COMPUTER GENERATED LINE DRAWING OF S-DNA.

	CONFORMATION		
	A	B	C
SUGAR PUCKER	C3'-ENDO	C2'-ENDO	C2'-ENDO
PITCH (A)	28.2	33.8	31
BASES PER TURN	11	10	9.3
RISE PER BASE-PAIR (A)	2.56	3.4	3.3
BASE TILT ANGLE	19	-6	-8
TURN PER RESIDUE	32.7	36	38.6
GROVE WIDTH (A)			
MINOR	11	5.7	4.8
MAJOR	2.7	11.7	10.5
GROVE DEPTH (A)			
MINOR	2.8	7.5	7.9
MAJOR	13.5	8.5	7.5
DISPLACEMENT D(A)	4.72	-.16	-2.13

TABLE 3.1 THE PARAMETERS DEFINING THE THREE CONFORMATIONS OF NATIVE DNA IN FIBRES.

It is thought to be the predominant form in solution and hence in biological systems. A computer generated side and end view of the model is given in Fig. 3.5c. The helical parameters listed in Table 3.1. The glycosidic bond takes on high anti conformation while the backbone angles from α to ε of Fig 3.2 are t, g(-), t, g(+) respectively. The molecule is a 10 base per turn right handed helical structure with almost horizontal base pairs packed in the centre core. It has two equally deep grooves, a wide major one and a narrower minor one.

The C-form is similar but with 9.3 bases per turn and the bases displaced slightly further from the helix axis. In this case the glycosidic angle is anti and the torsion angles t, t, g^-, t, g^+. The C-form, however, exists under opposing conditions compared to B of low salt concentration and low humidities.

The B-form observed from fibres has been found to comprise a family of structures exhibiting small variations dependent on the counter ion present and the type of DNA used[12] . Comparison of the B and C forms (Figs. 3.5a and c and table 3.1) show many similarities. The C form may be considered a member of the B family.

The A-form of DNA is stouter with a very deep narrow major groove, and a shallow, wide minor groove. The base-pairs are more tightly packed with a rise of 2.6A compared with 3.3A and are displaced well away from the helix axis leaving a hollow core. They are also tilted at an angle of 19^0. The glycosidic angle is anti and the to torsion angles are t, g^-, g^-, t and g^+.

The Z form is a novel structure first described in a crystal study of the complementary hexanucleoside pentaphosphate d-CpGpCpGpCpG by Wang et al[13] in 1979. It is a left handed helical structure with a dinucleotide repeating unit. The latter is due to the alternating position of the O1' of the deoxyribose sugar. The helix has 12 bases

per turn (6 dimers), a rise of 3.7A and a base tilt similar to the B-form. Examination of Fig. 3.5d shows that the backbone follows a discontinuous zig-zag path, in place of the major groove is a converse surface while the minor groove is present but very deep. The glycosidic torsion angle alternates from syn when associated with dG to anti with dC, the sugar pucker also alternates from C3' endo to C2' endo.

The descriptions given above refer to the averaged structures obtained from fibre diffraction studies. The possibility of small local variations is not precluded. The B-form of the alternating copolymer poly (dA-dT) was studied by Klug and coworkers[14] who proposed that the phosphate backbone structure alternated with sequence. This was termed the "alternating-B" structure. The possibility of sequence dependent structure and its implication with respect to recognition had been discussed previously for example by Arnott[15], Bram[16] and Wells[17], These ideas have subsequently been strengthened by a detailed dodecamer C-G-C-G-A-A-T-T-C-G-C-G carried out by Drew, Dickerson and coworkers[18,19].

It was found that the sequence formed just over a turn of B-helix with the correct average rise, twist angle and tilt. The average propeller-twist was 12^{o}. In addition a wealth of sequence dependent structure was observed. Purine -3', 5'-pyrimidine base-pair steps were shown to roll their base planes so as to open towards the major groove while pyrimidine-purine steps opened towards the minor groove. Homopolymer (Pur-Pur, Pyr-Pyr) steps were rigid resisting roll in either direction. This behaviour was attributed to the preference of pyrimidines for more negative glycosyl torsion angles. Variations in local helical twist angles were observe, CpG steps show smaller values than GpC as through in compensation for their smaller intrinsic base overlap. The propeller twist of G.C. base-pair was found to be less

than for A.T this was considered to be due to hindrance from interstrand base overlap rather than the presence of the third hydrogen bond.

Another important consequence of the B-DNA dodecamer study was the observation of 72 ordered water molecules which has given valuable information on hydration. A general preference for association with the polar N and O atoms at the exposed edges of the base-pairs was observed. Hydration within the minor groove was ordered, regular and apparently cooperative a geometric spine was seen filling the groove often bridging to phosphate oxygens. The presence of purine N-2 amino groups had a disruptive influence on the structure. In the case of the major groove order was restricted to a first hydration shell around the polar N and O groups other water molecules in the groove were disordered. Structural disorder was also found on the phosphate backbone except in the region of 5-methyl groups on thymine residues.

Recently, a solution NMR study of 5'd(C-G-T-A-C-G)$_2$ was carried out[20]. The use of the nuclear overhauser effect allowed 190 interproton distances to be obtained. Structure refinement were then carried out using two B-DNA starting models and a similar final structure was found from both. This was similar to the dodecamer, all base-pairs were propeller-twisted. The magnitude of local structural variation was found to be less.

The other commonly encountered conformation, A-DNA, has also bee observed in a single crystal x-ray study. The structure of the octamer d(G-G-T-A-T-A-C-C) and its 5-bromouracil containing analogue was solved to 1.8A resolution by Shakked et al[21]. This showed similar average parameters to the fibre model structure, 2.7A rise per step, 18^{o} tilt from the global helix axis, and a rotation per residue of 33^{o} leading to a 10.9 bases per turn helix. Sequence dependent structure was observed particularly with regard base stacking. A tendency for

interstrand purine purine partial tacking was observed. Electrostatic stacking interactions between adjacent guanine and thymine base produce symmetric bending of the double helix and a major groove widening. Correlations in the glycosidic bond and backbone torsion angle variations were shown and assigned to the requirement for energetically efficient base-stacking. In general the backbone distortions were found to be less than in the B-dodecamer. A study of thermal motion suggested that rigid-body librational motion of the double helix about is axis existed. Again, comparison with the B-dodecamer would seem to indicate that the B-form shows greater conformational disorder and perhaps greater flexibility than the A-form.

Further evidence on the degree of variation within the A- and B-forms of DNA has come from ^{31}P NMR studies of highly oriented fibres[22,23], measured as a function of humidity and angle. Due to the phosphorous chemical shift anisotropy the range of orientation and motion of the backbone phosphate groups was determined. For fibres of natural DNA in the A-form the observed range of phosphate orientation was in agreement with the classical A-DNA model[24]. No motion was observed on the NMR time scale. In the case of the B-conformation motional effects when seen these were considered to originate from three sources, conformational fluctuations, restricted rotation about a tilted axis, and rotational diffusion about the helix axis. A wide range of phosphate orientation was deduced consistent with those from single crystal studies.

As has been mentioned previously, sequence dependent structure is likely to be of great biological significance. In order to understand the observed variations of the B-dodecamer Calladine[25] has applied structural mechanics of deformable elastic systems. The conformation is considered to be a consequence of simple steric repulsive forces between purine bases in consecutive base-pairs but on opposite strands.

These forces are resisted by stresses in the helical backbone. The purine steric dash is due to propeller-twist and base-pair overlap it may be avoided by four possible motions: (1) suppression of propeller-twist (2) base-pair roll; (3) a base-pair sideways shift (4) a small rotation about the helix axis. The hypothesis was proposed that the purine clash exerted specific "pushing apart" forces on the base-pair resulting in motions (3) and (4). The shift was related to the sum of major and minor groove repulsions while the twist angle variation was in proportion to their difference. The observed anticorrelation between the backbone torsion angle at the site of the base-pair and the variation in the helix twist angle was reproduced by the application of the hypothesis and elastic mechanics.

So far the various possible structures that a DNA molecule may adopt have been discussed but nothing has been said about how the transition between the forms may occur. Our understanding of the mechanism of the transition and the conditions required to initiate it are incomplete. Work involving studies on natural DNA fibres has shown that, under conditions of low salt, the molecules may be induced to follow the transition pathway C→A→B with increasing the humidity from 33% to 98%[12]. The A conformation existing generally over the 66% to 75% range. At intermediate humidities x-ray patterns exhibiting conformation mixtures, (C/A) or (A/B) have been observed. Mahendrasingam[12] has given an explanation of these patterns in terms of the temporal effect of water migration and the possibility of ion concentration gradients within the fibre. At these intermediate humidities the fibre may be divided into zones of differing environmental conditions, hence structure. The point of transition has been observed to be dependent on both base sequence and water activity. Fibre studies have shown that poly (dA-dT) remains in the B-form regardless of water content, others such as poly (dA-dT) and poly

(dG-dC) readily switch from B to A upon drying. The polymer poly (dG).poly (dC) is found to favour the A-form even at high humidities.

Recently Calladine and Drew[28] have attempted to rationalise the observed behaviour of the A to B transition. Originally the transition was thought to be due to a rigid, bistable phosphate backbone, but this is inconsistent with the observed sequence dependent structure of the B-dodecamer. Calladine and Drew have argued that the bistability is an inherent feature of certain dinucleotide steps. The backbone acts to communicate this bistability to neighbouring steps. Model building, with only stacked rigid base-pair units, using three variables, twist, roll and slide the B-A was reproduced. In fact it was found a base roll of 12^{o} associated with a 1.5A slide was sufficient to make the transition. Tabulation of the values for these variables for the 45 steps available from crystal data showed they were distributed along a line from $+3^{o}$, -0.5A to $+20^{o}$, +2A. It was them identified that pyr-pur steps occupied the two extrema positions, the low side end representing the B form steps, the high roll and slide the A form steps. Of the sixteen possible steps three classes were found, bistable, weakly bistable and neutral. Steps such as C-G, C-A, T-G, and T-A were strongly bistable as the purines had to chose between good same strand overlap at slightly negative slide or good cross strand overlap at positive slide values. Propeller twist imposed the requirement for a 15^{o} roll in the latter case so as to allow the observed opening of the base-pair planes towards the minor groove. The steps C-C C-T, G-G and A-G were considered potentially bistable due to weak cross-strand overlap between the guanine 2-amino group and the pyrimidine ring. Finally, the neutral steps were A-A, A-T and T-T as those were free from steric hindrance.

Obviously such mechanist arguments, are by themselves insufficent, a causal link to hydration is required. It was observed

that those neutral steps were in fact those cross linked by water structure within the B-form. These steps fell in the central region of the roll slide diagram. It was suggested that to avoid large local variations in the phosphate backbone the slide parameter must be constant between base steps. This gave a mechanism for communication. Alteration in hydration was assumed to affect the balance between the water mediated stability of the neutral steps preferring low slide to the good cross stranded overlap in the bistable steps at high slide.

So far we have considered nucleic acid molecules as static only briefly mentioning the possibility of dynamic fluctuations however this is unlikely to be the case in vivo. Evidence for dynamic fluctuations has come from NMR studies[27] and more recently from the application of translation, libration, screw rigid (TLS) group model to high resolution x-ray data[28]. This divides the molecule into rigid molecular grouping and allows the calculation and comparison of anisotropic thermal factors. From this the direction and magnitude of motional vectors may be determined. Application of the technique to double-helical DNA and RNA has revealed the following base translations and librations; (1) fluctuations in propeller-twist and roll (2) buckling of the base-pairs and (3) sliding of the base-pair units. The first two motions are coupled to sugar librations and imply motion of the nucleoside unit. Such motions are consistent with the Calladine model, reducing cross strand steric hindrance. Fluctuations in roll may also be important in intercalation.

Many of the ideas developed within this section have only recently been proposed, they result largely from the results of oligonucleotide single crystal data. Consequently they must be considered tentative as insufficient data has yet been accumulated to raise them from the status of hypothesis. However, it would seem a coherent view of sequence dependent structure is beginning to emerge.

Recent advances in NMR are likely to allow structure determination in the solution state hence providing a valuable comparison to crystal structure observation.

3.4 Drug-Nucleic Acid Complexes

The small molecule nucleic acid interaction may involve one of the following three process (1) covalent bonding as with benzo pyrine diol epoxide or N-acetoxy-acetylamino fluorene; (2) intercalation, planar aromatic chromophores may be sandwiched between two base-pairs in a double helix, for example proflavin or daunomycin (3) by hydrogen bonding/ electrostatic attachment in a groove of the helix such as with netrospin. In fact the situation may be more complex, it is possible for part of the benzo pyrene diol epoxide to bind covalently while allowing the aromatic component to either intercalate or bind in the minor groove. Studies have also shown that molecules such as proflavin and ethidium bromide may intercalate via a mediating electrostatic binding mode and under certain conditions this may be the dominant interaction.

Before proceeding a few comments on drug structures relevant to this study will be made. The molecule of primary interest, ethidium bromide consists of a three membered, slightly non-planar, ring system termed the phenenthridium ring attached to which are a phenyl ring and an ethyl group. The former makes an angle of 97^{o} to the mean plane while the ethyl group is free to rotate about an N-C bond 84^{o} out of the mean plane. It has been found that the inclusion of a, near planar, heterocyclic ring system is a common feature of many intercalating small molecules. The chemical structures of ethidium bromide and two other known intercalators, acridine orange an proflavin are given in Fig. 3.6.

The process of intercalation is of particular interest as it has

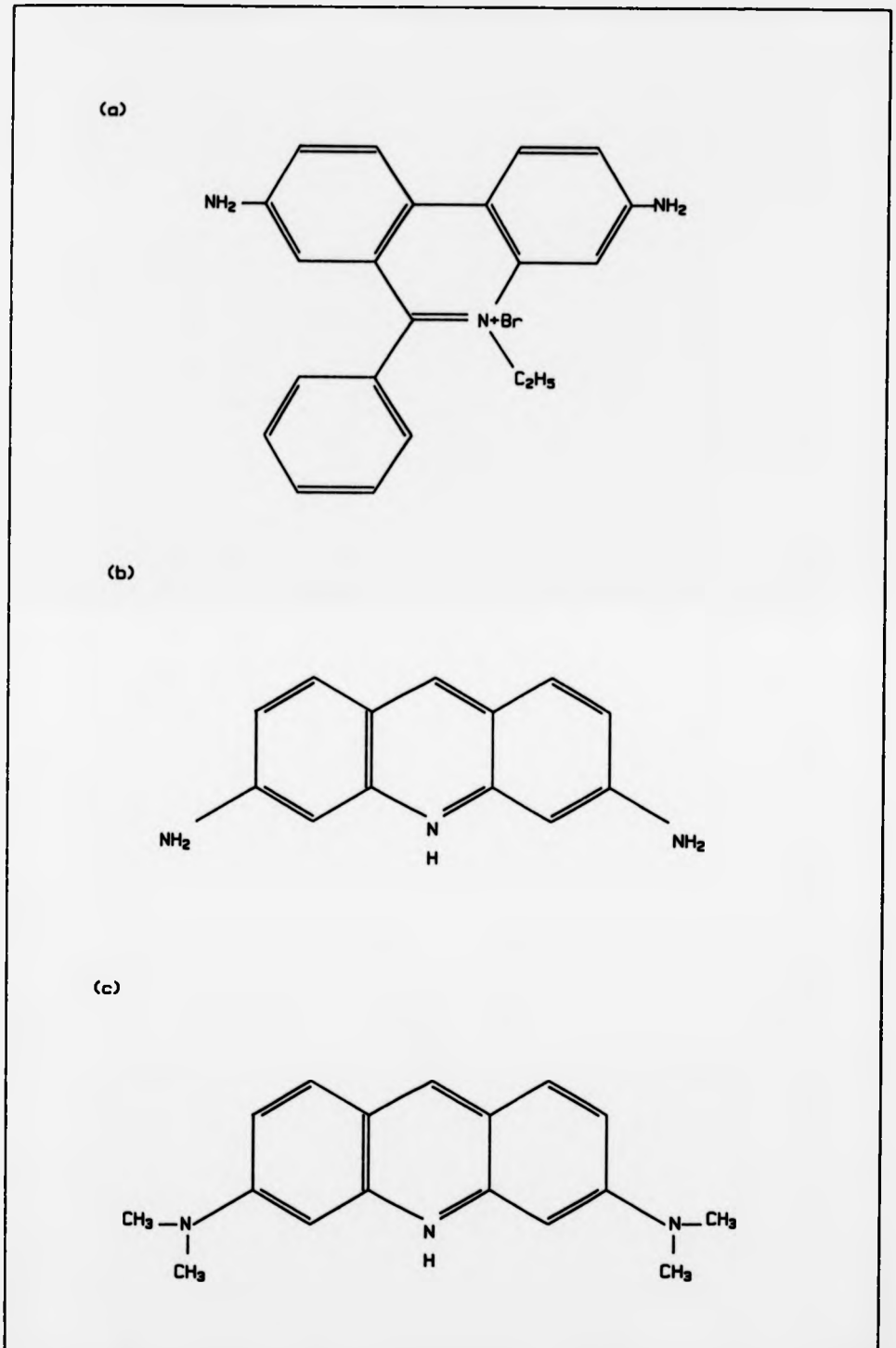

FIG. 3.6. A DIAGRAM OF THE CHEMICAL STRUCTURES OF (a) ETHIDIUM BROMIDE, (b) PROFLAVINE, (c) ACRIDINE ORANGE.

COMPLEX	CONTENTS OF CRYSTALLO-GRAPHIC ASYMMETRIC UNIT	SUGAR PUCKER	BASE TURN( )	RESOLUTION LIMIT OF DATA(A)	REFERENCE
PROFLAVINE CpG	1.5 PROFLAVINE. 1 CpG. $12H_2O$. . $5SO_4^{2}$	C3'ENDO(3'-5') C3'ENDO	32	0.85	(33)
PROFLAVINE CpA	1 PROFLAVINE. 1 CpG. $?H_2O$			0.8	(34)
PROFLAVINE 5. INDO-CpG	2 PROFLAVINE. 5iCpG. $15H_2O$. 1 METHANOL	C3'ENDO(3'-5') C3'ENDO	36	1.31	(35)
PROFLAVINE d(CpG)	2 PROFLAVINE. 2d(CpG). $27H_2O$	C3'ENDO(3'-5') C3'ENDO	17	0.89	(36)
PROFLAVINE (UpA) (CpG)	2 PROFLAVINE. 1UpA-1CpG. $?H_2O$	C3'ENDO(3'-5') C. C3'ENDO-A. C2'ENDO	16		(37)
ETHIDIUM 5. INDO-CpG	2 ETHIDIUM. 5iCpG. $27H_2O$. 4 METHANOL	C3'ENDO(3'-5') C2'ENDO	5	1.14	(38)
ETHIDIUM 5. INDO-UpA	2 ETHIDIUM. 5iUpA. $27H_2O$	C3'ENDO(3'-5') C2'ENDO	4	1.34	(39)

TABLE 3.2 STRUCTURAL DATA FOR DRUG-NUCLEIC ACID CRYSTALLINE COMPLEXES

been shown that certain molecules interacting in this way result in mutations. Lerman[29] was the first to propose the intercalation model as a result of a study on the interactions of several acridine dyes with DNA. Fibre x-ray diffraction patterns from the complexes showed that the presence of the bound drug resulted in considerable loss of information. The retention of the 3.4A meridional reflection, however, suggested that the planar chromophore substituted for a base-pair. Furthermore, solutions of the complexes showed an increase in viscosity and a reduction in the sedimentation coefficient in comparison to DNA solutions. These observations are consistent with a thinning and stiffening of the molecule on drug binding. The model requires adjacent base-pairs to move apart in order to accommodate the small molecule "sandwiched" between them. The arrangement is stabilised through π orbital interactions between the drug and the surrounding bases.

Following this initial work a series of fibre diffraction and associated model building studies were carried out, notably by Fuller and Waring[30] on ethidium, Neville and Davies[31] on acridine orange and proflavin, and Pigram et al.[32] on daunomycin. All were shown to be consistent with intercalation. In general they were unable to define the average structures to the same precision as for nucleic acids alone.

More recently progress in understanding the precise geometry of intercalation has been made through crystal structure determinations of duplex intercalation complexes. Up to the present over a dozen have been solved all show classical intercalation with an average drug to base-pair separation of 3.4A. A striking feature of all of these structures has been the presence of a pyrimidine -3', 5'-purine sequence at the binding site. As detailed in the previous section such sequences exhibit reactive base-pair roll opening towards the minor

groove in the B-form. This would suggest that intercalation would be mediated via this groove as is found to be the case with six of the eight intercalators so far studied. The two exceptions, proflavin and acridine orange, would seem to be able to reverse the natural base-pair roll. The B-dodecamer also suggest such pyr-pur steps have smaller than average twist angles to compensate for the weaker natural base-pair overlap in comparison to pur-pyr steps. Examination of the experimentally determined local twist values from crystal structures show a wide variation as Table 3.2 shows in the case of proflavin and ethidium. The daunomycin d(CGTACG) structure[42] is the only drug-oligonucleotide so far solved, this exhibits a twist of 36^{0} at the intercalation site and an unwinding of 8^{0} at adjacent sites. It is of interest to note that it is exactly these pyr-pur sequence steps that Calladine and Drew classify as bistable in their account of the A to B-DNA transition. The possible implications of this have yet to be investigated.

The complexes are also found to have similar backbone angles. They resemble those of A'-DNA invoking only an increase in δ from t to an intermediate t, g^{-} value and a reduction in the 3' end glycosidic value from low to high anti. In general a mixed C3' endo, 3', 5', -C2' endo pucker is preferred, however, in the case of proflavin this may be over-ruled possibly by solvent interaction see Table 3.2.

In order to obtain a better understanding of the significance o these crystal structures several model building studies extending the structure to the oligonucleotide level have been conducted. Two approaches have been used. Sobell and workers[40] relaxed the observed geometry to incorporate it in a standard B-structure the result involved linking at the binding site. A further study on the A to B transition postulated this linked structure as an intermediary. Berman and Neidle[41] constrained the backbone to that experimentally observed.

This resulted in an unusual conformation involving pronounced base-pair propeller-twist and bend.

Intercalation is considered to occur while the DNA is in the B-form as both base-pair separation and molecular flexibility are favourable in this case. Fibre diffraction and duplex to oligonucleotide model building suggest that the drug tilt and roll values would be consistent with those for B-DNA base-pairs. However, Hogan et al.[3] have interpreted the results of their transient electric dichroism and electric fluorescence dichroism on proflavin and ethidium giving tilt values of $14^{o} \pm 8^{o}$, $20^{o} \pm 8^{o}$ and roll values of $2^{o} \pm 8^{o}$, $10^{o} \pm 8^{o}$ respectively.

Many of the features of drug-nucleic acid interactions discussed in this section will only be clarified after many more drug-oligonucleotide structures have been resolved to high resolution.

3.5 EPR Spin-Label Studies of Nucleic Acids and Drug-Nucleic Acid Complexes

In these studies EPR has been used to probe the conformational behaviour and interactions of the macromolecule. Nucleic acids themselves are diamagnetic therefore spin-labelling or irradiation are the only methods available for obtaining an EPR signal. The technique has the disadvantage of requiring modification of the system hence there may be an associated perturbation. The method, however, has the advantage that if the position of the label is known then details of its local environment may be deduced. With other spectroscopic techniques applied to macromolecular systems interpretation is often made difficult by the quantity and complexity of the information obtained. Spin-labelling may be achieved either by covalent attachment to the nucleic acid itself or to an interacting intermediary molecule. In the former case

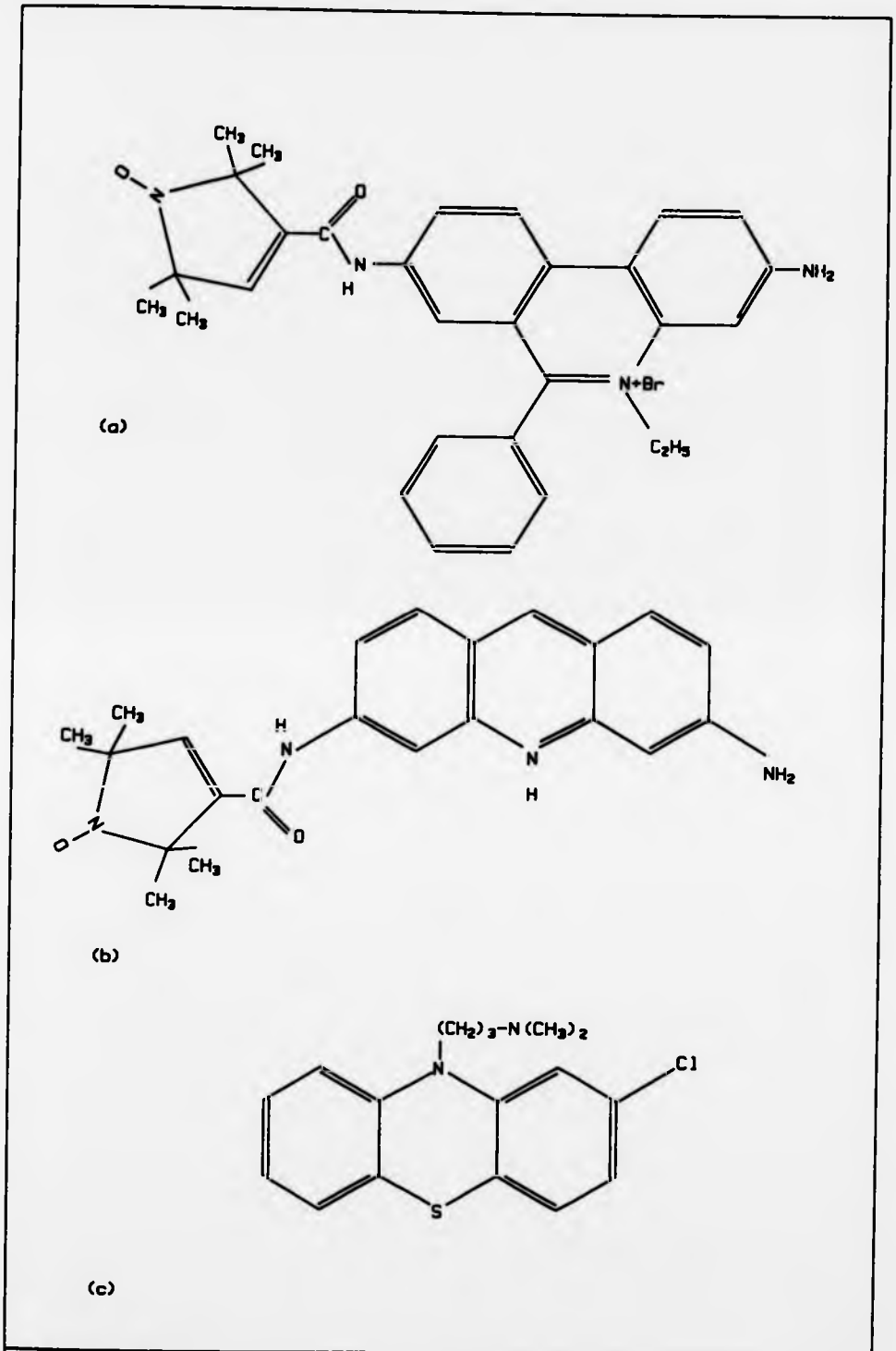

FIG. 3.7. A DIAGRAM OF THE CHEMICAL STRUCTURES OF PARAMAGNETIC DERIVATIVES OF (a) ETHIDIUM BROMIDE, (b) PROFLAVINE, (c) CPZ+.

labelling may be site specific or non-site specific. In the second class it is possible for the intermediary molecule to also be the label.

Spin-labelling of nucleic acids often involves the modification of some of the constituent bases. An example of non-site specific labelling is the interaction of pyrolidine bromoacetamide which was found to react covalently to all the bases. The extent of labelling was as follows: G 20%, A 3%; C, U and T less than 1%. In both the specific and the non-site specific cases the studies are carried out in solution and information is taken from the correlation time of the label. In general this is in the fast motion regime. Often Arrhenius plots[44] are used were the correlation time is monitored as a function of temperature. These studies have been applied to a wide range of nucleic acid systems to obtain information on helix coil transitions. The subject has been reviewed in more detail by Bobst[43], Kamajolova and Postnikova[44] and Dugas[45].

More recently Bobst and co-workers[41] have site-specifically labelled deoxyridine triphosphates with tethers of variable length which have then been enzymatically incorporated in a poly (dT) copolymer. This was then annealed with poly (dA) to cform a $(dT)_n(dA)_n$ structure. The label motion was monitored as a function of tether length from which it was deduced that the B-form major groove had a depth of 8A consistent with the x-ray result. By applying computer simulations assuming anisotropic motion and the non-coincidence of the magnetic and diffusion tensor parallel with the helix axis was deduced. A correlation time of the order of nanoseconds was obtained for the motion of the base-pairs.

The first drug-nucleic acid complex to be studied was with the positive ion radical of chloropromazine (see Fig. 3.7c). This was carried out by Ohnishi and McConnell[47] using flow orientated samples

which showed orientation dependent spectra. This arose from the hyperfine and g-anisotropy and was consider to be consistent with intercalation. A more detailed study of the system was then carried out by Porumb and Slade[48]. This was orientated fibres similar to those used in x-ray diffraction and applied the technique of spectral simulation similar to that detailed in the previous chapter. The results suggested the plane of the chromophore was perpendicular to the fibre axis.

Hong and Piette[49] used orientated DNA films to investigate the interactions of the spin-labelled drugs ethidium bromide (see Fig. 3.7a), aminofluorene, and aminothracene. In the case of ethidium bromide they observed an orientation splitting that varied from 2.8 mT with the fibre parallel to the field to 1.8 mT in the perpendicular orientation. It was argued on the grounds of steric hindrance that the label would be coplanar hence that the drug was intercalated. This was followed by a study of spin-labelled nitrobenzene DNA interactions[50]. Orientations studies showed the presence of two components coincident at both parallel and perpendicular orientations while at 45^{0} one showed a minimum splitting ($2A_{zz}$ = 3.4 mT) and the other a maximum ($2A_{zz}$ = 6.8mT). This was interpreted as showing intercalation with the nitroxide label z-axis at an angle of 45^{0} to the helix axis.

Intercalating probes have also been used to investigate the internal motions of nucleic acids. Robinson, Lerman and coworkers[51,52,53] have studied spin-labelled ethidium, a close derivative propidium and several amino acridines bound to DNA. The immobilized splittings for the two ethidium derivatives, 6.39mT and 6.3mT respectively, where found to considerably greater than for the acridines. The estimated correlation times were of the order 10 to 40 ns for the former compared with less than 1 nS for the latter. The ethidium correlation times were also obtained using saturation transfer

spectra and a value 100 nS calculated. It is also of interest to note that spectral lineshape simulation was carried out with an assumed angle of tilt between the plane of the nitroxide and that of the phenanthridium ring of 40^{0}. It was considered that the ethidium probe was essentially rigid with respect to the base-pairs and hence the correlation time reflected the internal motion of the nucleic acid. This motion was modelled by a simple elastic twisting, each base-pair torsional coupled to its neighbours.

Recently Strange[54] has completed a study on spin-labelled proflavine bound to DNA in the solution, gel and orientated fibre states. It was found that changing the humidity induced spectral changes and that these were consistent with conformational transitions as monitored by x-ray fibre diffraction. Spectral simulations were carried out using the method detailed in the previous chapter. It was postulated that the A-form spectra were consistent with the probe bound electrostatically orientated in the major groove. Fitting of the B-form spectra was found difficult due to the presence of motion and the possibility of both intercalated and externally bound drug been present.

In conclusion it may be seen that EPR can give valuable information on the geometry and dynamics of drug-nucleic acid and interactions.

REFERENCES

1. Shearman, L.W. Foryett, M.M. and Loeb, L.A. (1983), J. Biol.Chem. 258, 4483.
2. Sarma, R.H. and Dhingra, M.M., "Topics in Nucleic Acid Structure", ed. Neidle, S., Macmillan, (1981), 33.
3. Hogan, M.,Dattagupta, N. and Crothers, D.M., (1979), Biochemistry,

18, 280.

4. Urabe, H., Hayashi, H., Taminaga, Y., Nishima, Y., Kubota, K. and Tsuboi, M., (1985), J. Chem. Phys., 82, 531. 5. Ivanov, V.I. Minchenkovic, L.E. Mingat, E.E., Fauk-Kamenetskii, D. and Schafolkina, A.K., (11974), J.Mol.Biol., 87, 817.

6. Muller, W. and Crothers, D.M. (1968), J. Mol. Biol., 35, 251.

7. Watson, J.D. and Crick, T.H.C., (1953), Nature, 171, 738.

8. Franklin, R.H., Gosling, R.G., (1953), Acta. Cryst., 6, 678.

9. Fuller, W., Wilkins, M.H.F., Wilson, H.R. and Hamilton, L.D. (11965), J. Mol. Biol., 12, 60.

10. Arnott, S., and Hukins, D.W.L. (1973), J. Mol. Biol., 81, 93.

11. Marvin, D.A., Spencer, M., Wilkins, M.H.F. and Hamilton, L.D., (1961), J. Mol. Biol., 3, 547.

12. Mahendrasingam, A., Ph.D. Thesis, University of Keele (1983).

13. Wang, A.H., Quigley, G., Kolpak, F.J., Crawford, J.L., van Boom, J.H., Marel, G., Rich, A., (1979), Nature, 282, 680.

14. Klug, A., Jack, S. Viswamitra, M.A., Kennard, O., Shakked, Z. and Stectz, T.A. (1979), J. Mol. Biol., 131, 669.

15. Arnott, S. (1976), In 'Organisation and Expression of Chromosomes', (Allfrey, V.G., Bantz, E.K.F., McCarthy, B.J., Schmike, R.T. and Tissieres, A. eds.), Dahlen Konferenzen, Berlin.

16. Bram, S., (1971), Nature New Biol., 232, 174.

17. Wells, R.J., Blakesley, R.W., Hardies, S.C., Horn, G.T., Larson, J.E., Selsing, E., Bird, J.F., Chan, H.W., Dodgson, J.B., Jensen, K.F., Nes, I.F. and Wartell, R.M., (1977), CRC Crit Rev Biochem. 4, 305.

18. Drew, H.R., Wing, R.M., Takano, T., Broka, C., Tanceka, S., Itakura, K.

and Dickerson, R.E. (1981), Proc. Nat. Acad Sci., USA, 78, 2179.

19. Dickerson, R.E. and Drew, H.R. (1981), J. Mol. Biol., 149, 761.

20. Clore, G.M. Gronenborn, A.M., Moss, D.S. and Tickle, I.J., (1985), J. Mol. Biol., 185, 219.

21. Shakked, Z., Rabinovich, D., Kennard, O., Cruse, W.B.T., Salisbury, S.A.

and Viswanitra, M.a. (1983), J. Mol. Biol., 166, 183.

22. Shindo, H., Fujiwara, T., Akutsu, H., Matsumarto, U. and Kyoyoka, Y.

(1985), Biochemistry, 24, 887.

23. Fujiwara, T., and Shindo, H. (1985), Biochemistry, 24, 896.

24. Nall, B.T., Rothwell, W.P., Waugh, J.S. and Rupprecht, A., (1981), Biochemistry, 20, 1881.

25. Calladine, C.R. (1982), J. Mol. Biol., 161, 343.

26. Calldine, C.R. and Drew, H.R. (1984), J. Mol. Biol., 178, 773.

27. Hogan, M.E. and Jardetzky, O. (1980), Biochemistry, 19, 3460.

28. Holbrook, S.R. and Kim, S.H. (1984), J. Mol. Biol., 173, 361.

29. Lerman, L.S., (1961), J. Mol. Biol., 3, 18.

30. Fuller, W. and Waring, M.J. (1964), Ber Bunsenges Phys. Chem., 68, 805.

31. Neville, D.M. and Davies, D.R. (1966), J. Mol. Biol., 17, 57.

32. Pigram, W.J., Fuller, W. and Hamilton, L.D. (1972), Nature, 235, 17.

33. Neidle, S., Achari, A., Talor, G.L., Berman, H.M., Carrell, H.L., Glusker, J.P. and Stallings, W.c. (1977), Nature, 269, 304.

34. Westhof, E., and Sundaralingain, M., (1980), Proc. Nat. Acad. Sci., 72,

628.

35. Reddy, B.S. Seshardri, T.P. Sakove, T.D. and Sobel, H.M. (1979), J.
Mol. Biol., 135, 787.

36. Shieh, H.S., Berman, H.M., Neidle, S., (1980), Nuc. Acids. Res., 8, 85.

37. Aggrwal, A., Islam, S.a., Kuroda, R., and Neidle, S. (1984), Biopolymers,
23, 1025.

38. Jain, S.C., Tasai, C.C. and Sobel, H.M. (1977), J. Mol. Biol., 114,
217.

39. Tsai, C.C., Jain, S.C. and Sobel, H.M. (1975), Proc. Natn. Acad. Sci.,
72, 628.

40. Sobel, H.M., Tsai, C.C., Jain, S.C., and Gilbert, S.g. (1977), J. Mol. Biol., 114, 333.

41. Berman, H.M. and Neidle, S. (1979), In "Nucleic Acid Geometry and Dynamics
(ed. Sarma, R.H.), pp. 325, Pergamon Press.

42. Quigley, G.J., Wang, A.H.J., Ughetto, G., Van der Marel, G. Van Boom, J.
H. and Rich, A. (1980), Proc. Natn. Acad. Sci., 77, 7204.

43. Bobst, A.M. (1979). In "Spin-Labelling II : Theory and Practice"
(Berliner, L.J. ed.) Academic Press.

44. Kanzalova, S.G. and Postnikova, G.B., Quart. Rev. Biophys., 14, 244
(1981).

45. Dugas, H., (1977), Acc. Chem. Res., 10, 47.

46. Bobst, A.M., Kao, S.C., Toppin, R.C., Ireland, J.C. and Thomas, I.e.,

(1984), J. Mol. Biol., 173, 63.

47. Onishi, S., McConnell, H., (1965), J. Amer. Chem. Soc., 87, 2293.

48. Porumb, T. and Slade, E.F., (1976), Euro J. Biochem., 65, 21.

49. Hong, S.J. and Piette, L.H., (1976), Cancer Res., 30, 1159.

50. Hong, S.J. and Piette, L.H., (1978), Arch. Biochem. Biophys., 185, 307.

51. Hurley, I., Robinson, B.H., Scholes, C.P. and Lerman, L.S. (1979), In "Nucleic Acid Geometry and Dymamics" pp. 253 (Ed. Sarma R.H.) Pergamon Press.

52. Robinson, B.H., Lerman, L.S., Bethe, A.H., Frisch, H.L., Dutton, L.R. and Auer, C.J., (1980), J. Mol. Biol., 139, 13.

53. Hurley, I., Osei-Gyimah, P., Archer, S., Scholes, C.P., Lerman, L.S., (1982), Biochemistry, 21, 4999.

54. Strange, R.W., (1985), Ph.d. Thesis, University of Keele.

CHAPTER FOUR

ELECTRON PARAMAGNETIC RESONANCE INSTRUMENTATION

4.1 INTRODUCTION

This chapter which is concerned with instrumentation has been divided into three parts. The first reviews the effects of noise on spectrometer sensitivity and describes the spectrometers used in this study. The second details the saturation transfer experiment and the third is concerned with magnetic field regulation and computer control.

Part I starts by rationalising the various approaches taken in the literature for the assessment of the effects of oscillator noise on the overall spectrometer noise figure. A review of the other major noise source, detector noise, is also given. The discussion is limited to a homodyne reflection cavity spectrometer employing a circulator and field modulation. This material is then used to clarify the operation of balanced mixer detection. It is also used to explain the advantages of the Loop-Gap resonator design and the use of low-noise microwave pre-amplification. A description of the 10 GHz-band and 35 GHz-band spectrometers used in this study is then given.

Part II details the modifications to the 10 GHz-band spectrometer necessary to allow saturation transfer experiments. The method for, and results from, the calibration of the microwave magnetic field strength is given. Finally, the experimental procedure adopted and the necessary precautions are fully described.

The final part starts with an introduction to the theory of magnetic field regulation. A description of the two methods of field control used in this study is then given. A review of the computer control of EPR spectrometer and data acquisition systems and a discussion of the factors influencing their design are presented. The

system designed and implemented with the two spectrometers is then described.

PART I

4.1.1 Introduction

It was stated in Chapter 2 that a paramagnetic sample placed in a constant magnetic field will absorb energy from a transverse alternating magnetic field of the correct frequency. In order to observe this effect a spectrometer must consist of a generator and waveguide component or inductor to produce the alternating field a magnetic and a radiation detector. More specifically a modern EPR spectrometer uses a klystron oscillator feeding a reflection cavity the reflected power being detected by a schottky barrier diode operating in its linear region; that is giving an output current proportional to input electric field.

Resonance effects may be represented by small real and imaginary changes in the impedance of the conducting system[1]

$$r/R = \eta 4\pi Q_0 \chi'' \qquad -(4.1a)$$

$$x/R = \eta 4\pi Q_0 \chi' \qquad -(4.1b)$$

Where η is the filling factor defined as the ratio of microwave magnetic field integrated over the sample volume to the total integrated over the cavity volume; Q_0 is the unloaded Q-factor of the cavity; R is the waveguide resistance. Absorption is represented by small changes in he cavity resistance which effectively after the cavity Q-factor while dispersive effects are represented by small changes in the cavity impedance causing phase shifts.

One of the major objectives of spectrometer design is high sensitivity. Feher[2] obtained an expression for the minimum detachable signal assuming thermal noise to be the only source of amplitude fluctuations. The expression modified by Poole[3] is given below

$$\chi''_{min} = \frac{2}{\eta Q_o} \left(\frac{kT_d \Delta f}{P_o} \right)^{1/2} \qquad -(4.2)$$

P_o is the incident power; T_d the noise temperature of the detector; Δf the system bandwidth; k Boltzmanns constant. This figure is always exceeded in practice as other noise sources are present.

4.1.2 Noise sources

The problem of noise in a spectrometer system begins with the generator. This is one of the major noise sources. Thermal, shot and flicker noise within he oscillator result in amplitude and phase noise spectral density on the output. The amplitude limiting aspects of oscillators such as finite beam current and stabilised electrode potentials in the case of klystrons result in a reduction in amplitude fluctuations and a dominance of phase noise. Discrete components in the frequency spectrum may also be present such as modulation for frequency control and line frequency harmonics. THe output of an oscillator, therefore, is not a pure sine wave and may be represented as below.

$$E(t) = E_o \, (1+e(t)) \cos(\omega t - \theta(t)) \qquad -(4.3)$$

Where $e(t)$ represents fluctuations in amplitude and $\theta(t)$ random fluctuations in phase.

The spectrum of interest is that received at the detector diodes.

To obtain this, the output spectral density of the generator must be multiplied by the transfer function of the spectrometer microwave circuit. In general this reduces to a function of the cavity reflection coefficient as this is the dominant frequency dependent element.

To the received microwave noise spectrum is now added mixer and amplifier noise. The noise spectral density of microwave diodes has two components, a constant white noise contribution from shot noise and a component showing a 1/f dependence due to several junction barrier effects. Shot noise is common to junction devices and is a result of the random nature of the passage of the discrete charge carriers over a potential barrier and increases with bias current. The 1/f component may be due to variations in the barrier height or to charge trapping events at the junction. The output of the mixer diodes is then fed into an amplifier chain which will add noise of its own. The noise voltage present on a recorded spectrum is dependent on the bandwidth of the spectrometer detection system. The noise power is proportional to bandwidth, and on the content of 1/f noise power. In order to minimise both these contributions lock-in amplifier techniques are used. The signal is modualted by high frequency magnetic field modulation at the cavity.

4.1.2.1 Klystron Noise

In this section the various approaches presented in the literature to the problem of obtaining an expression for the noise power at the detector are reviewed. The klystron output fluctuates in amplitude and phase. However, on transmission though the spectrometer, conversion from phase (or frequency) fluctuations into amplitude fluctuations takes place. It is this amplitude noise component along with the transformed amplitude fluctuations that constitutes noise

voltage on detection. Hence it is an expression for this conversion that must be obtained. In general for a 10 GHz-band reflex klystron the level of frequency modulated (FM) noise is some 10 dB greater than amplitude modulation (AM) noise[4,5]. An additional factor to be taken account of is the effect of any fluctuations in the cavity tuning as this is indistinguishable from FM noise at the detector.

The first attempt to address the problem was presented by Feher[2], but no explicit term for the klystron noise spectrum was included. This was assumed to be incorporated in the cavity detuning term. Expressions for noise are dependent upon the microwave circuit. The theoretical analysis assumes that the reflection spectrometer comprises a critically coupled reflection cavity connected to the generator and detector by a three-port lossless circulator. It is also assumed that microwave bias ('bucking') is applied to he detector in phase quadranture to maximise absorption mode signals. Taking account of these restrictions, Feher's formula, rewritten in terms of noise power at the detector P_N takes the form given below

$$P_N \simeq P_o \frac{(\Omega_o-\Omega_g)^4}{B^4} + \frac{2(\Omega_o-\Omega_g)^4}{B^4\Gamma_o} + \frac{4(\Omega_o-\Omega_g)^4}{B^4\Gamma_o^2} \qquad -(4.4)$$

Where P_o is incident power, B cavity bandwidth, Ω_o cavity resonant frequency, Ω_g generator frequency and Γ_o the reflection coefficient at resonance.

The anaylsis by Standberg[4] involved noise spectral density functions explicitly. This is of importance as it is possible from noise measurements on oscillators to deduces these functions. Standberg also recognised the need to obtain an expression at the field modulation frequency for it is noise centred about this frequency that will pass the lock-in detector. As a consequence a modified expression for the cavity reflection coefficient was obtained. The resulting

expression, taking account of the previous restrictions is given below.

$$P_N(\mu_s) = B.G\ \frac{D_{fm}(\mu_s/2\pi).P_o}{2\pi\mu_s^2}\ \frac{(\Omega_q-\Omega_o)^2}{B^2}.\cos^2\xi + \Gamma_o^2+\mu_s^2\ s\ in^2\xi \qquad -(4.5)$$

Where μ_s is the modulation frequency, ξ the phase angle between bucking and signal fields and D_{FM} the frequency-modulation noise spectral density defined below.

$$D_{FM}(f) = (2\pi f)^2\ 4_o\int^{\infty} \phi(\tau)\ \cos 2\pi f\tau\ d\tau \qquad -(4.6)$$

The function $\phi(\tau)$ is the autocorrelation function of the $\theta(t)$ term of Eq. 4.2.

The most recent approach was presented by Meijer[5] who followed a similar general method as Strandberg, but with two important differences. The first was to recognise that the conversion of phase fluctuations to amplitude fluctuations is non-linear, the result of which was to allow all parts of the FM noise spectrum to contribute to noise about the modulation frequency. The procedure also explicitly takes account of the effect of possible discrete modulation frequencies, such as the modulation for automatic frequency control (AFC). The second feature of importance was to demodulate the transformed microwave spectrum against a carrier also exhibiting phase fluctuations. Strandberg demodulates against a pure carrier. The result of these were to introduce noise terms dependent on microwave bucking power. The expression for converted FM noise is given below.

$$P_N(\mu_s) = P_o^4 + 4P_o^2\frac{|E_B||E_C|}{4P_B^2} + 4P_BP_o\ \frac{\pi\Delta\omega^4}{8(B/2)^3}\ +\ \frac{\Delta\omega^2(\Omega_q-\mu_r) + 2\Delta\omega^2(\Omega_q-\Omega_o)^2}{((B/2)^2+\mu_r^2)^2}\ \frac{}{(B/2)^4}$$

-(4.7)

Where μ_r represents possible discrete frequency modulation components, P_B bucking arm power and $\Delta\omega$ is the square root of the statistical mode of the frequency modulated spectral density function $D_{FM}(f)$.

For a complete description of klystron noise at the detector the transmitted amplitude modulated noise must be considered the expressions due to Strandberg and Meijer are quoted below.

$$P_N(\mu_s) = B.G \quad \frac{D_{AM}(\mu_s/2\pi).P_o}{2} \quad \Gamma_o^2 + \frac{\mu_s^2}{B^2} \quad \cos^2\xi \qquad -(4.8)$$

$$P_N(\mu_s) = \frac{m(\mu)^2}{2} \quad P_B + P_o \frac{\mu_s^2}{(B/2)^2} \qquad -(4.9)$$

where $D_{AM}(\mu_s/2\pi)$ is the amplitude modulated spectral density function at the modulation frequency and $m(\mu)^2$ represents the modulation index.

4.1.2.2 Detector Noise

Schottky barrier diodes or any other form of detector may be characterised by two numbers their noise figure (NF) and conversion loss (L). The noise figure is defined as

$$NF(dB) = 10\log F \qquad -(4.10)$$

where F is termed the noise factor and represents the ratio of the input signal to noise to the output signal to noise ratios. Both these figures are functions of microwave power, the conversion loss increases with power while the noise figure falls. They are also functions of the video or intermediate frequency chosen. In order to bias the diode for optimal noise factor a constant level of microwave power must be applied this is one of the functions of bucking arm power. The noise

figure varies with frequency due to contributions from 1/f noise dominating shot noise at low frequencies.

In order to obtain an overall noise figure for a cascade of networks the individual noise factors F_n and gains (1/L) G_n are combined as below

$$F = F_1 + \frac{F_2-1}{G_1} + \frac{F_3-1}{G_1G_2} + \qquad -(4.11)$$

The conversion gain of microwave detector diodes is less than unity. It follows from eq. 4.11 that the first stage of amplification will give the greatest contribution to system noise figure.

4.1.2.3 Dispersion Suppression

When observing absorption the addition of a dispersive component, for example through slight mistuning, results in both lineshape distortion and additional noise. From equation 4.5 it may be seen that presence of a dispersive component ($\xi = \pi/2$) results in an increased conversion of FM klystron noise into amplitude fluctuations.

The signal voltage present at the detector diode is the vector sum of the voltage reflected from the resonant cavity and that from the bucking arm. The latter is microwave power fed onto the diode to bias it into the region of maximum sensitivity on the characteristic curve.

In order to gain a clearer understanding of absorption and dispersion in terms of their affects on cavity impedance the component voltages may be plotted in a complex plane diagram as shown in Fig. 4.1. From eqn 4.1(a) and (b) and the equivalent circuit for the reflection spectrometer expressions for the reflected voltage (V_L) in terms of R and X may be obtained. The loci of varying R and X are plotted in Fig. 4.1(i). A matched

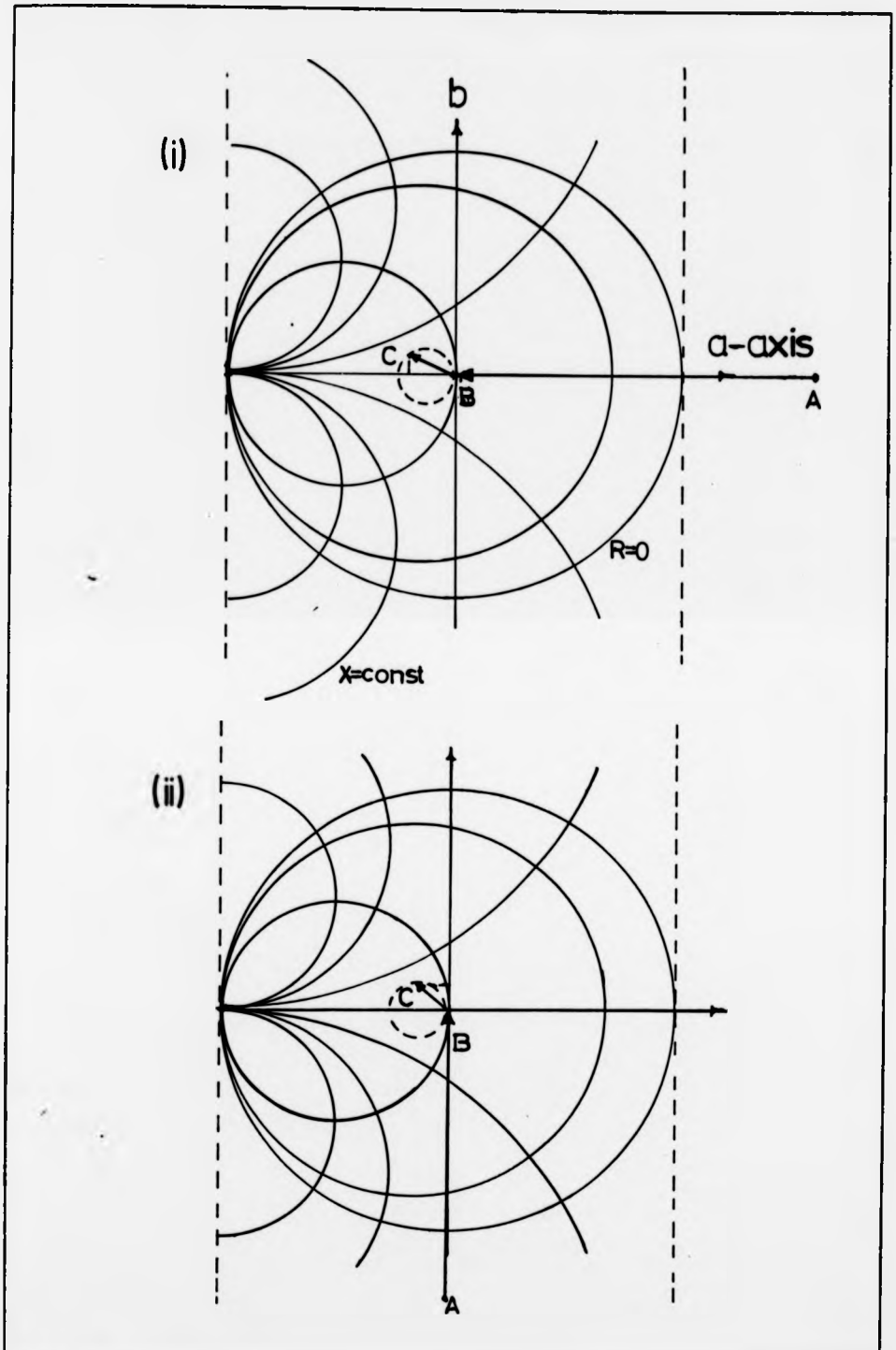

FIG. 4. 1. A COMPLEX PLANE DIAGRAM SHOWING THE VOLTAGE VECTORS PRESENT AT THE DETECTOR FOR A REFLECTION BRIDGE SPECTROMETER TUNED FOR (i) ABSORPTION, (ii) DISPERSION.

reflection cavity in a magnetic field distant from resonance results in zero reflected voltage equivalent to the origin position of Fig. 4.1(i). As field traverses resonance so vector V_L traces out a path around the small circle. The voltage at the detector will be the addition of V_L to the bucking arm vector AB. In Fig. 4.1(i) this vector is planned to lie along the a-axis or real axis only that components of V_L parallel to AB will cause a fluctuation in the detected signal. This represents purely resistive or absorptive mode. If a small degree of mistuning is introduced then a constant component of V_L would be present as shown by the vector AC. The diode voltage BC would respond to both resistive and reactive changes on passage through resonance resulting in mode mixing. Similarly by correctly phasing the bucking arm vector the dispersive mode may be isolated as shown in Fig. 4.1(ii).

Thus for the case of a single ended mixed reduction of mistuning and increasing the bucking arm voltage will result in dispersion suppression.

4.1.3 The 10 GHz-Band Spectrometer

Refer to Fig. 4.2 the microwave generator was an EMI-Varian klystron consisting of a cavity (25157) and plug in tube (R9696A) able to produce up to 100 mW of power. Up to 1200 mW could be made available by switching in a G.E.C. travelling wave tube amplifier. An isolator and attenuator were placed before the switch.

A 10 dB directional coupler was used to supply bucking, power this arm contained an attenuator and a phase shifter and fed the H-port of the balanced mixer. The cavity arm contained a 20 dB sidewall coupler for the frequency counter (Hewlett-Packard 5246L counter with 5257A transfer oscillator), and isolator, an attenuator and a 20 dB side wall coupler feed the power meter (Marconi 6460). Power was fed

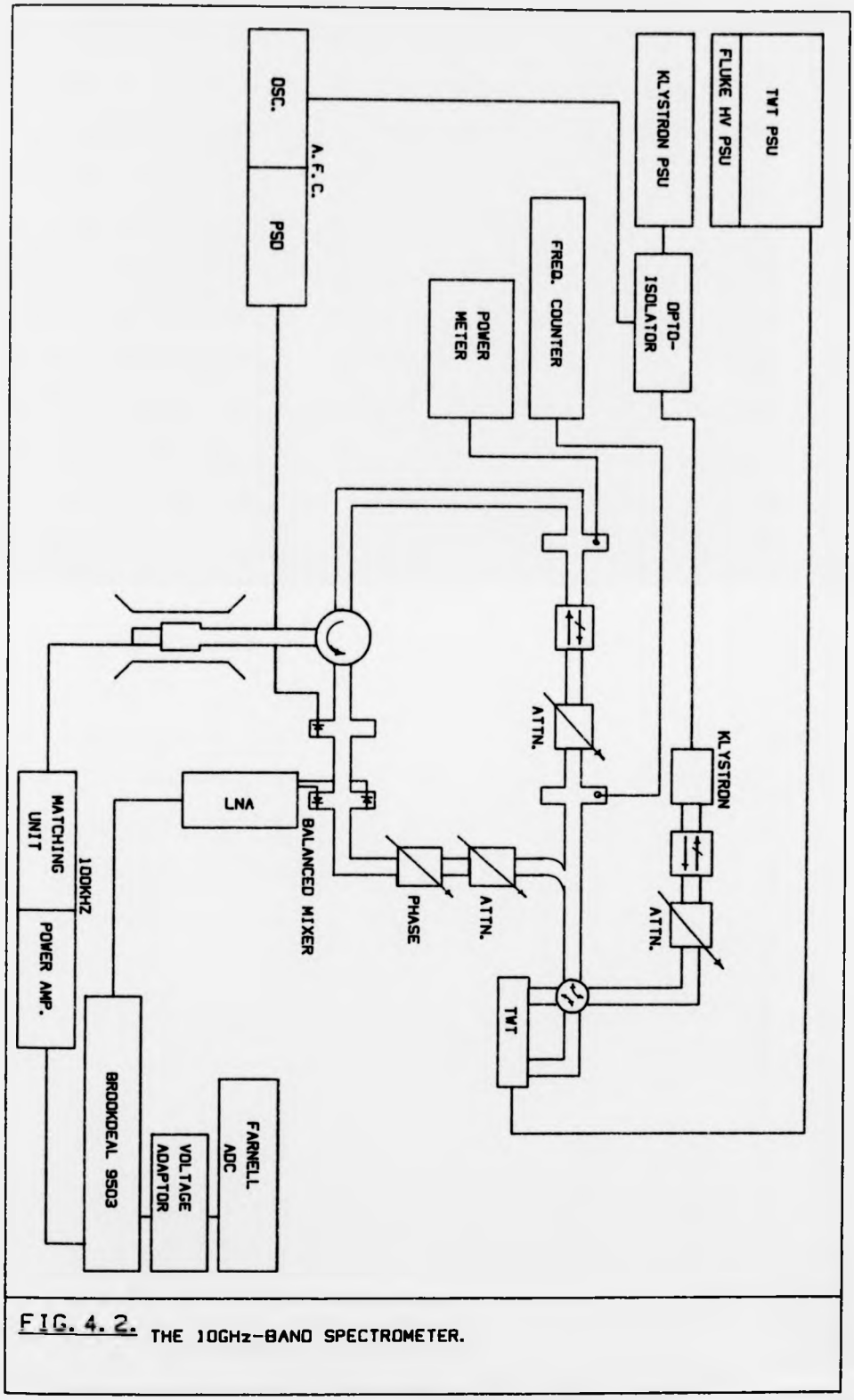

FIG. 4.2. THE 10GHz-BAND SPECTROMETER.

via port 3 of a Systron-Donner circulator to a Varian V-4531 TE_{102} rectangular cavity ($Q \simeq 3200$). Reflected power was taken from port 1 to a 20 dB side wall coupler to feed a diode for AFC. Finally, the power was fed into the E-port of the balanced mixer.

The balanced mixer contained a reversed match pair of silicon schottky barrier diodes, either AEI DC 1504F for normal operation or DC1590H for high power work. The manufacturers noise figures are 7.0 dB and 9.0 dB respectively and a conversion loss of 5.5 dB is quoted for the DC1504F. The noise figure measurements were made by detecting the single side band noise power at an intermediate frequency of 30 MHz and using an amplifier with a 1.5 dB noise figure. Directly attached to the balanced mixer was a low noise pre-amplifier. The amplifier had a noise figure of 2 dB at 100 kHz and a voltage gain of 55 designed around a plessey 5L561C interpreted circuit which gives optimum noise performance for impedance mismatch between the diodes and amplifier[6]. Two output were available one direct the other via a twin T notch filter at the AFC frequency, this output fed into an Ortec Brookdeal 9503C precision lock-in amplifier with 5012F oscillator and 5011F active filter in band pass mode options.

Automatic frequency control was achieved by modulating the klystron reflector at 6 kHz, the error signal was detected by the AFC diode forward of the balanced mixer and synchronously detected. The amplifier error signal was filtered and applied to the reflector using an opto-isolator amplifier[7].

4.1.4 The Balanced Mixer

In this section an attempt is made to clarify the advantages of the balanced mixer arrangement over a single ended mixer. The balanced mixer is a four part device. Microwave power entering port 3 is ports 1 and 2. Power entering port 4 is again split into two equal

components but they are divided in phase-quadrants between ports 1 and 2.

From Fig. 4.3 it follows that as the noise voltages are uncorrelated the powers add, while for the correlated signal voltages must be added. The effective noise figure is equivalent to that of a single mixer. However, it should be noted that it has to be assumed no power is lost within the hybrid. A similar assumption is in fact required in the single ended case as either a magic-T or a directional coupler are used.

The consequences of using a balanced mixer are summarised below.

1. The bucking power is divided in phase-quadranture and hence when the two currents from the microwave diodes are added the amplitude fluctuations are cancelled. The analysis of King[29] shows that at low powers more generally both amplitude and phase fluctuations on the bucking or reference would be eliminated.

2. As has been stated previously (Section 4.1.2.3) the contribution of amplitude to noise is 10 dB below that caused by FM noise, the latter being converted into amplitude fluctuation by the cavity. It was proposed by Wilmshurst[30] that the use of a balanced mixer resulted in suppression of the dispersion mode independent of bucking power. The suppression factor being given by

$$S = 2.\frac{\delta f}{(\Delta f)_u}$$

where δf is a measure of the FM noise and $(\Delta f)_u$ is the cavity bandwidth.

3. A consequence of the above is that the bucking arm power may now be set to optimise the diode noise figure without the constraint of suppressing dispersion as was the case in the single ended mixer where a compromise was required.

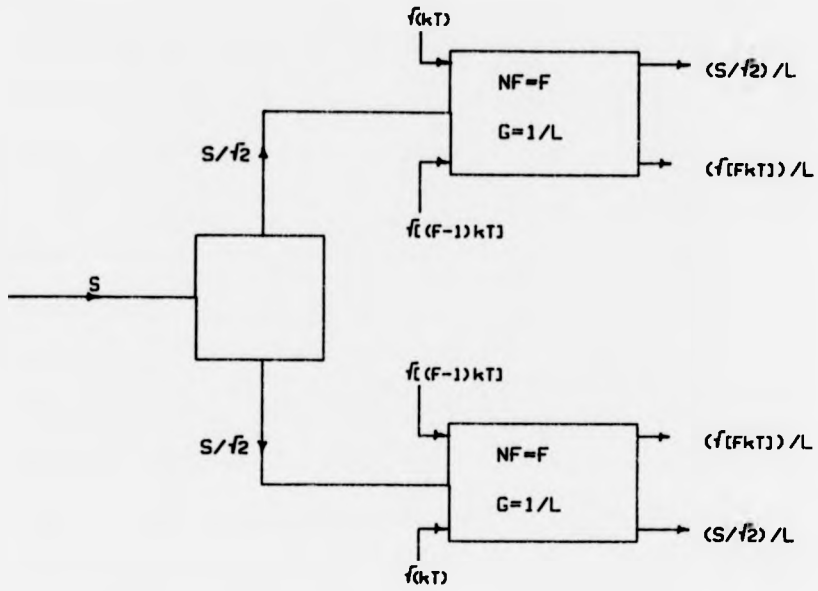

FIG. 4.3. THE BALANCED MIXER. A REPRESENTATION OF NOISE AND SIGNAL VOLTAGES PRESENT.

NO LNA		LNA NO. 1		LNA NO. 2	
SIGNAL	NOISE	SIGNAL	NOISE	SIGNAL	NOISE
830	7	1017	26	892	33
850	9	1059	22	932	40
840	8	1038	24	912	36.5
S/N=105		S/N=43		S/N=25	

TABLE 4.1. RESULTS OF THE 10GHz-BAND LOW NOISE AMPLIFER TEST.

4.1.5 Low Noise Microwave Pre-Amplifiers

Low noise amplification of the microwave power prior to detection may potentially improve the detection system noise figure. The importance of the first stage of amplification is illustrated by Eqn. 4.11. The use of several types of device are reported in the literature such as parametric amplifiers[8], microwave masers[8] and travelling wave tube amplifiers[11]. None of these devices have found common usage on modern EPR spectrometers. In recent years a rapid development in GaAs FET technology for 12 GHz communications satellites has occured consequently 10 GHz-band GaAs low noise microwave pre-amplifiers are becoming available at low cost. These devices have the potential advantage of good performance and single operation at low cost.

Two such amplifiers were obtained from JVL Electronics Limited, the quoted performance was a gain of 10 dB and noise figure of 2 dB with a centre frequency of 9.3 GHz. In order to test the performance the amplifier was placed just before the balanced mixer in the spectrometer described in Section 4.1.3 DC1504 diodes were used and the noise figure of the high gain 100 kHz low noise pre-amplifier was measured as 2 dB. Signal to noise ratio for the spectrometer system was determined by running spectra from standard spin-label solutions. The spectra were recorded digitally (see Section 4.3) and mean squared values for the signal and noise obtained.

If the diode noise figure and gain quoted in section 4.1.3 are used in eqn. 4.11 then the system noise figure would be expected to improve from 8.5 dB to 3.4 dB on insertion of the microwave pre-amplifier. The results obtained are summarised in Table 4.1. These are clearly not in agreement with the calculated figures. The possibility of facility components can not be discounted as no test facilities were available.

4.1.6 The Loop-Gap Resonator

The conventional resonant structure used for EPR is the resonant cavity, other devices such as travelling wave tube helices[10] and strip-line resonators[12] have found specialised application but are inferior to the cavity for most work. Recently a novel type of structure, termed a loop-gap resonator was tested by Froncisz and Hyde[13]. It is a cylindrical slotted device, the loop forming an inductive element and the slot a capacitance. Resonators have been constructed operating at 3 GHz and 9 GHz and show significant improvements in signal to noise ratios over a conventional rectangular TE_{102} cavity. This improvement is due to the structure's low Q but high filling factor. The consequence of the high filling factor is to produce a magnetic field strength at the sample up to a factor 8 larger for the same incident microwave power. The effects of this are two fold. Firstly, it allows a conventional klystron source to achieve for higher field strengths for saturation studies, also when operating at normal field intensities the contribution of klystron noise to he system noise is reduced as equations 4.6 and 4.8 show. Advantage is also gained from the lower Q-factor for this further reduces the sensitivity to generator noise as the two equations show ($Q_0 = \Omega_0/B$).

The resulting 10 GHz-band device is of small size (typically 10 mm long) and has an external diameter of 6 mm. It may be constructed from machinable glass ceramic with a silver layer of several microwave skin depths added to its internal surface. The device must then be placed in a conducting radiation shield. It was considered that this would form an ideal ENDOR structure as the radiation shield could be replaced with a small radio frequency coil.

As a result of the advantage outlined above an attempt to construct such a device was made. Two methods were used: that of Froncisz and Hyde and a modified version of a method developed by

Bowman[14]. The attempts were unsuccessful and a more detailed account may be found in Appendix B.

4.1.7 Spectrometer System Noise Measurements

In order to gain a better understanding of the relative importance of the contributing factors affecting the noise performance of the spectrometer described in Section 4.1.3 a series of measurements were performed. The aims were to determine a noise figure for the balanced mixer, to look at the variation of noise power as a function of incident power and to observe the variation of signal to noise as a function of cavity coupling - Feher claimed that an improvement in signal to noise could be gained by slight overcoupling[2].

In order to obtain a noise figure for the balanced mixer a noise generator diode WB2703 from the Microwave Ltd. was used, an excess noise ratio of 11 dB at 9.5 GHz was produced for a current of 14 mA. The output port of the diode waveguide was attached to the balanced mixer of the spectrometer system shown in Fig. 4.2 in place of the cavity arm. A matched load was placed on the other port of the diode waveguide. In order to determine the noise the signal from he mixer was monitored at the lock-in amplifier forward of the demodulator but after the AC gain step. The monitors used were an oscilloscope, a Tektronix 7603 frame with 0-5 MHz spectrum analyser plug-in and a Hewlett Packard 312B selection voltmeter centred at 100 kHz with a 3.1 KHz bandwidth. On switching the diode on an off no change in the output noise level could be discerned by any of the monitors. No method to check the operation of the noise diode was available. Assuming correct operation the minimum noise figure consistent with this result, allowing for a minimum detectable change of output of 10%, is 6.5 dB.

To determine the spectrometer system noise level about 100 KHz, the spectrometer of Figure 4.2 was tuned for normal operation, however,

the output was monitored as above using the latter two frequency discriminating monitors. In both cases, however, despite using the highest available gain setting the noise level could not be brought above the noise floor of the measuring device. Hence to obtain a measure of noise a series of EPR spectra were recorded and the noise level obtained by the method detailed in Section 4.1.5. The results of measuring noise voltage as a function of incident microwave power are shown in Figure 4.4. The variation in noise as a function of power is seen to be random no trend for the noise power to increase with microwave power could be discerned.

In order to study the effect of coupling on noise a convenient method of determining the coupling parameter β must be found. The coupling parameter may be related to the reflection coefficient by the formula below.

$$\Gamma = \frac{1 - \beta}{1 + \beta} \qquad -(4.11)$$

The function is plotted in Figure 4.5. The voltage present at the mixer diodes is given by the incident microwave voltage multiplied by the reflection coefficient. The bucking power level was adjusted to 1 mW hence from Figure 4.6 it may be seen that the diodes were operating in the linear region of their characteristic where output current is proportional to field. If a low frequency saw tooth waveform is now applied to the klystron reflector the well known klystron mode display is obtained. If the klystron and cavity are on time a cavity mode dip will be visible. The reflection coefficient may be determined from the ratio of the depth of the cavity dip to the overall height of the mode display. The sign of the coefficient may be determined from the direction in which the cavity dip moves for increased coupling, if the dip moves towards the base line the cavity is overcoupled if it moves

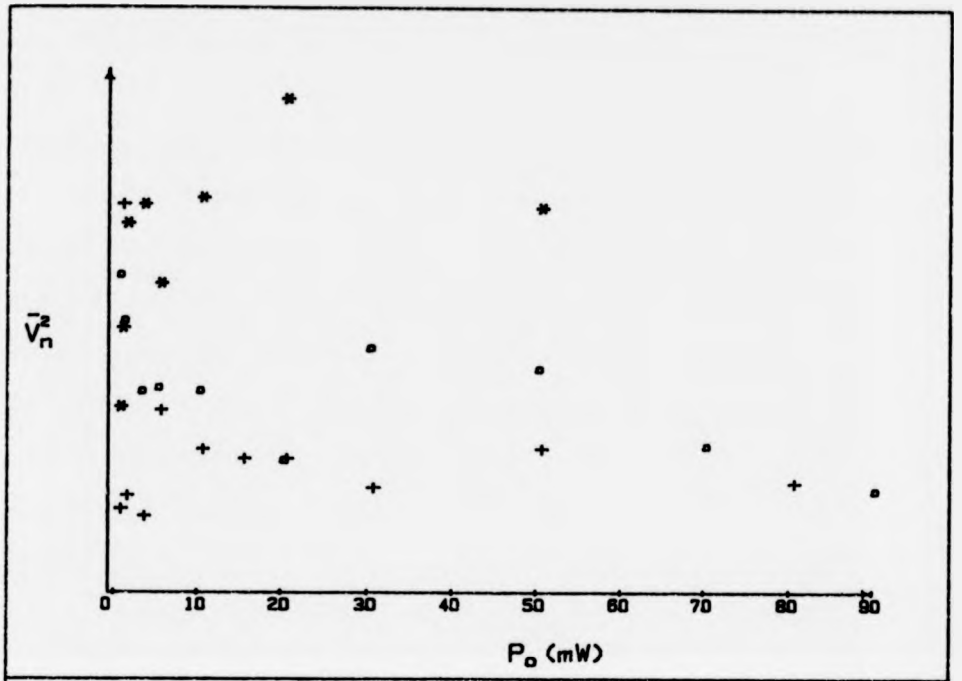

FIG. 4.4 A GRAPH OF NOISE POWER AGAINST INCIDENT CAVITY POWER.

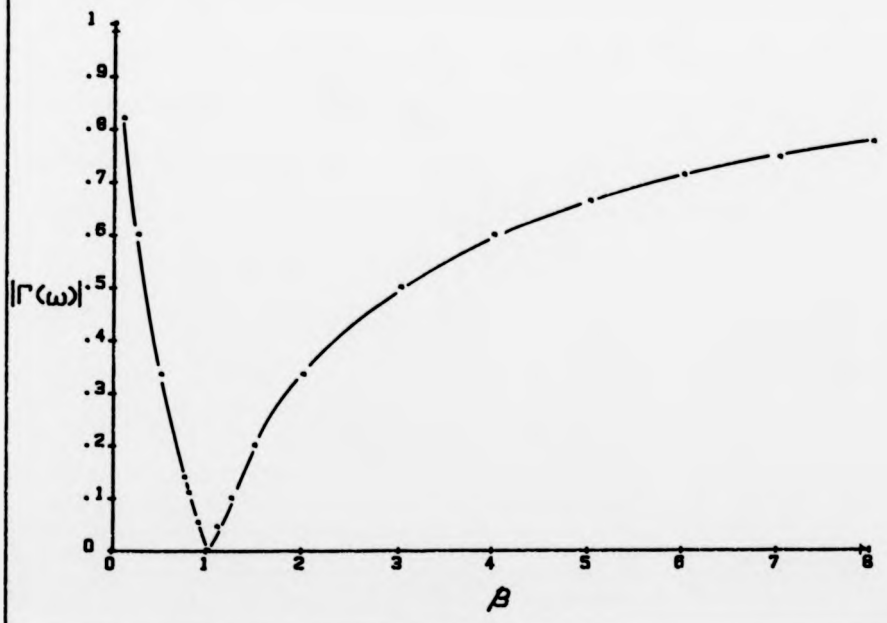

FIG. 4.5 A GRAPH OF THE MODULUS OF THE REFLECTION COEFFICIENT AGAINST THE COUPLING COEFFICIENT.

away it is overcoupled. Again, in order to determine the signal to noise ratio as a function of coupling, the methods detailed in section 4.1.5 was used. The results of the signal to noise measurements are presented in Figure 4.7 and those for noise power against coupling in Figure 4.8. From Figure 4.7 the signal to noise peaks strongly around critical coupling Figure 4.8 shows a weak trend to lower noise for overcoupling this is masked by the stronger functional dependence of the signal. A phase change of π occurs on passing through critical coupling hence it is necessary to adjust slightly away from this point, however, the results presented here indicate the choice of side is not critical.

4.1.8 The 35GHz-Band Spectrometer

A diagram of the spectrometer may be found in Figure 4.9. An EMI-Varian 5146A klystron with a tuning range from 33.8 GHz to 35 GHz was used powered by a Phillips klystron power supply in conjunction with a Fluke 2kV high voltage supply. The power is fed via an isolator a 3dB directional coupler which extracted bucking arm power. This was fed through a phase shifter and an attenuator before entering a magic-T to supply the diode. The diode was an AAY34 schottky barrier type held in a GEC diode holder. A mica isolated junction was used onto the magic T. The cavity power was fed via an attenuator, a wavemeter and a 22dB side wall coupler (to fed power meter head) to port 3 of an MESL 3 port circulator. The cavity was constructed in the departmental workshops from non-magnetic brass it resonated in the TE_{011} mode at 34.34 GHz (D=L=11.43 mm). Coupling was via a 2 mm hole at $\lambda/2$ along one side wall. The coupling plunger was a brass tipped PTFE rod. Two holes 1 mm in diameter were bored in the centre of the two end plates, one to allow the passage of humidified air into the cavity, the other for sample mounting. Port 1 of the circulator fed

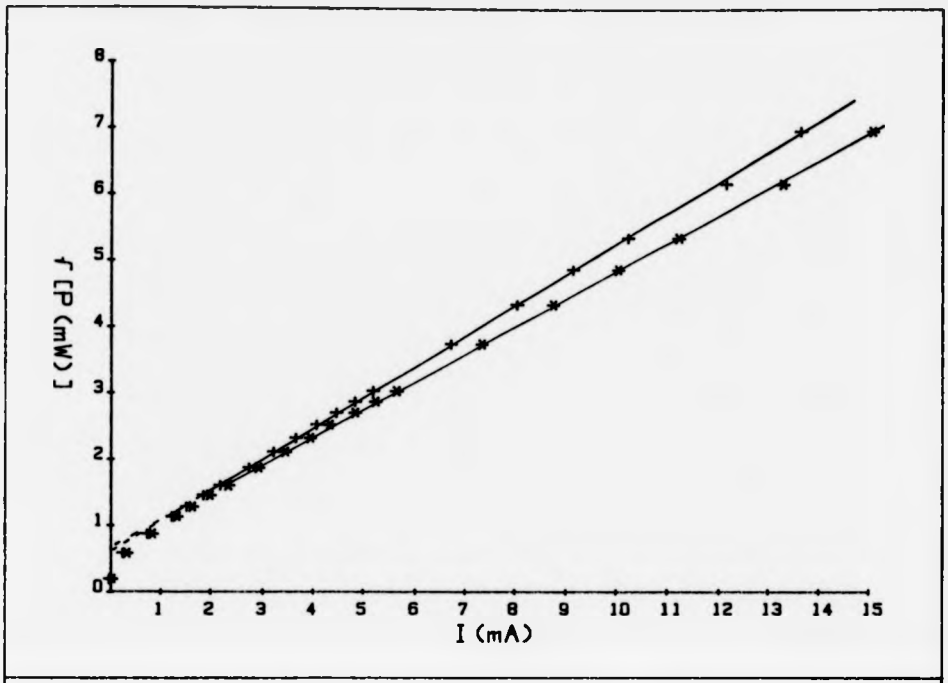

FIG. 4.6. A GRAPH OF THE LINEAR REGION OF THE DIODE CHARACTERISTIC FOR OC1504 (+) AND OC1590 (*) DIODES.

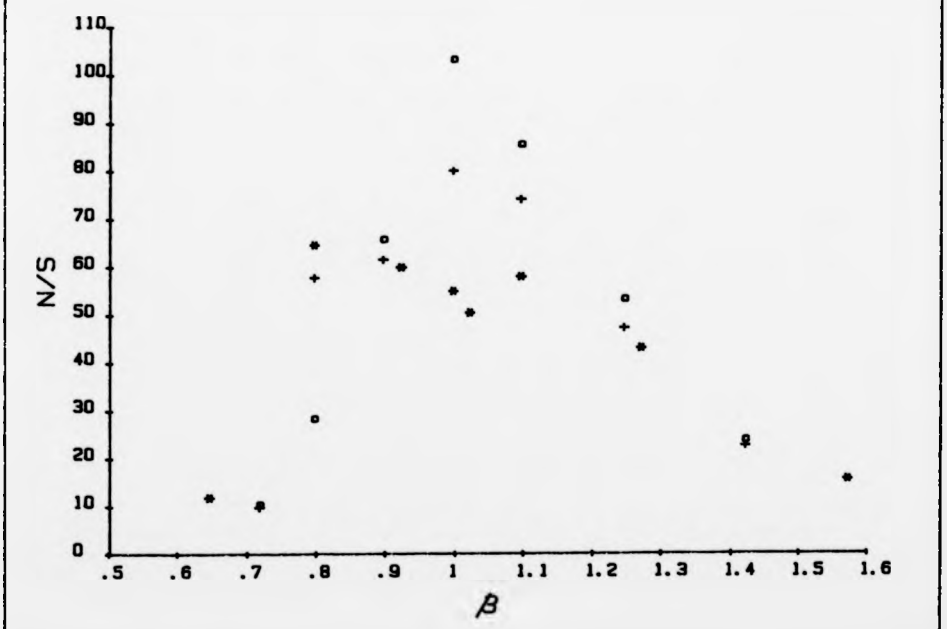

FIG. 4.7. A GRAPH OF SIGNAL TO NOISE AGAINST COUPLING COEFFICIENT.

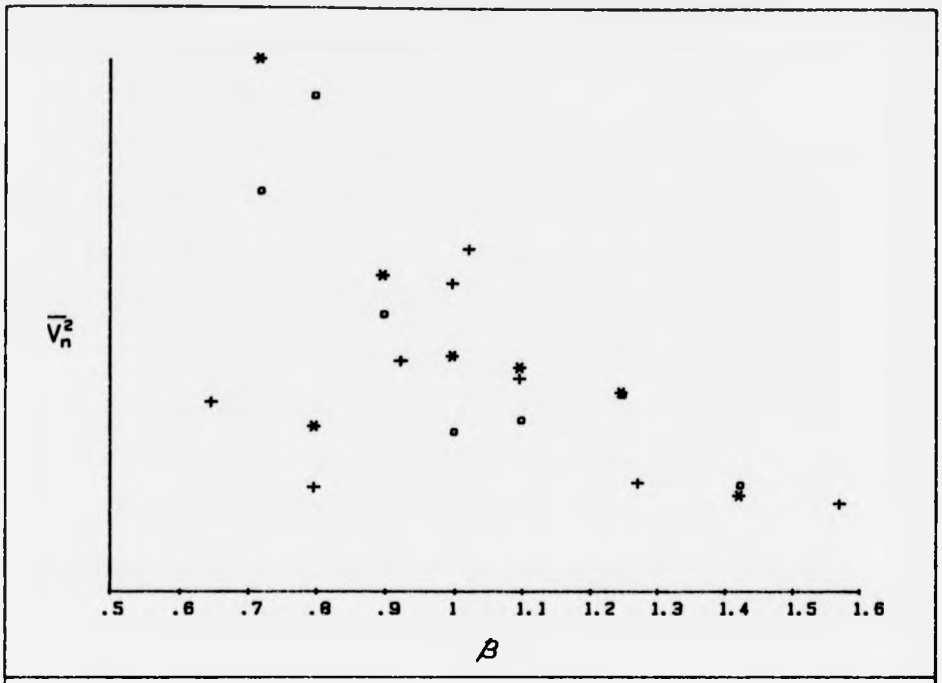

FIG. 4.8. A GRAPH OF NOISE POWER AGAINST COUPLING COEFFICIENT.

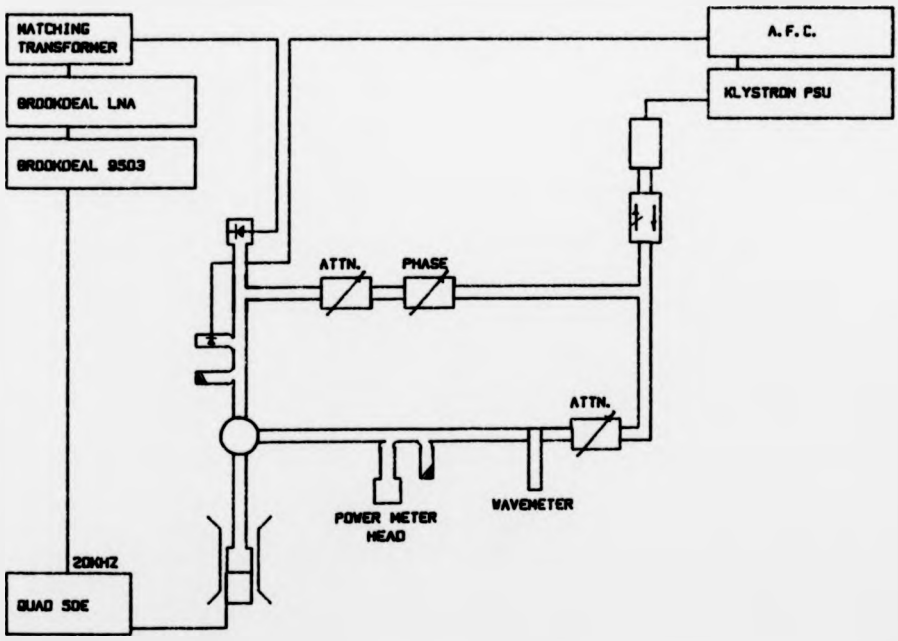

FIG. 4.9. THE 35GHz-BAND SPECTROMETER

the reflected power via a 22 dB sidearm coupled for the AFC diode to the magic-T to supply the detector diode.

The signal was fed via a matching transformer to a Brockdeal LA350 low noise amplifier and then to the Brockdeal 9503C lock-in amplifier. The output of the 5012F oscillator option was fed via a Quad 50E audio power amplifier to a pair of Varian modulation coils mounted to the cavity block. A modulation frequency of 20 kHz was used as this still allowed a field of 0.1 mT to penetrate the cavity. The output of the AFC diode was fed via the 10 GHz-band low noise amplifier to the 10 GHz-band AFC unit a similar opto-isolator amplifier took the error signal onto the reflector of the 35 GHz klystron power supply.

4.1.9 Summary

The results of the measurement of noise as a function of microwave power suggests that klystron noise does not dominate detector noise in this system. This implies that the detector diodes and low noise microwave pre-amplifier have noise figures and gains very different from those quoted by the manufacturers. The noise measurements carried out could be improved if a more precise method for measuring system noise around 100 kHz was used.

Before improvements to the present 10 GHz-band spectrometer can be made the uncertainties produced by the noise measurements must be removed. If the noise and gain figures for the detector diodes and low noise microwave per amplifier are assumed to correspond to those given by the manufactuers than the addition of the amplifier should result in a three fold decrease in system noise figure. From the discussion in Section 4.1.6 it follows the introduction of a loop-gap resonator would result in a decreased conversion of converted FM noise.

PART II

4.2.1 Introduction

This section is devoted to an account of the necessary modifications to a conventional EPR spectrometer, and to the experimental procedure necessary, for performing slow motion sensitive saturation studies. The theoretical background to saturation transfer EPR was given in Chapter 2, part II. The method used to study saturation transfer in this study was second harmonic detection of the out of phase magnetisation in the presence of a saturating microwave field. A justification of this method is given below.

The literature, up to the present, contains five methods of observing motionally induced saturation transfer: (1) progressive saturation[15] which involves the observation of conventional absorption spectra as a function of microwave power (2) the EPR dispersion signal using high frequency field modulation detecting the 1st harmonic response with the reference phase set at 90^{0} out of phase[16]. (3) the EPR absorption spectrum using high frequency field modulation recording the 2nd harmonic response with the reference power set at 90^{0} out of phase[15]. (4) electron-electron double resonance (ELDOR)[17], this allows a portion of the spectrum to be saturated and the transfer of this saturation to be monitored by a second microwave source at another part (5) two-dimensional electron spin echo spectroscopy[18] where a two pulse electron spin echo sequence is used to determine the variation in natural linewidth (T_2) across a spectrum. This variation is related to rotational reorientation.

The first method is unsatisfactory as it is sensitive only over the 10^{-4}s to 10^{-5}s motion range. The dispersion method shows a greater range of sensitivity, also the spectral shapes are found to be unaffected by variations in experimental parameters (microwave field

intensity H_1, modulation amplitude H_M, T_1). The shape is found to be determined by the $\tau_R\omega_m$ product. However, dispersion mode detection on a reflection cavity bridge spectrometer is more sensitive to noise as outlined in section 4.1.2.3. The second harmonic absorption display has a wide range of motional sensitivity, however, the spectral shapes are not uniquely determined by the $\tau_R\omega_m$ product and show greater sensitivity to experimental parameters. The last two methods offer a more direct way of monitoring saturation transfer but the complex experimental arrangements required make them impractical.

The method used in this study was the second harmonic absorption spectrum recorded with phase-quadranture reference. The 10 GHz-band spectrometer described in Section 4.1.3 was modified by the addition of 50 kHz and 25 kHz field modulation frequencies. The Brockdeal lock-in amplifier allowed the second harmonic of the reference to be detected and hence this form of display was easily obtainable. The method also has the advantage of an extensive literature base to aid interpretation. The experimental procedure and precautions along with reference spectra have been published by Thomas[15].

4.2.2 Microwave Field Strength Measurement

Several methods for microwave field strength measurement have been developed. Thomas[16] used the method of perturbing spheres which the cavity Q-factor is measured with and without a metal sphere at the sample position. The method is difficult to perform and suffers from large errors. A more satisfactory method was proposed by Beth[19] involving the saturation characteristics of perosylamine disulflorate (PADS). Vistnes and Dalton[20] used single crystals of N-methylphenazinium tetracyanoquinodimethan (NMP-TCNQ) which have the advantage of a linear variation of linewidth with field above 0.01 mT.

It was the latter method used in this study crystals of NMP-TCNQ

were supplied by Dr. A.I. Vistnes. The crystals were of small size and were mounted at the sample position at the end of 2 mm diameter quartz rod. Care was taken to orientate the long axis parallel H_1 for minimum perturbation of the field. The results of the linewidth against incident microwave power are shown in Figure 4.10 and the H_1 calibration in Figure 4.11.

It should be noted that caution should be exercised in the interpretation of saturation spectra of fibres as a function of angle due to the possible variation of cavity dielectric properties with sample position. DNA possesses an induced anisotropic dipole moment parallel to the helix axis giving rise to a dielectric susceptibility and also the degree to which the sample will perturb the cavity electric field will change with angle. Dielectric susceptibility is a complex quantity, the real part causes a shift in cavity resonant frequency as well as a concentration of magnetic and electric fields while the imaginary component models absorption or changes in cavity Q. These effects may cause variations in the magnetic field strength within the sample. The concentrating effect is termed the lens effect a useful qualitative and quantitative discussion is given by Dalal, Eaton and Eaton[21].

4.2.3 Magnetic Field Modulation

A range of field modulation frequencies is preferable for saturation transfer experiments hence the present 100 kHz modulation unit was modified to also give 50 kHz and 25 kHz with field amplitudes up to 1.5 mT peak to peak.

The source of modulation was the 1 Hz to 110 kHz Brookdeal 5012F oscillator. The output was fed to a field strength control unit where the amplitude could be set by two range potential

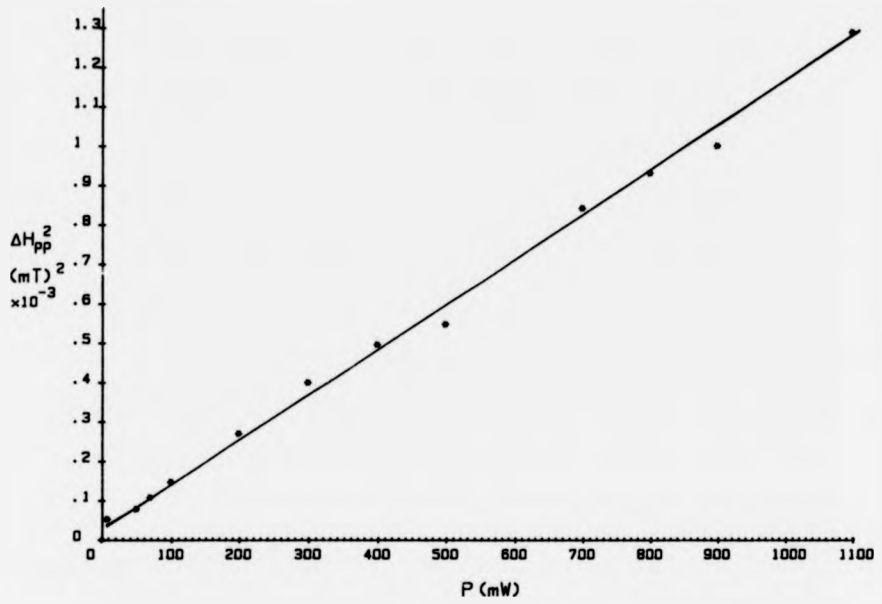

FIG. 4.10. A GRAPH OF THE PEAK TO PEAK LINEWIDTH SQUARED AGANIST MICROWAVE POWER FOR A CRYSTAL OF NMP-TCNQ.

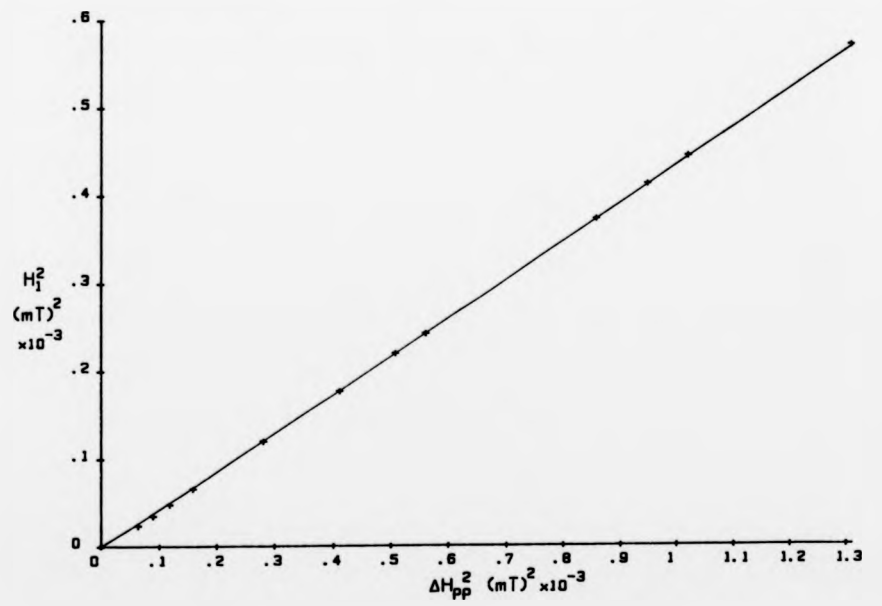

FIG. 4.11. A GRAPH OF MICROWAVE FIELD STRENGTH SQUARED AGANIST PEAK TO PEAK LINEWIDTH SQUARED FOR NMP-TCNQ.

divider (0.02 mT and 0.2 mT). This was amplified (AIM power amplifier) and fed to the cavity coil matching unit. Here the power amplifier output was impedance matched to the cavity coils by a transformer. A zobel network was added to the primary. The cavity coil circuit was a series resonant circuit to obtain the required voltage and to ensure spectral purity. The required frequencies were obtained by switching extra series capacitance in place and returning the Brookdeal oscillator. A second transformer was present to allow the current to be monitored via a bridge rectifier the output was taken to a calibrated meter in the field strength control unit.

4.2.4 Experimental Method

The field modulation was set at 50 kHz at am amplitude of 0.5(mT) peak to peak. The microwave incident power was adjusted to 1 mW to avoid saturation and hence to obtain zero signal with the reference phase at phase-quadranture. The lock-in amplifier gain was increased by an order of magnitude from that required to observe the EPR signal, first harmonic detection was used. The sweep was set to cover the largest spectral feature this was monitored using the VDU unit of the controlling microcomputer. The reference phase was adjusted in 10^{0} steps until a minimum was found the gain was then further increased and steps of 1^{0} phase used. This procedure defined the phase-quadranture position the lock-in was then switched to 2nd harmonic detection and the microwave power adjusted to 80 mW (0.025 mT, H_1).

4.2.5 Summary

The experimental procedure could be significantly simplified if a digital phase sensitive detector similar to that described by Vistnes et al[22] was introduced. This allows two components 90^{0} apart to be recorded simultaneously, the components at intermediate phases may then

be constructed. Theoretically both first and second harmonic responses could also be recorded simultaneously, however, at present this results in reduction in the signal to noise ratio.

Ideally the results of second harmonic absorption measurements should be combined with first harmonic dispersion data, however, as has been mentioned high sensitivity dispersion mode measurements are difficult. This could be improved with the introduction of a loop-gap resonator an added advantage to both displays would also be the high microwave field intensity.

PART III

4.3.1 Introduction

The advantages of obtaining EPR spectra in digital form has been recognised for several years, and consequently a number of papers on the acquisition of digital spectra exist. The ability to perform easily and accurately functions such as integration, differentiation, difference and resolution enhancement through multi-scan averaging or digital processing are some of the advantages. The development of spectral simulation as a major tool in EPR has also produced a need for digital spectra. The computations involved are often large and complex hence mainframe facilities are often required.

As stated above the data processing of EPR spectra often require the facilities of a mainframe, however, the total or partial dedication of such machines to real time control is rarely possible. The advent of microprocessors has allowed the control and data acquisition of spectrometers to be carried out separately and the resultant digital spectrum to be transferred to a mainframe. Early papers in this field used microprocessor development systems[23,24]. More recently authors[25,26,27] have utilised one of the rapidly developing, relatively

powerful, commercial microcomputers now available at low cost. The approach adopted in these designs has been to construct hardware, machine specific, interface unit containing the required analogue to digital converter (ADC), digital to analogue converter (DAC), voltage adaption circuitry and input output ports (IO ports). In this work a system was designed around commercially available interface instrumentation utilising the standard IEEE-488 general purpose interface bus (GPIB) for data and control information transfer. The advantages of such an approach are that the resultant control system is not machine specific, any computer with a GPIB facility may act as the controller. The system designed in this manner is simple in construction.

An EPR spectrum is a set of voltage-field data pairs, which ideally both should be obtained simultaneously, but many systems imply the field value from a calibrated linear sweep. This may be achieved using a Hall effect based system or a linear sweep generator calibrated with an NMR magnetometer. Such arrangements are susceptible to calibration errors due to long term drift. In this study two forms of magnetic field control were used both affording the precision of the NMR method for each data point.

4.3.2 Model of Magnet and Power Supply

In order to design a stable control system for the magnetic field a transfer function for each element if the system is required. A linear analysis in the Laplace Domain will be constructed. The electromagnet consists of two coils in series. Each is formed from many parallel winding so the resistance of the coils is considered negligible compared to their inductance (refer to Fig 4.13). The transfer function of the electromagnet and power supply reduces to that of an inductor as the field produced is proportional to current flowing

I(t). The voltage across the coils is given by V(t).

$$I(t) = 1/L \int_0^t V(t)dt' = K/L \int_0^t V_o(t)dt'$$

Where V_o is the integrator output and K the voltage per unit current given by the power supply. In the Laplace domain, this becomes

$$I(s) = K/sL\ V_o(s)$$

The transfer function for the electromagnet and power supply P(s) is given by

$$P(s) = I(s)/V_o(s) = K_p/s$$

where $K_p = K/L$ is a system constant.

4.3.3 Bruker Field Control System

In order to obtain a field control system with NMR precision the Bruker B-NM20 NMR magnetometer and BR-R20 field regulation units were used refer to Figure 4.12. The combined units were designed to regulate static field to high stability, this mode would be of use for future ENDOR work, however, in this study they were used to produce a computer controlled field sweep. The majority of results presented were obtained with this system.

The NMR magnetometer consisted of a voltage controlled oscillator able to lock into the resonance condition, the oscillator frequency is counted and the converted field information displayed and made available in binary coded decimal (BCD) format at two parallel output ports. The frequency counter gate time was adjustable between 0.1 mS and 10 s.

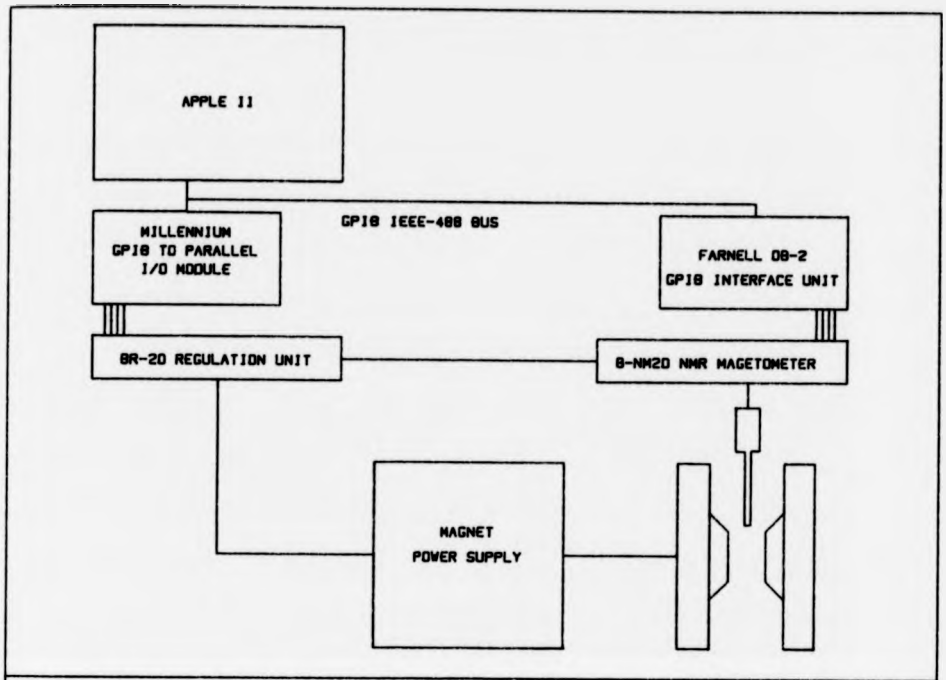

FIG. 4.12. A DIAGRAM OF THE BRUKER BASED FIELD CONTROL SYSTEM

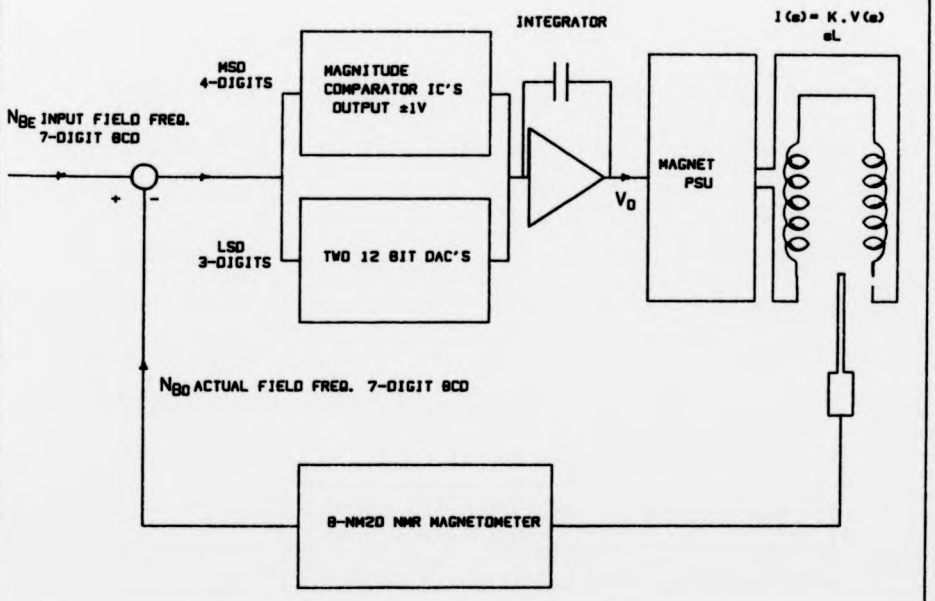

FIG. 4.13. A CONTROL LOOP DIAGRAM FOR THE BRUKER SYSTEM

The field regulation unit received current field information from one of the magnetometer output ports. This was compared to the set value and the error voltage developed fed to the Bruker BN120/125 magnet power supply. A diagram of the control loop is given in Fig. 4.13. Within the regulation unit the seven digit BCD input is divided into 4-digit and 3-digit segments. The set value is divided similarly. The two most significant 4-digit segments from the inputs to four 7485 magnitude computer integrated circuits (IC's). If a difference is present one of the two relays switched approximately 1 volt onto the appropriate input of a differential integrator, dependent on the sign of the difference. This result in the magnet power supply being driven at a maximal rate in the desired direction. If the difference is zero the both relays open and the differential input is driven from two 12 bit DAC's into which the least significant digits are fed achieving fine control. The unit was designed to operate with a magnetometer gate time of 1s, the integrator acts to smooth the output voltage due to these discrete 1s steps itself having a 5s time constant. This is a sampled system consequently it has a settling time much greater than the gate time this period was reduced by cutting the gate time and integrator time constant by an order of magnitude.

The maximum sweep rate used to record an EPR spectrum is dependent upon the narrowest linewidth present and the required lock-in amplifier time constant. The time taken to sweep through the narrowest line is required to be an order of magnitude greater than the time constant if sweep direction dependent field position shift is to be avoided. This imposes a severe limitation on the sweep rate, values in the range 0.01 mTs^{-1} and 0.05 mTs^{-1} were found to be common. However, these rates are greater than with the Bruker system in lock, use of such rates results in a steady state error between the set point field and the acted field. The problem was resolved by obtaining the field

value for the data pair direct from the magnetometer rather than the set point.

The system was operated both at 10 GHz-band fields 0.340 T and at 35 GHz-band fields 1.25 T, however, to obtain consistent locking of the B-NM20 magnetometer it was found necessary to increase the value of field modulation to the probe head to counteract inhomogenous broadening from the Bruker BE20 magnet.

4.3.4 Pulsed NMR Field Locking Magnetometer

To enable precision fast response magnetic field locking over a wide range of field strengths the pulsed NMR field locking magnetometer was designed in this laboratory. The instruments allows field locking from 0.12 T to 1.64 T (5 to 70 MHz). It is dependent for its operation on the phase change that occurs on passing through the central crossing point of the dispersion signal. A diagram of the system is given in Fig. 4.14.

The required field frequency is obtained from a digitally programmable phase-locked loop frequency synthesiser covering 5 to 70 MHz in 100 Hz increments. The output is gated and drives a power amplifier. The radiofrequency pulses are passed via a hybrid to a wideband probe. The free induction decay is separated by the hybrid, amplified and passed to the signal port of a balanced mixer. The local oscillator port receives power directly from the frequency synthesiser. The resulting free induction decay, which may be observed on an oscilloscope, is integrated and applied to the magnet power supply, see Fig. 4.15. Initially the frequency may be adjusted for resonance, at this point no output from the balanced mixer is obtained, any small shifts away from resonance result in a polarity dependent DC output. The magnetometer is in lock and will remain so as long as the field steps are not so great as to take the free induction decay away from

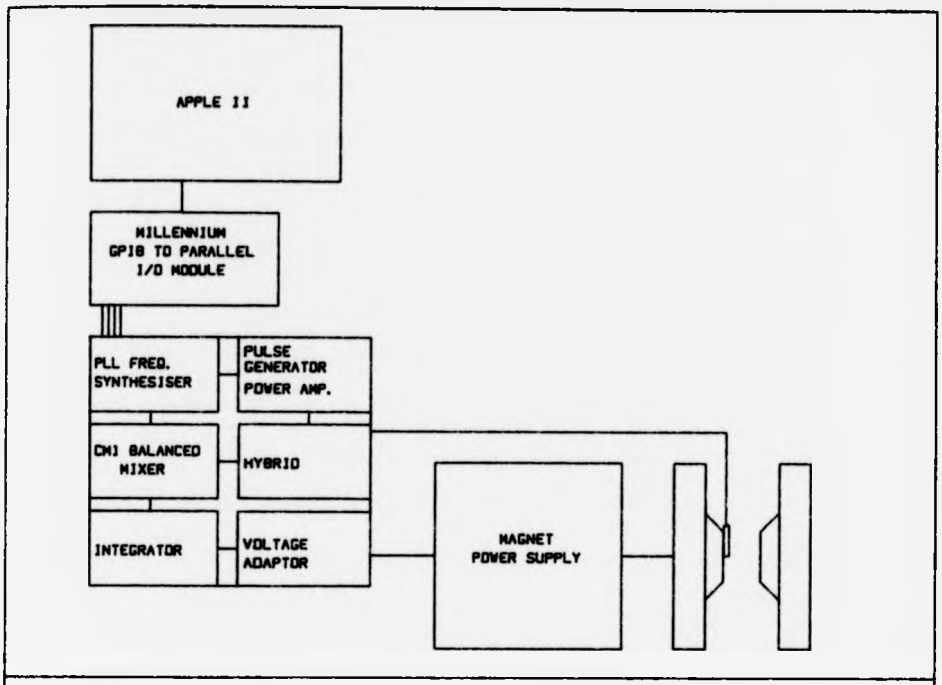

FIG. 4.14. A DIAGRAM OF THE PULSED NMR FIELD CONTROL SYSTEM

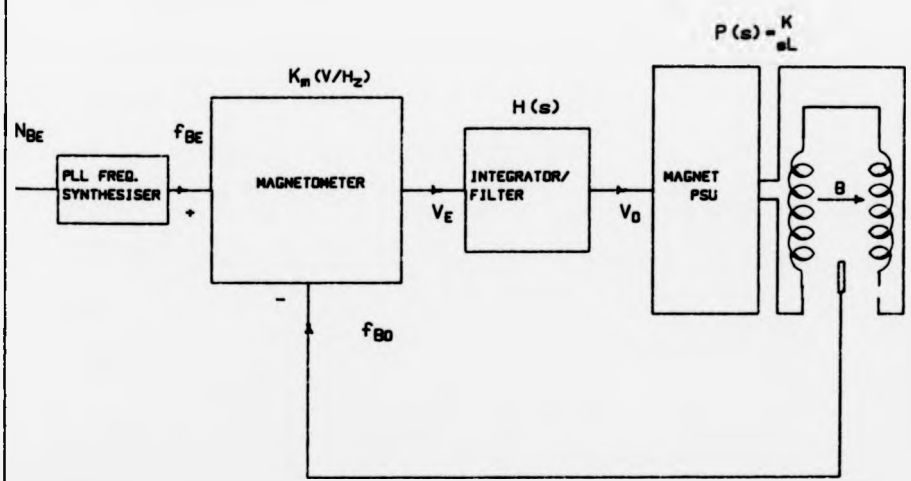

FIG. 4.15. A CONTROL LOOP DIAGRAM FOR THE PULSED NMR SYSTEM

the centre region.

The design of the wideband probe was based on the delay time probe of Lowe and Whitson[28] to allow power transfer over the required frequency band. To achieve this the impedance of the probe was made approximately 50Ω over the range. A series of probes were constructed with the aim of reducing the overall probe width while retaining a constant impedance and signal strength. The sample used was a gelatine-ferrous sulphate gel which allowed a good filling factor to be achieved. The probe was enclosed in a screening mesh backed by two thin copper side plates to reduce interference and radiation. The side plates also allowed the impedance to be varied by altering the distributed capacitance. The probe dimensions (50 x 40 x 5 mm) allowed mounting between the cavity and pole face. Thin (2.5 mm) non magnetic coaxial cable was used to attach the probe as this is a matched system the length used is not critical.

The magnetometer control system may be modelled as shown in Fig. 4.15 suitable choice of a function H(s) should lead to optimum loop characteristics. The model for the magnet and power supply has been detailed in section 4.3.2. The magnetometer may be represented by a transfer constant K_m (Volts Hz^{-1}), the error signal applied to the power supply is a function of the frequency, equivalently field, deviation.

$$V_E = K_m [F_{BE} - (\tau B/2\pi)]$$

The observed field frequency is related by the resonance condition $2\pi f = \tau B$ to the field Note also

$$V_o = H(s)V_E$$

and

$$B(s) = (K_p/s).V_o$$

An expression is required for the loop transfer function, the input set point F_{BE} or F(s) in terms of the resultant magnetic field B(s).

$$V_E = (s/H(s)).(B(s)/K_p)$$

Hence

$$\frac{sB(s)}{H(s)K_p} = \frac{-K_m\gamma B(s)}{2\pi} + K_m F(s)$$

$$\frac{B(s)}{F(s)} = \frac{2\pi K_p K_m H(s)}{2\pi s+\gamma K_p K_m H(s)}$$

The D.C. loop gain is given by $\gamma/2\pi\ K_p K_m$ hence the above expression may be rearranged in the form of a dimensionless transfer function given below.

$$\frac{(\gamma B(s)/2\pi)}{F(s)} = \frac{G_L H(s)}{G_L H(s)+s}$$

A suitable form for the filter transfer function must now be substituted in order to have a stable low pass response. The following was tried.

$$H(s) = \frac{-1+s\ \tau_2}{s\tau_1} \qquad \tau_2 = R_2C \qquad \tau_1 = R_1C$$

This represents an integrator with a phase lead. R_2, in effect, determining loop damping. On substitution into the transfer function the following expression is obtained.

$$\frac{\tau B(s)/2\pi}{F(s)} = \frac{(G_L\tau_2/\tau_1) + G_L 1/\tau_1}{s^2 + s(G_L\tau_2/\tau_1) + G_L 1/\tau_1}$$

Consider the form of a standard second order transfer function with damping factor η and loop natural frequency ω_n.

$$G(s) = \frac{2\eta\omega_n s + \omega_n^2}{s^2 + 2\eta\omega_n s + \omega_n^2}$$

Hence, equating terms, an expression for the loop frequency ω_n and damping factor η maybe obtained.

$$\omega_n = (G_L/\tau_1)^{1/2}$$

$$\eta = (\tau_2\omega_n/2)$$

The values of the two resistors and capacitors were chosen assuming critical damping ($\eta = 0.707$) and a settling time ($4/\omega_n$) secs. The values were tuned from these starting values to give reliable locking over the decade frequency range (d.c. gain varies with frequency).

4.3.5 Computer Control and Data Acquisition System

The computer control and data acquisition system was designed around the GIPB. This is a parallel bus transmitting eight-bit bytes of data, the bus is comprised of sixteen lines, the eight data lines and eight control lines responsible for the transfer protocol. GIPB interfaces are now available for a wide range of commercial machines.

The bus may often be controlled from a high level language and no knowledge of the transfer protocol is required. The theoretical maximum data transfer rate of the bus is one megabyte per second (1 MByte s^{-1}), however, when under high level control rates of 1-2 KByte s^{-1} are more normal. The use of machine code routines may allow rates of 20-50 KBytes s^{-1} to be achieved.

The system described here utilised two GIPB interface instruments, a Farnell omnibus OB-2 and a Millennium GIPB to parallel input output module, refer to Fig. 4.16. The Farnell unit allowed, in input (talker) mode 13 x 4 bit words and one analogue input of ± 1.999V full scale reading to an ADC, in output (listener) mode 3 x 4 bit words were available. This unit received the spectrum. The adapted lock-in amplifier voltage formed the ADC input while the 7 binary coded decimal (BCD) digits representing the field from the B-NM20 magnetometer used 7 out of the 13 word inputs. A consequence of this is that when the GIPB controller poles the Farnell both voltage and field are received simultaneously. The control of the magnetic field sweep was effected by the Millenium, configured as an output device 7 BCD digits represent magnetic field for the Bruker system or proton frequency equivalent to that field for the pulsed magnetometer. The digits were latched and sent to the appropriate device in parallel. In order to monitor the present status of the Millenium a display was constructed, the parallel outputs were fed via a set of buffers, latches and decoder drivers to a 7 segment display.

An Apple II Plus 48 KRAM microcomputer with twin disk drives was used as the system controller. An Apple GIPB interface card was used in one of the eight available input/output slots. Another slot was used for a GEC 4190 terminal emulator interface card that allowed the Apple to transfer files onto the University mainframe computer. The Apple high resolution graphics (256 x 196) were used for displaying

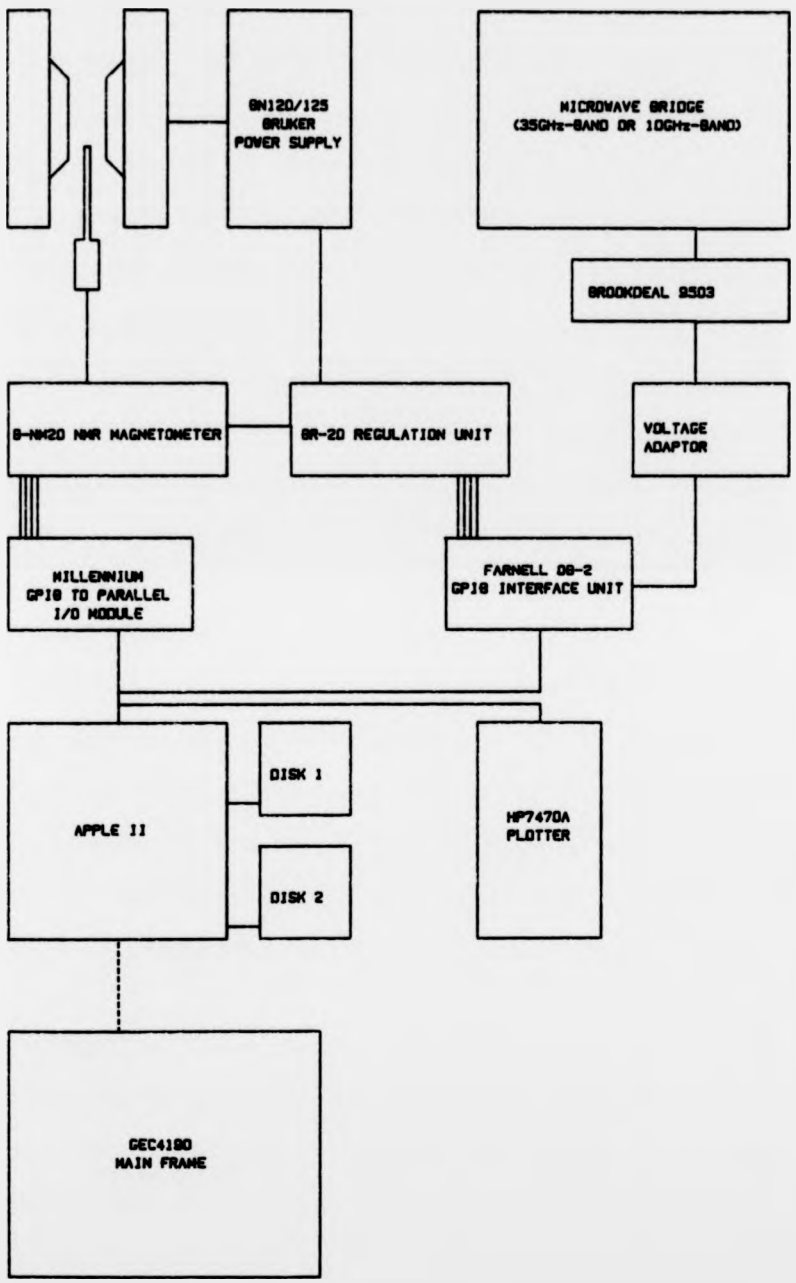

FIG. 4. 16. A DIAGRAM OF SPECTROMETER CONTROL AND ACQUISITION SYSTEM.

spectra.

The control software was written in BASIC as adequate sweep rates were attainable. The control program defined the start field, sweep interval, sweep direction and sweep rate. The number of data points was set at 500. The use of string variables by the Farnell set this limit as these variables are accumulated in memory and string clearance could not occur during a sweep. In order to overcome this problem an attempt was made to run machine code fast transfer routines, but it was found that the Farnell used a non-standard procedure for settling the status register of the Texas 9914 GIPB controller integrated circuit. On completion of a sweep the spectrum could be displayed and or stored on floppy disk. Experimental and instrumentational parameters could be stored with the spectrum. A hard copy could be obtained from a Hewlett Packard 7470A plotter.

It should be noted that for digital data to be meaningful the sampling rate should be such that the highest frequency component multiplied by twice the step size should be less than or equal to one. This is Shannon's Theorem. In the present case it requires that at ;least two samples be taken for the narrowest linewidth component present in the spectrum[28].

4.3.6 Summary

Both magnetic field control systems were found to operate satisfactorily in the 10 GHz-band and 35 GHz-band field ranges. The limitation on the loop settling time in the systems was found to be due to the discrete nature of the error signal. The correct analysis, for both systems should be in terms of the z-transform, however, the loop response time was made greater than the sampling period allowing the s-transform to be used in both. The fundamental difference between the two systems was in the magnitude of the sampling period. In the Bruker

system this was the gate time 100 mS while for the pulsed NMR system it was the pulse period of a few milliseconds. The improved response time of the pulsed NMR magnetometer allowed sweep rates of 0.2-0.3 mT S^{-1} to be achieved with zero set point error. With this system the set point is the actual field there is no need to measure the field. This allows spectral averaging, the klystron may remain stable to 1 m10^5 over many sweep periods, spectra recorded under identical sweep conditions may be added. In the case of the Brucker system the field-signal data points are accurate, however, the position in field at each sample may vary between sweeps. In this case interpolation is required.

The Apple-GPIB control and data acquisition system proved reliable and convenient, the spectra could be transferred directly to the mainframe hence signal to noise degradation due to manual digitisation was avoided.

REFERENCES

1. Wilmshurst, T.H. (1960), Ph.D. Thesis, University of Southampton.

2. Feher, G., (1957), Bell Syst. Tech. J., 36, 449.

3. Poole, C.P., Electron Spin Resonance, A Comprehensive Treatment of Experimental Techniques, Wiley-Interscience, New York, 1983, p.395, (2nd Ed).

4. Strandberg, M.W.P., (1972), Rev. Sci. Inst., 43, 307.

5. Meijer, G.C.M., (1975), J. Appl. Sci. Eng. A., 1, 129.

6. Grannell, P.K., Unpublished circuit.

7. Minshall, J., Unpublished circuit.

8. Sims, G.D. and Stephenson, I.M., Microwave Tubes and Semiconductor Devices, Blackie, 1963.

9. Siegman, A.E., Microwave Solid-State Masers, McGraw-Hill, 1964.

10. Wilmshurst, T.H., Electron Spin Resonance Spectrometers, Adam Hilger, London, 1967, p. 217.

11. Wilmshurst, T.H., Gambling, W.A. and Ingram, D.J.E. (1962), J. Electron. Control, 13, 339.

12. Johansson, B., Haraldson, S., Petterson, L., and Beckman (1974) RSI, 45, 1445.

13. Froncisz, W. and Hyde, J.S. (1982), J. Mag. Reson., 47, 515.

14. Private Communication, (1984), Dr. A.I. Vistus.

15. Goldman, S.a., Bruno, G.V. and Freed, J.S., (1973), J. Chem. Phys., 59, 3071.

16. Thomas, D.D., Dalton, L.R. and Hyde, J.S. (1976), J. Chem. Phys.,

65, 3006.

17. Hyde, J.S., Smigel, M.D., Datton, L.R. and Dalton, L.A. (1975), J. Chem. Phys., 62, 1655.

18. Millhauser, G.L. and Freed, J.H. (1984), J. Chem. Phys., 81, 37.

19. Beth, A.H., Balasubramanian, K., Robinson, B.H., Datton, L.R., Venkaturance, S.D. and Park, J.H., (1983), J. Phys. Chem., 87, 359.

20. Vistnes, A.I., and Datton, L.R., (1983), J. Mag. Reson., 54, 78.

21. Dalal, D.P., Eaton, S.E. and Eaton, G.R., (1981), J. Mag. Reson., 44,

415.

22. Vistnes, A.I. Wormald, D.I. and Isachsen, S., (1984), Rev. Sci. Instrum., 55, 527.

23. Lindsay, P.N.T. and Peake, B.M. (1982), J. Mag. Reson., 47, 365.

24. Herring, F.G., Mayo, J. and Phillips, P.S., (1979), J. Mag. Reson.,

34, 413.

25. Howie, R.A., Hunter, C.J., Regan, C., and Smith, D.B., (1981), Chem.

Industry, 7, 771.

26. Trousson, P. and Rinne, M., (1984), Rev. Sci. Instrum., 55, 1989.

27. Ireland, J.C., Willett, J.A. and Bobst, A.M. (1983), J. Biochem. Biophys. Methods, 8, 49.

28. Lowe, I.J. and Whitson, D.W. (1977), Rev. Sci. Instrum., 48, 268.

29. King, R.J, Microwave Homodyne Systems, Peter Peregrinus Ltd, Stevenage, 1978, p. 16.

30. Wilmshurst, T.H., Electron Spin Resonance Spectrometers, Adam Hilger,

London, 1967, p. 186.

CHAPTER FIVE

MATERIALS AND METHODS

5.1 Preparation of Spin-Labelled Ethidium Bromide

The procedure initially adopted was similar to Hurley et al[1], however, modifications were found necessary particularly in the method of purification before the desired compound could be isolated in a high state of purity.

The details of this modified procedure are given below. 2,2,5,5-tetramethyl-3-pyrrolin-1-oxy-3-carboxylic acid (Kodak) was first converted to the corresponding acid chloride. To a suspension of the acid (0.66 g) in dry benzene (10 cm^3) was added dry trielthylamine (0.6 ml) whereupon the acid dissolved. Thionyl chloride (0.4 ml) was then added dropwise to the stirred solution at room temperature and the The mixture was stirred for half an hour at room temperature and the volatile components then removed using a rotary evaporator. To ensure no moisture entered the rotary evaporator a silica gel guard tube was placed in the line to the pump.

To the residue was then added dry dimethyl formamide (8 cm^3). This solution contained the desired spin-labelled acid chloride. Ethidium bromide (0.66 g), previously dried at 57^o under reduced pressure 0.01 mm Hg, was added to dry formamide (20 ml). Dry triethylamine (1.5 cm^3) was then added. To this mixture was added, in small portions, the solution of spin-labelled acid chloride previously prepared.

The resulting mixture was allowed to stand overnight and the dimethyl formamide then removed under reduced pressure (60^o at 0.01 mm Hg). The residue, the crude spin-labelled ethidium bromide, was then dried.

Purification

The crude spin-labelled ethidium bromide was taken up in minimum volume of methanol and loaded onto a cellulose column (1.5 m x 3 cm). The column was then elevated with methanol containing a little aqueous ammonia (5% by volume of 0.88 NH_4 OH) at a rate of 60 ml/hr. The resultant major bands were, in order of decreasing Rj, coloured yellow, orange, and purple-red. The yellow band was observed to give an EPR signal but neither this nor the optical spectrum showed any change on the addition of DNA. The orange band contained the majority of the spin-label as shown by EPR. Since the optical absorption maximum of this material at 455 nm shifted to 485 nm on the addition of DNA and the EPR spectrum of the solution consisted of a large immobilised component this could be identified as the desired spin-labelled ethidium bromide. The purple-red band had an optical absorption at 480 nm consistent with that from ethidium bromide. Since this component gave only a weak EPR signal it was assumed to be unreacted starting material. Those fractions from the chromatography column which were shown by t.l.c. on both cellulose and silica to contain only the desired component were combined and the solvent removed under reduced pressure. Final traces of solvent were removed at 50^{o} under vacuum using an oil pump. The compound was obtained in the form of a solid red residue exhibiting an extinction coefficient at 455 nm of 5000.

In earlier reactions the purification procedure of Hurley was followed. This involved the use of preparative silica t.l.c. plates. In one case conversion of the spin-labelled ethidium bromide to the chloride form was achieved by refluxing a methanolic solution over AgCl, however, as expected this was observed to have little effect on the number, colour and Rj values of the resultant t.l.c. bands. In both cases elution of the silicon t.l.c. plate with El-OH-$CHCl_3$ (2:1) gave bands which appeared to be in agreement with those previously

reported[1], however, on drying the colours were observed to change making it difficult to identify the desired bands. A systematic study involving both optical spectroscopy and EPR of the resultant bands from both a preparative t.l.c. plate and a rotating disk chromatron revealed no band with the correct optical absorption, the EPR signal intensity was distributed in a broad spread across the plate. No band was found that gave a significant immobilised component in the EPR spectrum on addition of DNA. Several solvent schemes were tried without success. Attempts to re-run those tubes containing the most spin-label also failed to separate a component with the correct characteristics.

During our work on the preparation of the spin-labelled ethidium bromide several modifications to Hurley's method were introduced. In order to reduce the proportion of the purple-red component in the crude product the amount of ethidium bromide with respect to spin-label was reduced. It was also found that the addition of benzene to a solution of the crude product in dimethyl formamide resulted in a red precipitate and a pale yellow solution. The t.l.c. plates showed that the pale yellow component probably corresponded to the unreacted spin-label acid. For this reason the reaction residue was washed with benzene prior to column chromatography to reduce significantly the amount of this component in the crude mixture.

5.2 Preparation of DNA-Drug Complexes

The DNA used in these studies was Calf Thymus DNA type I, highly polymerised, sodium salt, No D-1501 obtained from the Sigma Chemical Company. The DNA solutions were made from distilled deionizer water at a concentration of 2 mg/ml then dialysed against the required salt concentration. The dialysis was run for at least 48 hours during which the solution was regularly renewed. The phosphate concentration of the DNA solutions was then determined from absorbance at 255 nm by

ultra-violet spectroscopy. The solutions were stored at 4°C and used within two weeks.

The spin-labelled ethidium bromide solutions were made from the dried solid, a molecular weight of 560 was assumed and distilled deionized water. The solution was stirred for 24 hours and any solid removed by filtration. The concentration was calculated from the absorbance at 545 nm (ε = 5000), solutions of the order of 1 mM were used.

The DNA-drug complex was formed by adding the appropriate volume of drug solution dropwise, while stirring, in order to prevent precipitation of the DNA. Gels were then obtained by sedimentation f the complex in an MSE DP Pegasus 65 ultracentrifuge using a 6 x 4.2 cm^3 rotor at 50,000 rpm for 8-12 hours. the supernatant was removed to prevent the gel redissolving if the gels were not used immediately they were stored at 4°C.

5.3 Preparation of Fibres

Orientated fibres of DNA-Drug were made using the method of Fuller et al[2]. Two thin glass rods with bulbous ends 200-500 ηm in diameter were mounted with plasticine within a pulling frame similar to that described by Fuller. The tip to tip separation was adjusted to approximately 200 ηm as a drop (15-40 ηl) of gel added from a 5-50 ηl Finnpipette, the fibre was formed by allowing the gel to dry.

It was possible to obtain thin well ordered fibres by letting the gel dry naturally, however, the orientation maybe improved for some gels by stretching before completely dry. The fibres used in this study were formed by allowing the gel to dry down to the diameter of the glass rods then it was carefully stretched to a length of approximately 2 mm. The dried fibre was then removed with a scalpel. Difficulties may be encountered dependent on the salt concentration of

the gel, low salt causes necking of the gel, high salt gels are elastic and difficult to manipulate.

An indication of the degree of order was obtained from observing the quality and position of the optical birefringence fringes. An Olympus microscope fitted with a rotary compensator with calicite combination plates was used. Only a qualitative estimate of order could be obtained due to the colour of the fibres used in this study.

Due to the benefits or producing well aligned fibres an investigation into the orientating influence of high electrostatic fields was undertaken. DNA is known to have an induced anisotropic dipole moment[3], however, a negligible permanent dipole moment. Fibres were dried under the influence of electrostatic fields up to 2 kV cm^{-1}, however, no significant increase in order was observed from the x-ray diffraction patterns. Further details of this experiment may be found in Appendix A.

5.4 Visible and Ultraviolet Spectroscopy

Two spectrophotometers were used a Cary 118C of this department and a Varian DMS100 belonging to the Department of Chemistry. The concentration of the drug and DNA solutions were calculated assuming the Beer Lambert law from

$$C(M) = [AxDxl(cm)]/E(M^{-1}cm^{-1})$$

where C(M) is concentration, A measured absorbance, l path length, D dilution factor and E molar extinction coefficient. The values taken for the molar extinction coefficient were 6600 $M^{-1}cm^{-1}$[4] for Calf Thymus at 258 nm and 5000 $M^{-1}cm^{-1}$ for spin-labelled ethidium bromide at 545 nm[1]. The latter figure was confirmed by measurement. The ratio between the amounts of DNA and drug sedimented by centrifugation can be

calculated from

$$P/D = (P_o - P_1)/(D_o - D_1)$$

where P_o = the initial DNA concentration

P_1 = the concentration of the DNA in the supernatent

D_o = the initial drug concentration

D_1 = the concentration of drug in the supernatent

In practice it was found that the influence of the P_1 and D_1 terms was negligible.

5.5 The Control of Relative Humidity

In order to control the degree of hydration of the fibres and gels during an EPR experiment air was pumped, using a Hyflow pump through a saturated salt solution and circulated through the cavity. This could be achieved by placing a rubber pipe onto the exit port of the Varian 1GHz band cavity or onto an entry pipe machined on the end wall of the 35GHz-band H_{011} cavity. The air was passed through three glass jars in series, the first contained distilled water, the second the saturated salt solution and the third was empty to collect any condensed water. The flow rates used were slow so as to allow the air to saturate on its passage through the salt solution. This was also aided by a porous diffuser placed at the end of the entry pipe. The following salts and indicated relative humidity values at 20^oC[5] are listed.

Salt	RH(%)
Calcium chloride	33
Potassium carbonate	44
Sodium bromide	57
Sodium nitrite	66
Sodium chlorate	75

Potassium chloride	86
Sodium sulphite	95
Potassium chlorate	98

REFERENCES

1. Hurley, I., Osei-Gyimah, P., Archer, S., Scholes, C.P. and Lerman, L.S. (1982), Biochemistry, 21, 4999.
2. Fuller, W., Hutchinson, F., Spencer, M. and Wilkins, M.H.F., (1967), J. Mol. Biol., 27, 507.
3. Jennings, B.R. and Rindler, P.J., (1977), Chem. Phys. Letts., 45, 550.
4. Fredericq, E., and Houssier, C., Electric dichroism and electric birefringence, Clarendon Press, Oxford, 1973.
5. O'Brien, F.E.M. (1948), J. Sci. Instrum., 25, 73.

CHAPTER SIX

EPR STUDIES ON SPIN-LABELLED ETHIDIUM BROMIDE DNA COMPLEXES

6.1 Introduction

In this chapter the experimental results obtained from EPR studies on spin-labelled ethidium bromide (SLEB) DNA complexes and the associated spectral simulations will be presented and discussed. The effects of relative humidity on SLEB-calf thymus DNA are studied in detail by EPR at 9 GHz. In order to confirm the validity of spectral simulations measurements at 35 GHz were also taken. The work of Robinson et al[1] suggests that motion of the order of 30 ns occurs in SLEB-DNA. To investigate the effect of relative humidity on SLEB motion ST-EPR spectra were recorded.

6.2 Experimental Method

The SLEB and SLEB-DNA complexes were prepared as described in Chapter 5. The 9 GHz and 35 GHz spectrometers and the procedure adopted for ST-EPR is described in Chapter 4. The conventional EPR spectra were recorded with 5 mW incident power at 9 GHz and 1 mW at 35 GHz. The zeeman modulation amplitude was maintained at 0.2 mT for the SLEB-DNA complexes. The solution spectra were recorded using a Varian flat solution cell while the SLEB-DNA gel and fibres were mounted on a 2 mm quartz rod held in a goniometer. At 35 GHz the samples were placed on a 1 mm quartz rod.

The Varian E231 cavity was humidified by air from a Hyflow pump passing through a three bottle humidity control, described in Chapter 5, and entering the lower sample port. The 35 GHz cavity was designed in the TE_{011} mode so air could be passed through a 1 mm hole in the centre of the end wall. At 98% RH the sample and

FIG. 6.1 THE SOLUTION SPECTRUM OF SPIN-LABELED ETHIDIUM BROMIDE. g=2.0053, a=1.61(mT).

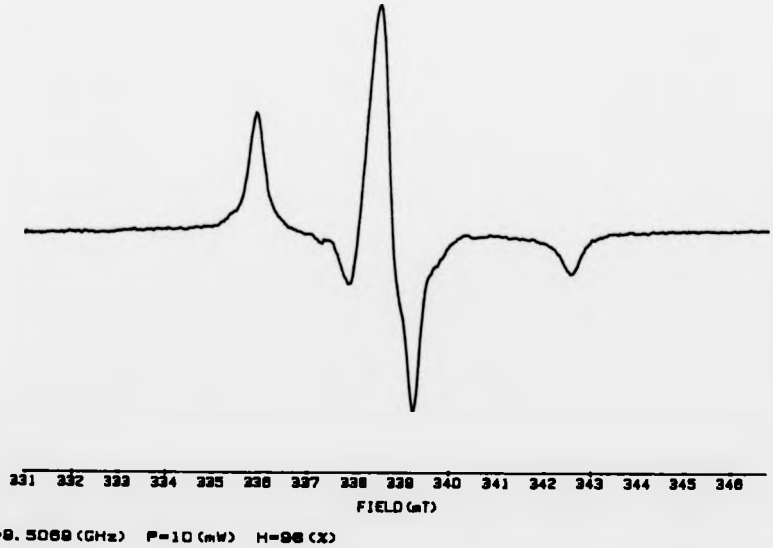

FIG. 6.2 THE GEL SPECTRUM OF SLEB-DNA 0.5MM NACL. g=2.0049, a=3.325(mT).

cavity were left for a minimum of 6 hours this period was reduced at lower RH values but was never less than 1 hour.

The majority of results presented here were taken with a single P/D = 70 fibre (0.5 mM NaC). Firstly a data set was recorded at 33% RH spectra recorded every 15^{o} of rotation of the fibre long axis to the magnetic field from 0^{o} to 180^{o}. The fibre was then humidified to 98% RH and a similar set recorded. The humidity was then reduced stepwise back to 33% RH, spectra recorded as a function of angle at each intermediate humidity. The initial and final 33% RH results were compared. ST-EPR spectra were also recorded at each humidity. The procedure as repeated with other P/D = 70 fibres and a P/D = 100 fibre. A powder spectrum was recorded from gel, similar to that used to form the original fibre, at 33% and 98% RH. The 35 GHz spectra were then recorded.

6.3 The Solution Spectrum

The spectrum from a 10^{-5}M solution of SLEB using distilled deionised water is shown in Figure 6.1. The g-value and isotropic hyperfine splitting are given below.

$g = 2.0053$ $\qquad\qquad$ $a_n = 1.61$ (mT)

These define the minimum value for the trace of the g-tensor and maximum value of the isotropic coupling constant a_n for the bound nitroxside as they were recorded in a fully hydrated environment.

6.4 Powder Spectra

Powder spectra were recorded from the centrifuge gel used to form the oriented fibres. The spectra recorded at 98% and 33% RH are shown in Fig. 6.2 and 6.3 respectively.

As discussed in Section 2.1 the anisotropy of the nitroxide hyperfine tensor allows the separation of outer hyperfine extrema with

$2A_{ZZ}$ where A_{ZZ} represents the largest component of the tensor. The extrema for a rigid limit isotropic distribution of spin-labels arise from those radicals for which the nitrogen $2p\pi$ orbital, defined as along the z-axis, is nearly parallel to the applied field direction. McConnell et al[2] have shown that the derivative shape of these extrema may be approximated to absorption curves with shape function characteristic of the inhomogeneous broadening. Mason and Freed[3] relate the peak to peak derivative. Lorentzian linewidth δ to the full width at half height of the extrema by $2\Delta_l^r = 1.59$ and $2\Delta_h^r = 1.81$ for the low and high field lines respectively.

The values measured are given below:-

33% RH	$2A_{ZZ} = 7.08$ (mT)	$2\Delta_l^r = 0.61$(mT)
		$2\Delta_h^r = 0.85$(mT)
98% RH	$2A_{ZZ} = 6.65$ (mT)	$2\Delta_l^r = 0.4$ (mT)
		$2\Delta_h^r = 0.5$ (mT)

6.5 Fibre Spectra at 33% Relative Humidity

The spectra recorded at 33% RH from 0^o to the applied magnetic field to 90^o are presented in Fig. 6.4 a-d. A complete data set from 0^o to 180^o is plotted in Fig. 6.5. The maximum hyperfine splitting $2A_{ZZ}$ was found to vary from 7.02 (mT) to 90^o to 7.14 (mT) at 0^o. The linewidth of the extrema varied from $2\Delta_l^r = 0.6$ (mT), $2\Delta_h^r = 0.7$ (mT) at 0^o to field to $2\Delta_l^{rr} = 0.8$ (mT) at 90^o. The high field line was partially obscured at 90^o hence an accurate measure of width was not possible.

6.6 The 98% to 33% R.H. Transition

A plot of spectra from 98% to 33% R.H. showing their relative peak to peak heights for the angles 0^o and 90^o are given in Figs. 6.6 and

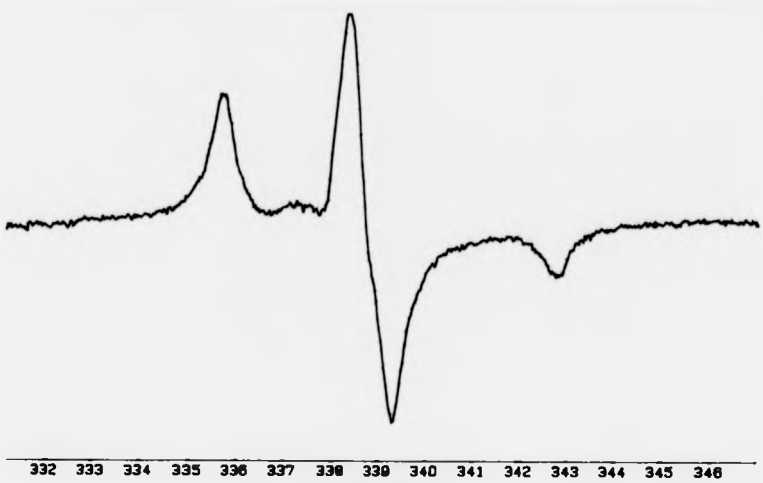

FIG. 6.3. THE GEL SPECTRUM OF SLEB-DNA 0.5MM NACL AT 33% RH.

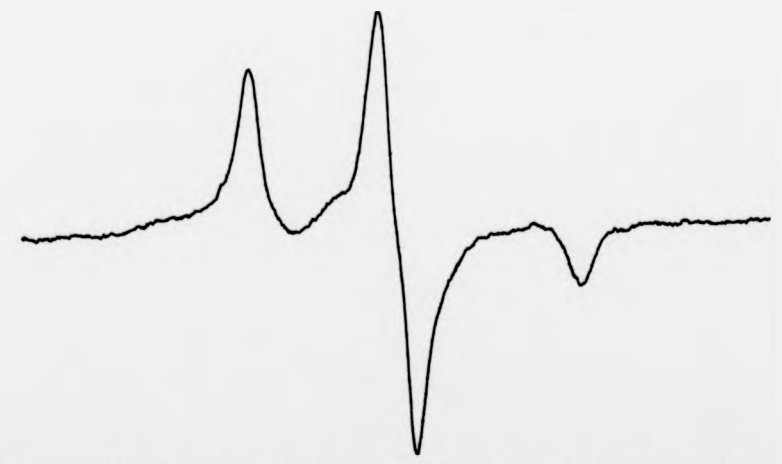

FIG. 6.4a SLEB-DNA FIBRE P/D=70 0.5MM NACL AT 0DEG TO THE FIELD. HUMIDITY=33%

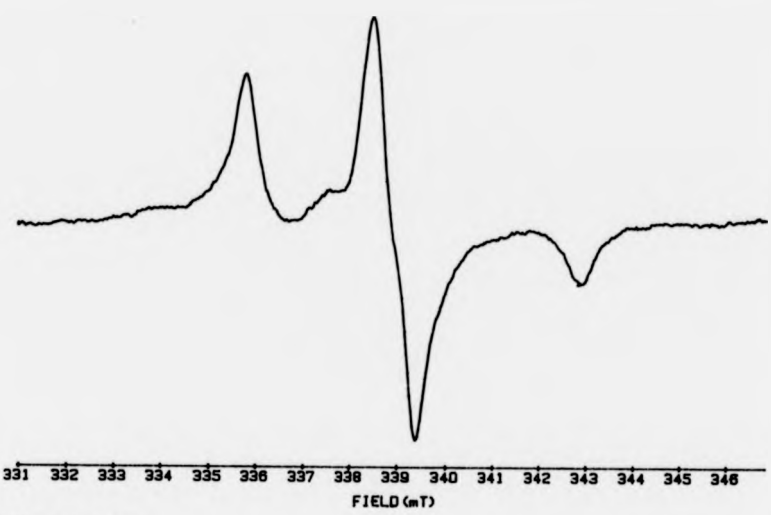

FIG. 6. 4b 30DEG TO FIELD.

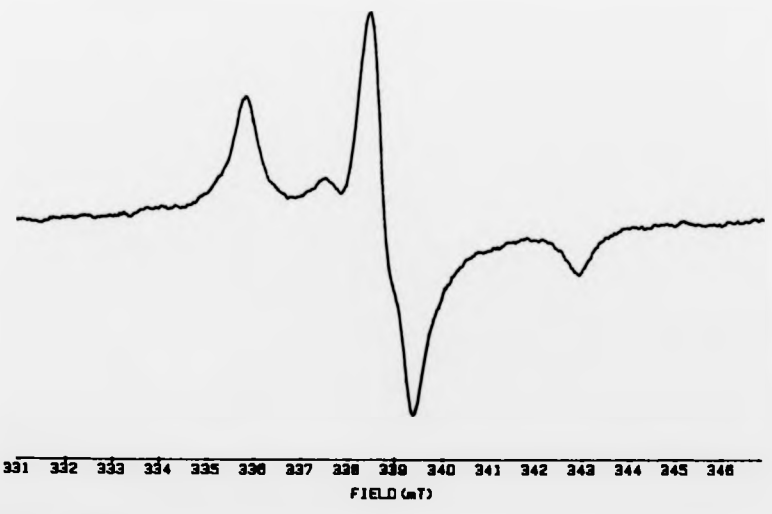

FIG. 6. 4c 60DEG TO FIELD.

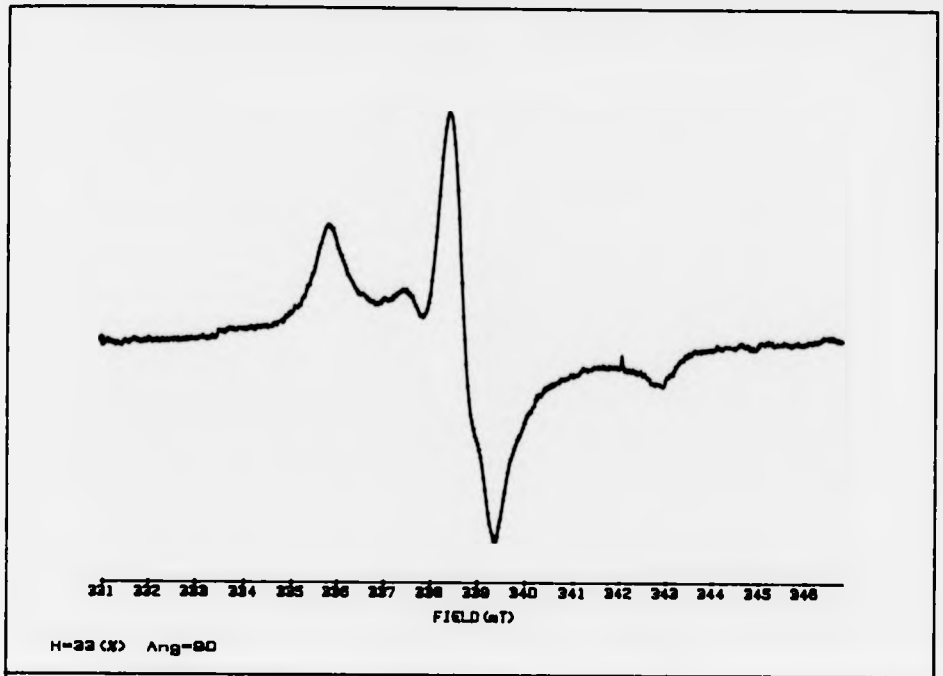

FIG. 6. 4d 90DEG TO FIELD.

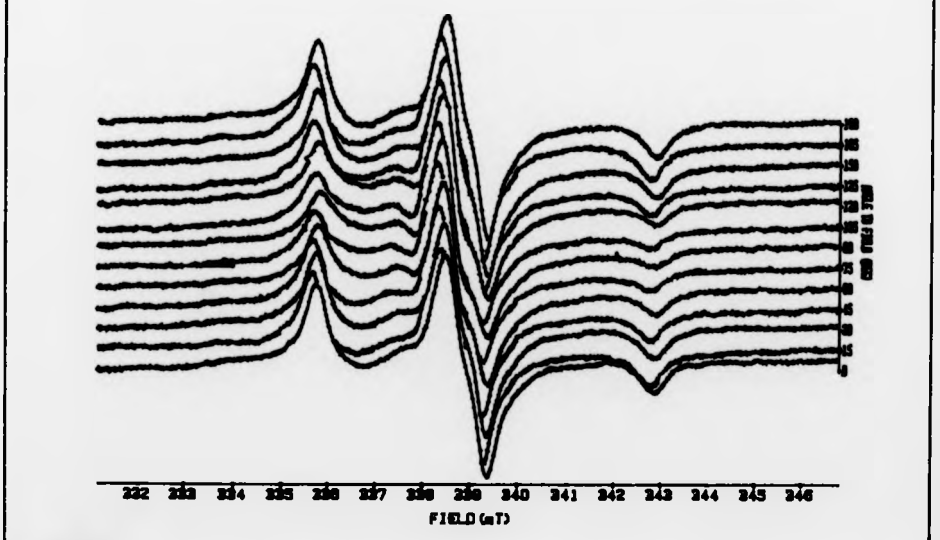

FIG. 6. 5 SLEB-DNA FIBRE P/D=70 0.5MM NACL AT 33% HUMIDITY AS A FUNCTION OF ANGLE.

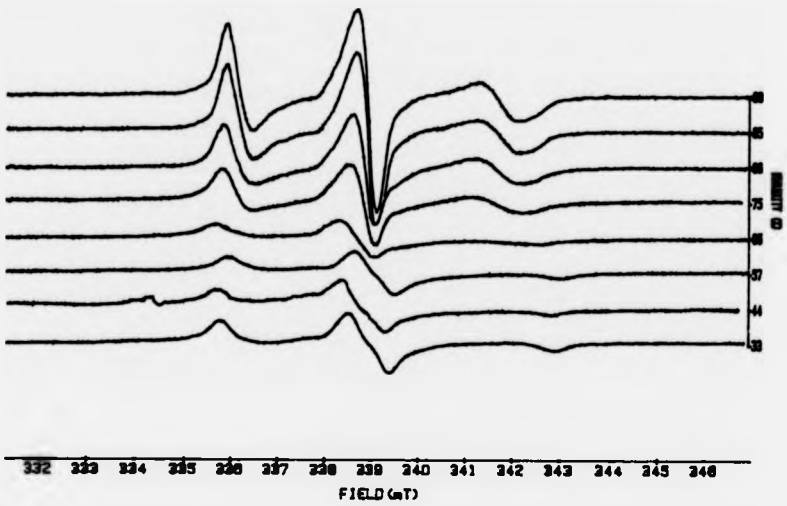

FIG. 6.6 SLEB-DNA FIBRE P/D=70 0.5MM NACL AS A FUNCTION OF HUMIDITY AT AN ANGLE OF 0DEG TO THE FIELD.

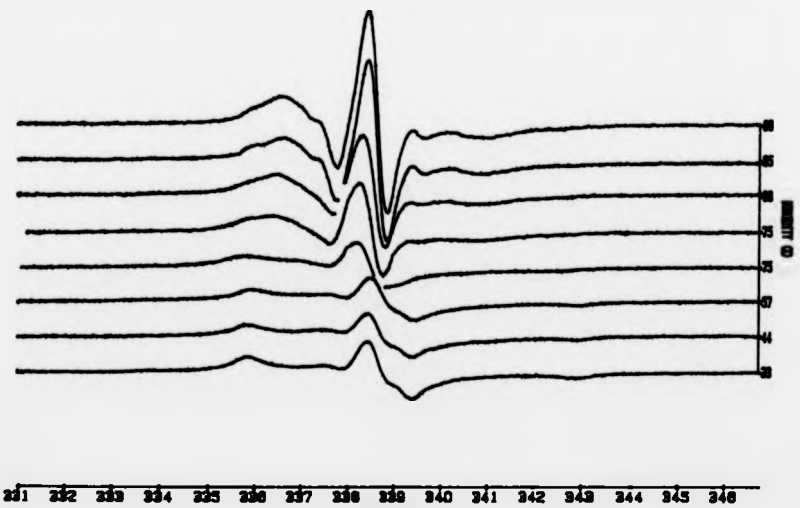

FIG. 6.7 SLEB-DNA FIBRE P/D=70 0.5MM NACL AS A FUNCTION OF HUMIDITY AT AN ANGLE OF 90DEG TO THE FIELD.

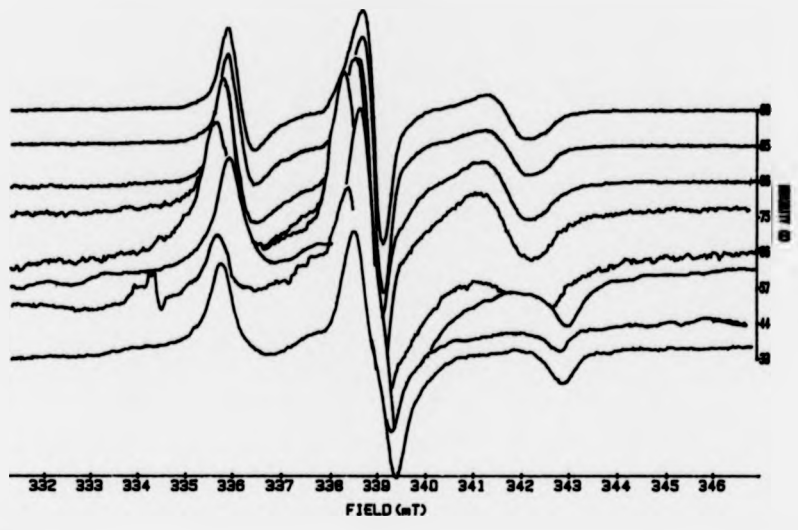

FIG. 6.8 SLEB-DNA FIBRE P/D=70 0.5MM NACL AS A FUNCTION OF HUMIDITY AT AN ANGLE OF 0DEG TO THE FIELD. NO SCALING.

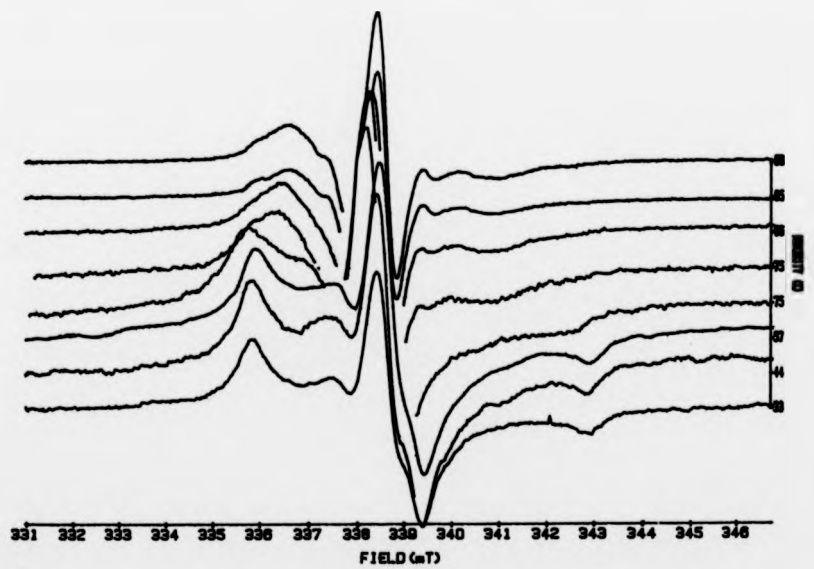

FIG. 6.9 SLEB-DNA FIBRE P/D=70 0.5MM NACL AS A FUNCTION OF HUMIDITY AT AN ANGLE OF 90DEG TO THE FIELD. NO SCALING.

6.7 respectively. It may be seen that the peak height remained constant between 33% and 66% but began to increase at 75%. This was associated with a change in the lineshape as demonstrated in the plots of normalised spectra in Figs. 6.8 and 6.9. The reduction in the maximum hyperfine splitting at 75% is clearly seen in the 90^{o} spectra. The increase in peak height continues up to 98% R.H. associated with a decrease in linewidth.

6.7 Fibre Spectra at 98% Relative Humidity

Figure 6.10a-g shows spectra recorded as a function of angle at 98%, the complete 0^{o} to 180^{o} data set is plotted in Fig. 6.11. Associated with the increase in peak height with respect to the 33% spectra is a higher degree of angular variation. This is illustrated by the variation in g-value (as taken from the central zero crossing) and hyperfine splitting $2A_{ZZ}$ plotted in Fig. 6.12 and 6.13.

6.8 Computer Simulation of EPR Spectra from SLEB-DNA Complexes at 98% Relative Humidity

The simulations were carried out using the program described in Section (2.2.2). Of the thirteen input parameters listed the following are dependent variables:

1. Principal values (g_{xx} g_{yy} g_{zz}), (A_{xx} A_{yy} A_{zz})
2. Linewidths M(+1), M(0), M(-1)
3. Lineshape
4. Tilt of nitroxide θ_2
5. Twist of nitroxide ψ_2
6. Degree of fibre misalignment δ
7. Orientation of fibre to the applied magnetic field θ_0

For a powder spectrum simulation this list is reduced to the principal values, linewidths and lineshape. Consequently the

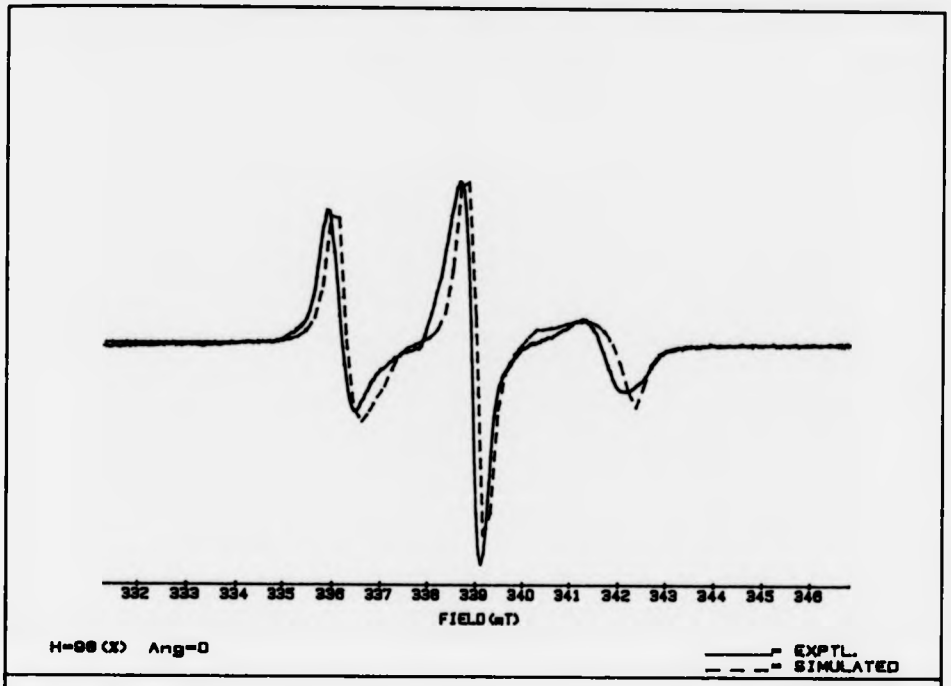

FIG. 6.10a SLEB-DNA FIBRE P/D=70 0.5MM NACL AT 0DEG TO THE FIELD. HUMIDITY=98%

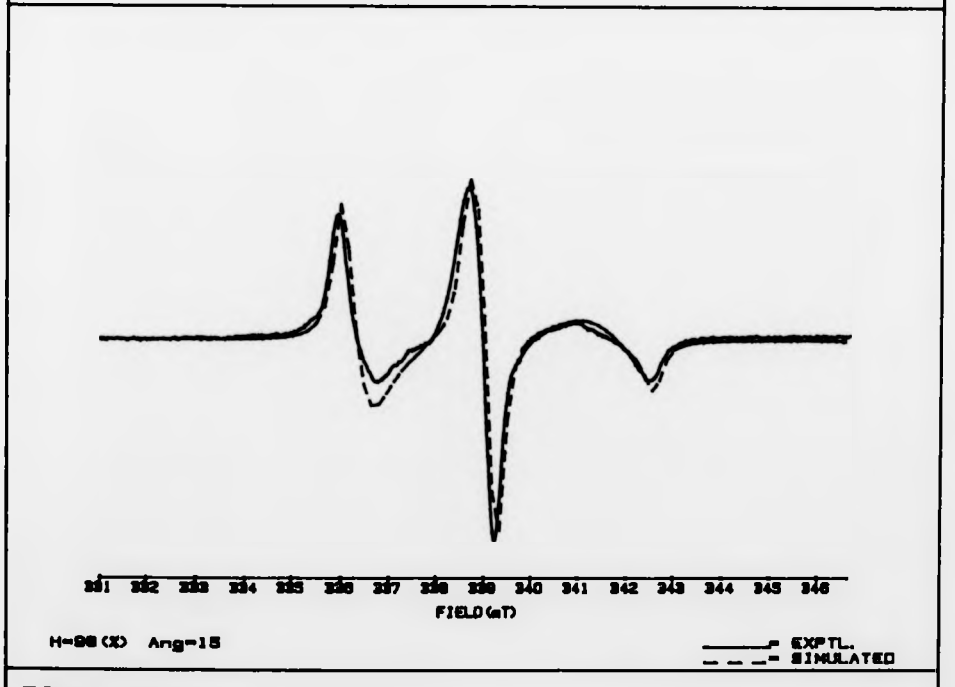

FIG. 6.10b 15DEG TO THE FIELD.

FIG. 6. 10c 30DEG TO THE FIELD.

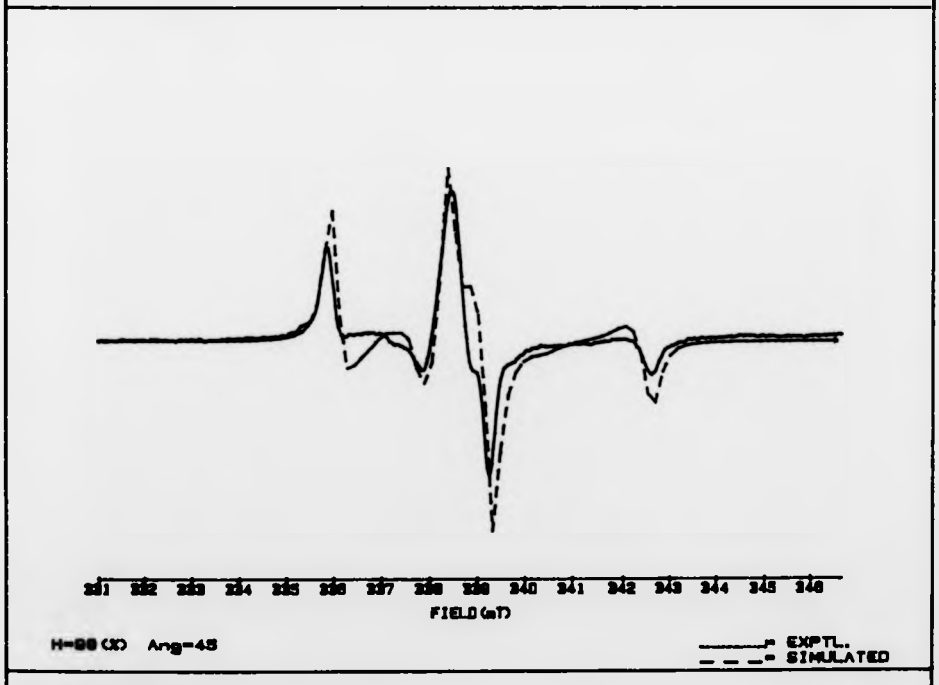

FIG. 6. 10d 45DEG TO THE FIELD.

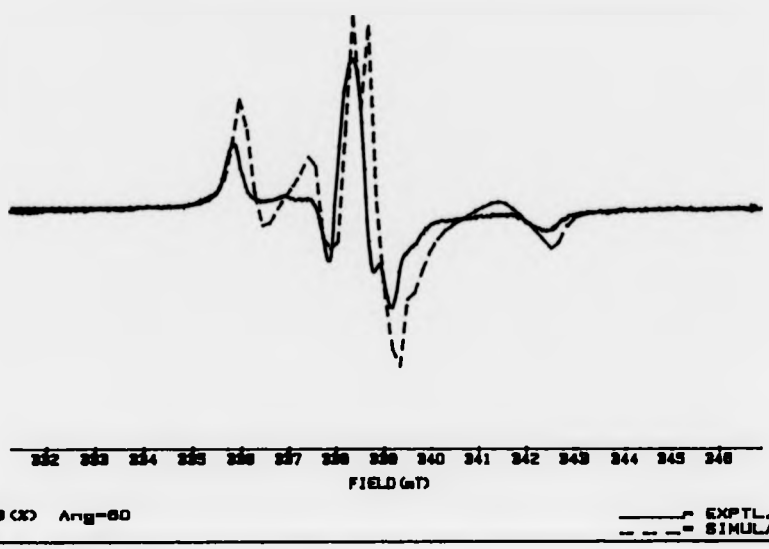

FIG. 6. 10e 60DEG TO THE FIELD.

FIG. 6. 10f 75DEG TO THE FIELD.

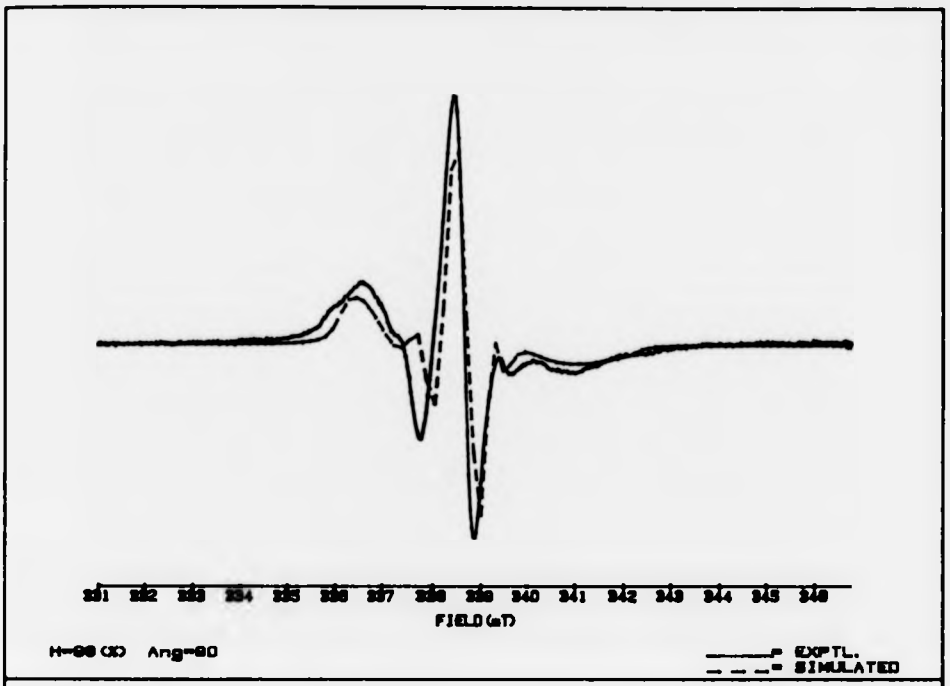

FIG. 6.10g 90DEG TO THE FIELD.

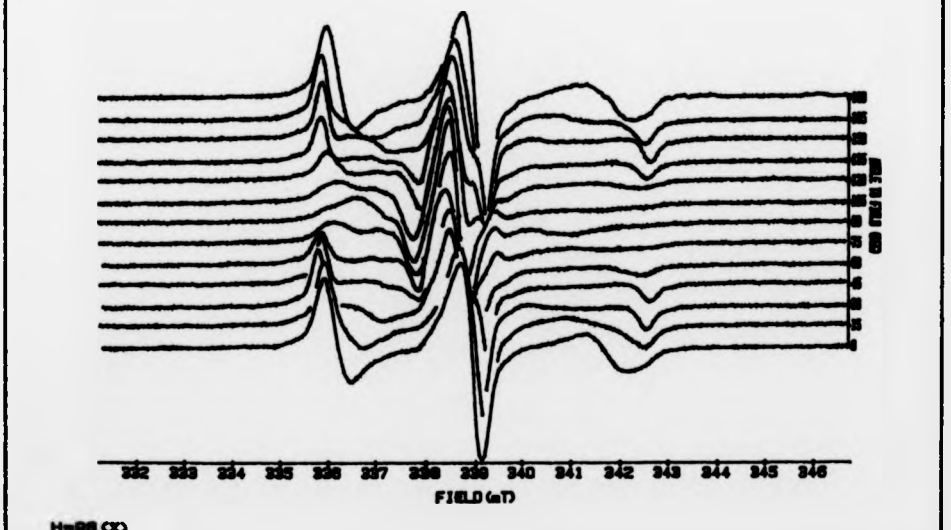

FIG. 6.11 SLEB-DNA FIBRE P/D=70 0.5MM NACL AT 98% HUMIDITY AS A FUNCTION OF ANGLE TO THE FIELD.

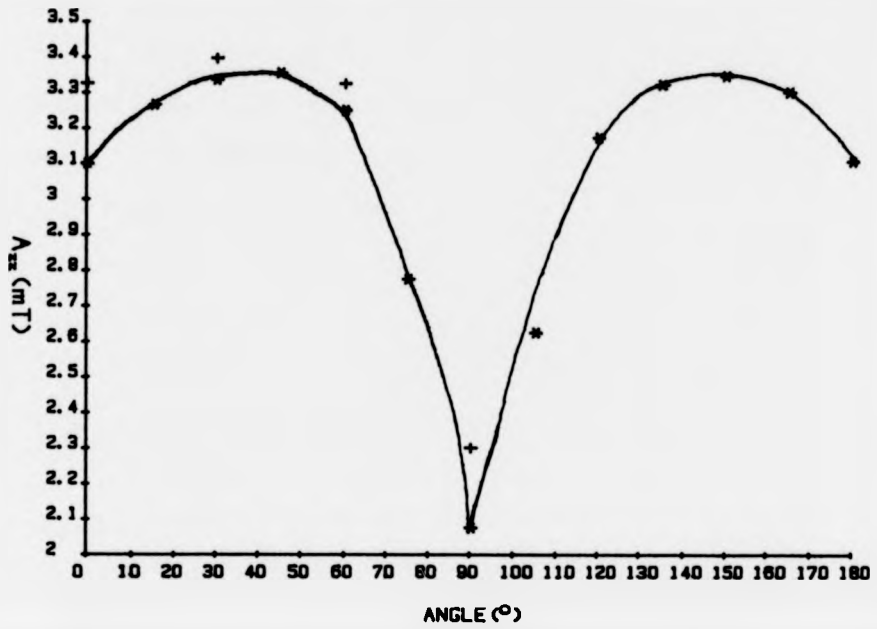

FIG. 6.12. A GRAPH OF THE MAXIMUM HYPERFINE SPLITTING AS A FUNCTION OF ANGLE TO THE FIELD AT 98% HUMIDITY (•) P/D=70, (+) P/D=100.

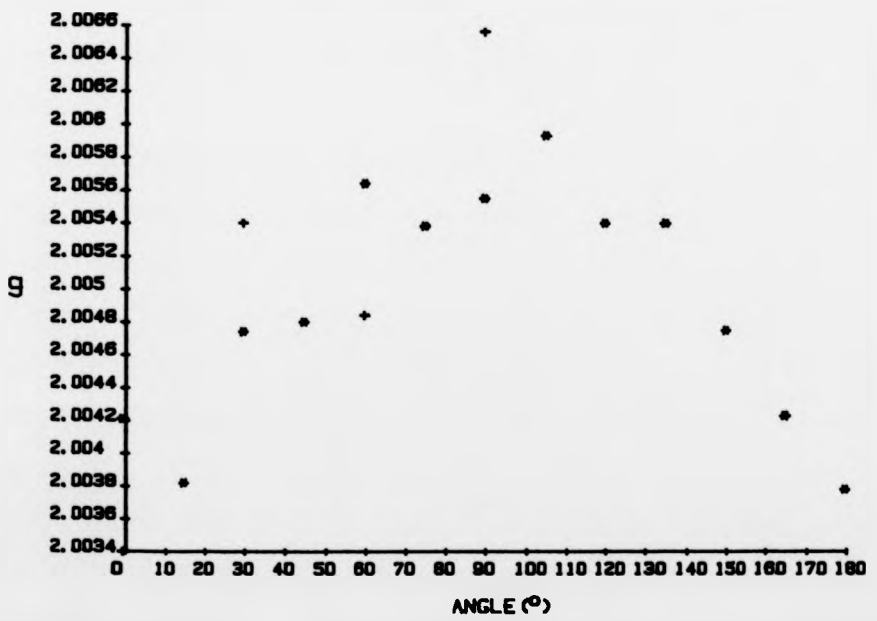

FIG. 6.13. A GRAPH OF g-FACTOR AGAINST ANGLE TO THE FIELD AT 98% HUMIDITY (•) P/D=70, (+) P/D=100.

simulation procedure began with the gel spectrum. The restriction imposed on the g-values by the solution spectrum of SLEB was observed. A starting value for linewidth Δ was obtained from the experimental spectrum. The resulting simulation is given in Fig. 6.3. The parameters used are listed below.

g_{xx} = 2.0080 A_{zz} = 3.32(mT)

g_{yy} = 2.0054 A_{yy} = 0.69(mT)

g_{zz} = 2.0025 A_{xx} = 0.69(mT)

Linewidths : M(-1) = 0.23(mT)

M(0) = 0.20(mT)

M(+1) = 0.22(mT)

Lineshape : Lorentzian

The line positions, width, and height are in good agreement, but the overall fit is not perfect. The above parameter set was found not to be unique, small variations in the nine variables showed other combinations that produced a similar standard of fit. The set presented above was the one found to give the best fit to the fibre spectra.

The fibre spectra were simulated by the following procedure. A set of parameters obtained from the powder simulations were used as starting values with the twist set to zero and a misalignment $\delta = 40^{0}$[4]. The tilt angle was then varied in 15^{0} steps from 0^{0} to 180^{0}, the 0^{0} and 90^{0} to field spectra simulated for each step. The procedure was repeated for different twist angles however little effect was observed. The degree of misalignment was then altered for the 0^{0} spectrum this was found to affect line position, width and the overall spectral shape. Small values of misalignment, less than 10^{0} were found to give poor overall shape, but clearly defined position and hence separation. By altering the angle of tilt the positions of the lines could be fitted. It was found that the angles δ and θ_2 were correlated, if δ

was increased the line positions could be maintained by reducing θ_2. The effect of increasing δ was to improve the overall shape. The optimum was found to be $\delta = 20^0$ and $\theta_2 = 15^0$. The 90^0 spectrum was simulated and found approximately correct, also the required hyperfine splitting maxima was found to be in the region of 45^0 to the field. If δ was further increased the linewidths became too broad and the maximum at 45^0 was lost.

The 0^0 spectrum was simulated using the optimum δ and θ_2 values the angle of twist ψ_2 was then altered but little effect was observed. The 90^0 spectrum was, however, found to be sensitive a best fit was obtained for $\psi_2 = 40^0$.

The 0^0 and 90^0 spectra were then simulated using the other compatible powder parameter sets. Alteration of δ, θ_2 and ψ_2 again found the best fit occurred in the $\delta \simeq 20^0$, $\theta_2 \simeq 20^0$, $\psi_2 \simeq 40^0$ region. The overall spectral shape of the 90^0 and 45^0 to field spectra were found to be most sensitive to changes in g, A and ψ_2 hence the parameter set giving the best fit was selected. This set was given at the beginning of this section. The parameter set supplemented by $\theta_2 = 15^0$, $\delta = 20^0$, $\psi_2 = 40^0$ was used in the simulations presented in Fig. 6.10a-g and in Fig. 6.4.

6.9 The Saturation Transfer EPR Experiments

Initial results recorded from the hydrated fibres were found to be incorrect due to a phase error introduced in the lock-in amplifier on frequency doubling the reference before demodulation. In subsequent experiments the second harmonic response at low power was minimised in the self nulling procedure refer to section (2.3).

The spectra recorded from gel at 33% and 98% R.H. are shown in figs. 6.14 and 6.15 respectively. Comparison with Fig. 2.7b and with spectra published elsewhere from anisotropic situations[5,6,7] show these

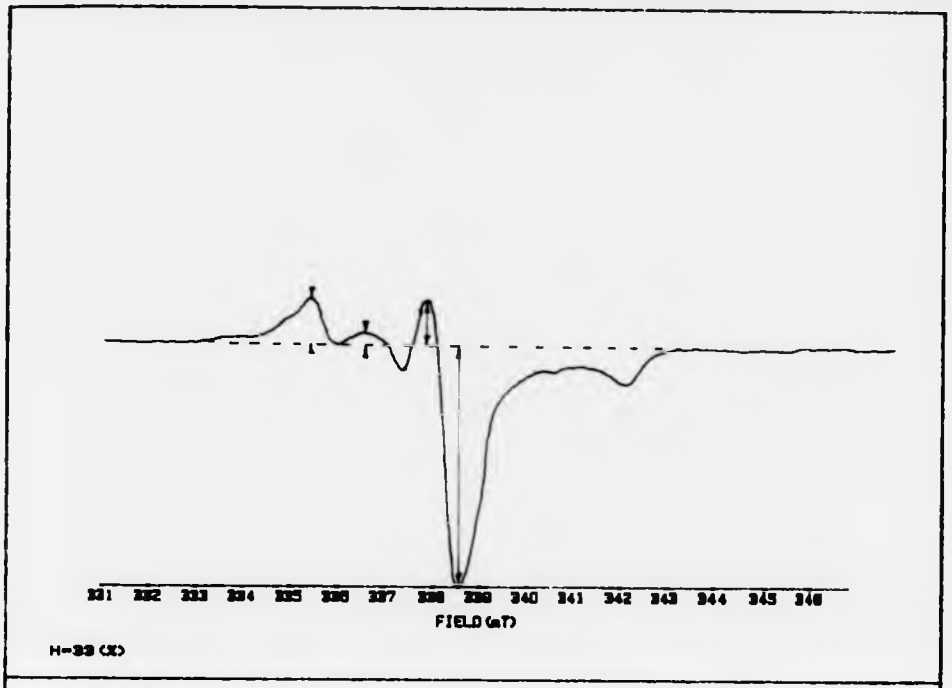

FIG. 6. 14 SLEB-DNA GEL P/D=70 0.5MM NACL ST-EPR SPECTRUM HUMIDITY 33%.

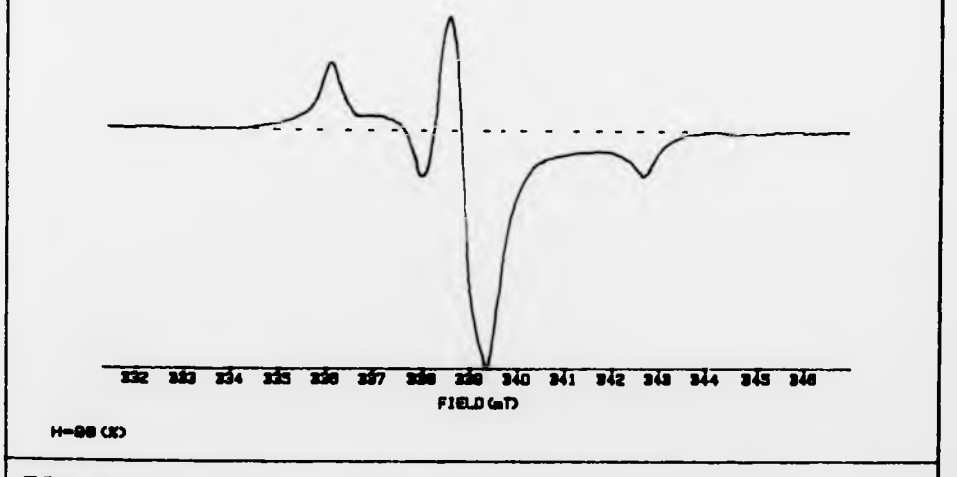

FIG. 6. 15 SLEB-DNA GEL P/D=70 0.5MM NACL ST-EPR SPECTRUM HUMIDITY 98%.

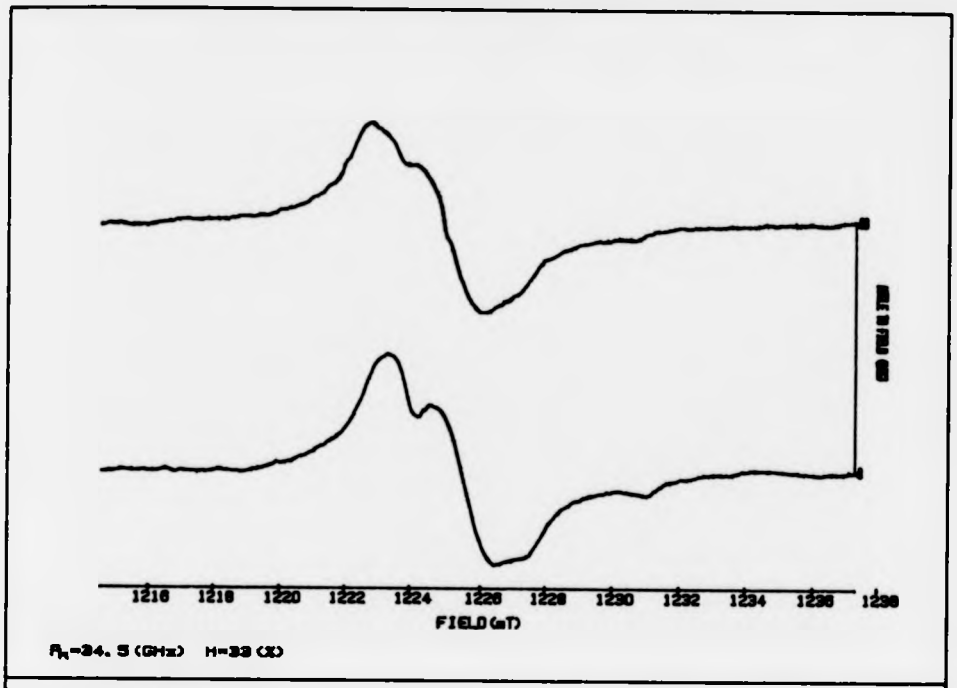

FIG. 6. 16 SLE8-DNA FIBRE P/D=70 0.5MM NACL AT 0DEG AND 90DEG TO THE FIELD. HUMIDITY 33%.

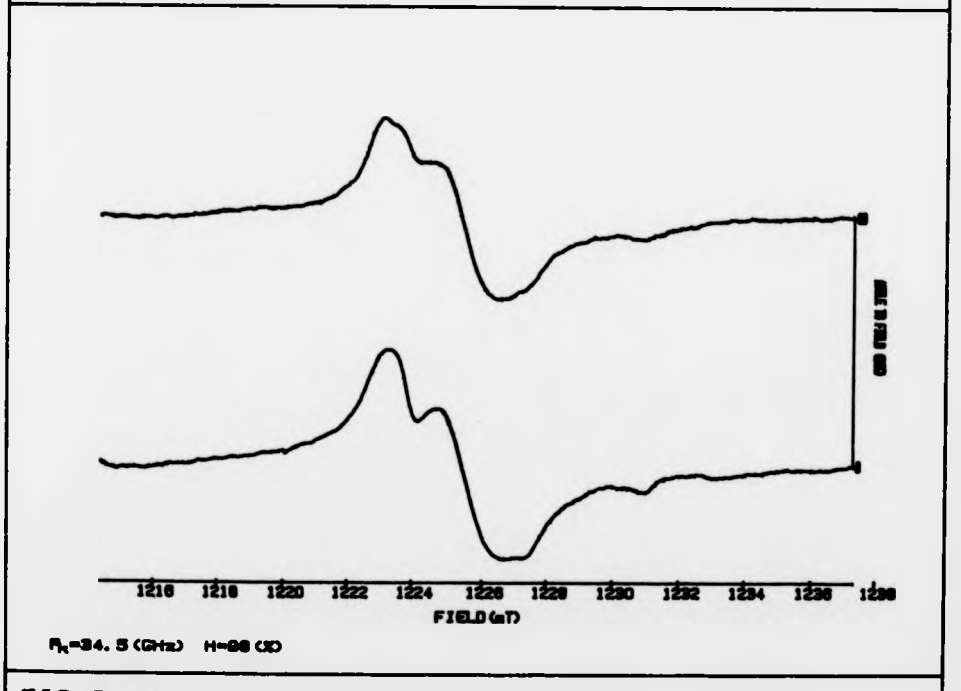

FIG. 6. 17 SLE8-DNA FIBRE P/D=70 0.5MM NACL AT 0DEG AND 90DEG TO THE FIELD. HUMIDITY 98%.

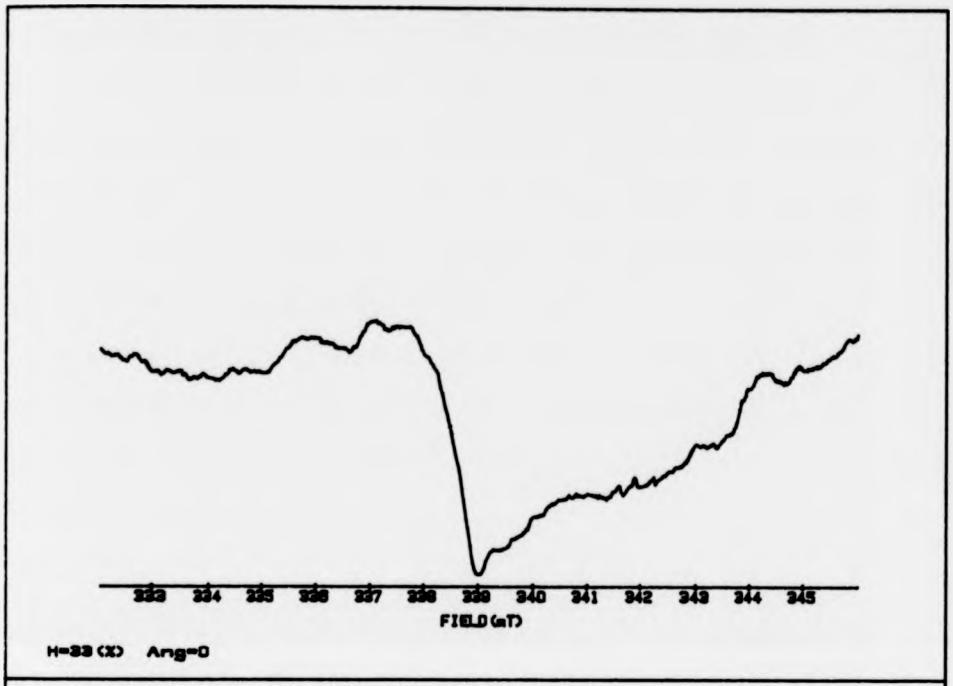

FIG. 6. 18 SLEB-DNA FIBRE P/D=70 0.5MM NACL AT 0DEG TO THE FIELD. HUMIDITY 33%.

results to be anomalous. This is illustrated in the high field regions of these spectra where the $M = -1\ d\theta/dB_{res}$ turning point intensity is below the baseline. The low field and central regions are approximately as expected. The low field ration L'/L shows the expected trend consistent with a shorter correlation time at 98% with respect to 33% as shown by published tables[6,7].

Care was taken in adjusting the reference phase at 1 mW incident power, however, the second derivative response was observed not to go to zero but pass through a broad minima. The uncertainty in the null phase position may explain the anomalous results presented above.

6.10 35 GHz-Band Fibre Spectra

In order to confirm the assignments of nitroxide tilt and twist proposed from the 9 GHz spectra results at 35 GHz were also recorded. A cavity was designed and constructed, as detailed in section (4.1) to allow humidification. The 33% and 98% R.H. spectra at 0^{o} and $90^{o}$to field are shown in Fig. 6.16. and Fig. 6.17. A value for the maximum hyperfine component A_{zz} may be obtained from the separation of the two high field features. These are observable in the 90^{o} to field spectra a value of 3.54 (mT) was extracted.

6.11 Discussion

The results presented exhibit inconsistencies. In particular the 35 GHz results do not show the variation in peak intensity with humidity or the angular variations clearly seen in the 9 GHz spectra. The geometric and magnetic parameters used in the simulation of the 98% RH 9 GHz results have been used to simulate the expected 35 GHz spectra and are presented in appendix C. Subsequent 9 GHz spectra from the same fibre showed a similar insensitivity to humidity variations. The fibre was stored and several weeks later the spectrum presented in Fig. 6.18

was recorded. The validity of the earlier 9 GHz results is confirmed by the similar behaviour of a P/D = 100 fibre the data from which is given in Appendix D.

The gel spectra presented in section (6.4) are characteristic of nitroxide radicals with a rotational correlation time $\tau_c \geq 10^{-9}$ sec. They, however, reveal a difference in the maximum hyperfine splitting between 98% and 33% RH, the splitting is increased by 0.43 (mT). Two independent mechanisms may affect the maximum hyperfine splitting, motion and degree of hydration of the nitroxide. The latter, however, would require the splitting to decrease.

Motion in the 10^{-9} sec $\leq \tau_c \sim 10^{-6}$ range results in limited lineshape variations accurate determination of the correlation time may be achieved by lineshape simulation based on the methods developed by Freed et al[8,9]. Approximation methods, however, exist. Goldman et al[10] have shown that τ_c may be estimated from the parameter $S = A'_{zz}/A_{zz}$ where A_{zz} is half the rigid limit value of the maximum hyperfine splitting. The splitting is reduced as τ_c decreases. Mason and Freed[3] have investigated the variation in linewidth of the outer extrema. The linewidth is determined by the inhomogenous broadening in the rigid limit. Near this limit residual motional broadening is present due to "uncertainty in lifetime broadening" and is given to a rough approximation by τ_c^{-1}.

The method of Goldman et al requires knowledge of the rigid limit splitting but this is difficult to obtain due to the restriction imposed by constant solution conditions. Examination of the linewidth results of section (6.4) and comparison of the fibre spectra show that the narrower linewidth occurs at 98% RH. This is in conflict with the observed reduction in A_{zz}.

To clarify the situation results at 35 GHz were recorded and the saturation transfer EPR technique employed. As mentioned in Section

(2.2.3) the rigid limit criterion is $(\Delta A + h^{-1}\Delta g\beta B)\tau_c >> 1$ hence it would be possible to fulfil this equality by experimenting at sufficiently high magnetic field. Hyde and Rao[11] have produced a calibration of the difference in maximum hyperfine component measured at 9 GHz and 35 GHz ($A_{zz}(Q) - A_{zz}(X)$) against correlation time for nitroxides. This has been found to be independent of the magnetic parameters. Uncertainty in the validity of the 35 GHz spectra has presented the application of this approach which would give an estimation of τ_c at both humidities free from ambiguity due to solution. It was hoped that the ST-EPR results could have confirmed these estimations.

The simulations presented in section (6.8) were carried out assuming the rigid limit criterion was valid. The program has been modified by Strange[4] to allow rapid restricted motion about a given axis after the model of Jost et al[12]. Simulations using motional averaging were attempted however, no satisfactory fit was attainable.

In simulating the 98% R.H. spectra the nitroxide tilt angle was stepped over the range $0^0 < \theta_2 < 180^0$. It was observed that the general form of the experimental spectral lineshapes for the 0^0 and 90^0 to field positions of the fibre were reversed in the simulations for tilt angles $45^0 < \theta_2 < 90^0$. The simulated spectra for a given angle to field were found to be unique over the range. The possibility that, from symmetry considerations, equal populations of nitroxides could exist with tilt angles θ_2 and $(180^0 - \theta_2)$ was investigated. The simulated spectra for the two orientations were weighted then added. It was not possible to fit the experimental spectra using this procedure.

Hong and Piette[13] studied oriented fibres of DNA-DNBSL, N-(4'-amino-1'-oxyl-2',2,6',6'-tetramethyl piperidine)-2, 4-dinitro benzene and DNA-FNBSL, N-(4' -amino- 1'-oxyl-2',2,6',6'- tetramethyl

piperidine)-2, 4-dinitro -5-fluorobenzene complexes. The resulting spectra were found to be similar to 0^0 and 90^0 to the field and to show a maximum hyperfine splitting at 45^0 to field. The high and low field extreme were observed to split in two, the outer giving rise to maximum splitting at 45^0 the inner reaching minimum separation. The model proposed to explain these results was that the nitrobenzene was intercalated with the nitroxide z-axis at a tilt $\theta_2 = 45^0$. The observation of two hyperfine splittings out of phase with each other was considered to be due to drugs bound on opposite sides of the DNA and consequently with a relative angle of 90^0 between the two nitroxide z-axes.

Cylindrical averaging in a perfectly ordered fibre should result in a population of nitroxides with relative angles between their z-axes between 0^0 and 90^0. The two turning points in the distribution may give rise to the observed extreme peaks. In order to test the feasibility of the model simulations were carried out assuming good fibre orientation and a tilt of 45^0. The results are presented in appendix E. It was found that the trends in hyperfine splittings could be reproduced.

In a previous study Hong and Piette[14] had examined EBSL-DNA complexes. The value maximum hyperfine splitting was given as $2A_{zz}$ = 6.72(mT) for precipitated complex. This is consistent with the results presented here. Oriented complexes were also studied. The maximum splitting at 0^0 to the field was $2A_{zz}$ = 5.7(mT) the value obtained for a fibre at 98% in the present study was $2A_{zz}$ = 6.25 (mT). This would infer a higher degree of motion in the oriented complexes of the former. The trend in hyperfine splitting and overall lineshape was similar to that observed with the 98% fibre. No maximum was observed at 45^0 to field the splitting reached its maximum at 0^0 to field. If the geometry of the two complexes is assumed similar the difference

could be explained by a higher degree of disorder within the fibre. Simulation showed the 45^0 maximum was lost when the gaussian misalignment was increased. This may, however, be a motional effect.

In Chapter 3 the drug nucleic acid interaction literature was reviewed. The orientation of the drug with respect to the nucleic acid was characterised by two angles tilt and roll. The former was a rotation about the short axis (x-axis) the latter a rotation about the long axis (y-axis). If the z-axis of the nitroxide was coincident with that of the drug and the N-O bond along the drug y-axis then the tilt and twist may be related to the above angles. If either the roll or tilt were zero the nitroxide tilt would equal the non-zero angle and there would be no twist. If both are non-zero, from Figure 2.5, tilt θ_2 may be considered as a rotation about the nitroxide y-axis and hence to drug tilt assuming $\phi = 0$. Rotation about the x-axis perpendicular to the DNA would be related to the nitroxide tilt (θ_2) and twist (ψ_2). Roll $\theta_R = \sin \theta_2 \tan \psi_2$.

REFERENCES

1. B.H. Robinson, L.S. Lerman, A.H. Beth, H.L. Frish, L.R. Dalton and C. Aver, J. Mol. Biol. (1980), 139, 19.
2. H.M. McConnell and B.G. McFarland, Quart. Rev. Biophys. (1970), 3, 91.
3. R.P. Manson and J.H. Freed, J.Phys.Chem., (1974), 78, 1321.
4. R.W. Strange, Ph.D. Thesis (University of Keele), (1985).
5. I. Hurley, P. Osei-Gyiman, S. Archer, C.P. Scholes and L.S. Lerman, Biochemistry, (1982), 21, 4999.

6. M.A. Hemminga and A.J. Faber, J. Magn. Reson. (1986), 66, 1.

7. B.J. Gaffney, J. Phys. Chem. (1979), 83, 3345.

8. J.H. Freed (1976) in "Spin-Labelling Theory and Applications" (Berliner, L.J., Ed.), Vol. I, pp. 53-132, Academic Press, New York.

9. J.H. Freed, G.V. Bruno and C.F. Polnagzek, J. Phys. Chem. (1971), 75, 3385.

10. S.A. Goldman, G.V. Bruno and J.H. Freed, J. Phys. Chem. (1972), 76,

1858,

11. J.S. Hyde and K.V.S. Rao, J. Magn. Reson., (1980), 38m 313,

12. P.C. Jost, O.H. Griffith, (1976) in "Spin-Labelling Theory and Applications" (Berliner, L.J. Ed.), Vol. I, Academic Press, New York.

13. S.J. Hong and L.H. Piette, Archv. Biochem. Biophys. (1978), 185, 307.

14. S.J. Hong and L.H. Piette, Cancer Res. (1976), 30, 1159.

CHAPTER SEVEN

CONCLUSIONS AND SUGGESTIONS FOR FURTHER WORK

This chapter is divided into four sections: Concluding remarks on instrumentation; suggestions for further work; concluding remarks on EPR studies of spin-labelled ethidium bromide-DNA complexes; suggestions for further work.

7.1 Concluding Remarks on Instrumentation

7.1.1 Spectrometer Noise Performance

The aims of this work were to determine the dominant noise sources within the 9 GHz spectrometer and to investigate the use of low noise microwave pre-amplifier and loop-gap resonator in improving the system performance.

The studies of Feher[1], Strandberg[2] and Meijer[3] on the character and transmission of klystron valve noise were reviewed and a common formalism adopted to allow comparison. The analysis of Meijer[3] was used to illustrate the advantages of the Loop-Gap resonator design. These are a reduced susceptibility to both frequency modulated and amplitude modulated due to the reduction of Q-value and the increased microwave field strength which allows lower incident power levels to be used.

Noise figure analysis of the spectrometer detection system was used to justify a study of low noise microwave preamplifiers. Solid state amplifiers are now available with quoted specifications NF = 2 dB, gain G = 12 dB, and insertion loss of less than 1 dB. If detector noise is dominant an improvement in performance should result if the detection system noise figure is greater than or approximately equal to

the figure for the microwave preamplifier. The measurement of noise power as a function of klystron output power implies that detector noise is infact dominant. As no improvement in signal to noise was observed this would infer either the noise figure of the diodes is of the order of 2dB or that this noise figure value is in error.

A subsidiary aim was to investigate the proposal of Feher that an improvement in performance could be achieved by slight overcoupling of the microwave cavity. The noise power was found to show a weak inverse dependence on cavity coupling while the signal response peaked at critical coupling. The signal to noise ratio consequently also peaked at critical coupling and no advantage in slight overcoupling was found.

In order to determine a value for the system noise figure a noise generating diode with an ENR = 11.5 dB at 9.5 GHz was used. However, no change in the monitored noise power could be discerned with or without the low noise pre-amplifier in place. This casts further doubt on the specification of the pre-amplifier used. These measurements also imply that the noise figure for the detection system is greater than that calculated from the diode characteristics and balanced mixer theory, but no method of testing the noise diode was available.

7.1.2 Saturation Transfer EPR

In order to perform second harmonic out of phase ST-EPR on the 9 GHz spectrometer variable matching to the cavity modulation coils was introduced to allow 50 KHz modulation and the microwave magnetic field strength was calibrated. The Brockdeal 9503 lock-in amplifier second harmonic function doubled the frequency of the reference signal from the reference oscillator. Calibration of the microwave magnetic field strength using a single crystal of NMP-TCNQ was found to be straightforward.

7.1.3 Computer Control and Magnetic Field Regulation

A computer control and data acquisition system for use with the 9 GHz and 35 GHz spectrometers was designed and constructed. The two common components, the Bruker BN100/120 magnet power supply and the Brockdeal 9503 precision lock-in amplifier, were interfaced. The system was controlled through the IEEE bus standard which allowed flexibility in the choice of microcomputer controller. A Commodore PET and an Apple IIe were used successfully. The results presented in this thesis were taken with the latter as this allowed data files to be transferred to the Computer Centre mainframe. The system proved both reliable and easy to use.

The microwave frequency was monitored by a Hewlett Packard frequency counter HP4267 which gave an accuracy of 1 part 10^4 over the period of a spectral sweep. For most applications this accuracy is sufficient for the g-values obtained from the spectrum. In order to realise this the magnetic field at the sample position must be reproducible and measurable to an accuracy of 1mT. This may only be achieved by the use of nuclear magnetic resonance methods. Two NMR field control schemes were examined. The first system as based on the Bruker BNM20 NMR magnetometer and BR20 regulation unit. The field was swept by updating BCD information to the regulation unit. The system has to be operated as an open control loop to obtain practical sweep rates consequently a reproducible magnetic field-time sweep profile was not possible. However, the degree of measuring accuracy required was achieved by constant polling of the magnetometer unit during the sweep.

The second magnetometer system overcame the above restrictions. A digitally controlled frequency synthesiser was used in a second order phase lock loop to lock the magnetic field to the given frequency via the frequency discriminating character of the proton NMR dispersion signal. Once the initial lock had been obtained sweep rates up to

$0.7mTs^{-1}$ were possible. The minimum step was 100 Hz (2.35μT) as the control loop was closed for this range of sweep rates the conditions of reproduciblity and accuracy are fulfilled. Sweeps were generated by updating the frequency in BCD form, to the synthesiser. The magnetometer was operated with a broad band transmission line probe consequently was able to lock over the range 10 to 70 MHz (0.15 T to 1.6 T).

7.2 Further Work

The intrinsic advantages of the loop-gap resonator highlighted in this work justify further research into construction. Despite the reduced advantage at 9GHz for fixed size samples such as fibres and crystal significant gains in sensitivity should still be achievable.

The ambiguity of the noise measurements requires clarification. Double sideband measurements of the shottky barrier diodes noise figure and conversion gain at 100kHz I.F. is required. Similar measurements on the balanced mixer arrangement would be of use to verify the equivalence with a single diode. If accurate figures were available then the operation of the excess noise diode could also be tested. These figures would also allow proper assessment of the effectiveness of low noise microwave preamplifiers.

If the present homodyne spectrometer system could be characterised as detailed above then it would be of interest to test the performance of balanced mixer with respect to single ended mixer detection. The reduction of amplitude fluctuations from the reference arm is well understood ,however, the influence on cavity arm amplitude fluctuations caused by FM noise conversion[4] requires clarification.

7.3 Concluding Remarks on EPR Studies on Spin-Labelled Ethidium Bromide DNA Complexes

The aim of this study as to evaluate the use of EPR in monitoring the binding of a spin-labelled analogue of the known intercalating molecule ethidium bromide as a function of relative humidity. Orientated fibres of low salt calf thymus DNA are known to undergo the conformational transition C→A→B-form as the relative humidity is altered from 33% to 98%.

The gel spectra showed that no nitroxide component of the complex was undergoing rapid rotation ($\tau_c = 10^{-9}$s). The observed maximum hyperfine splitting at 98% and 33% are consistent with bound motional restricted nitroxides. The difference in splitting indicates a degree of mobility at 98% relative humidity.

The orientated fibre sample at 98% relative humidity showed a marked variation in spectral profile as a function of angle to the external magnetic field. This may be attributed to a degree of order of the nitroxide z-axes with respect to the fibre axis. The maximum hyperfine splitting is seen to maximise around 45^{o} to field and to each a minimum at 90^{o}. The molecular hyperfine tensor is axially symmetric. The maximum splitting will correspond to the majority of the nitroxide z-axes being parallel to the field. Likewise the minimum splitting will occur when the field is more closely parallel to the x-y plane. This is consistent with the observed variation in g-value with angle.

The fibre spectra recorded at low humidity (33%) show only small variations as a function of angle to the field. This would indicate a wider distribution of molecular axes within the fibre. If the degree of order of the DNA molecules within the fibre is independent of humidity then it may be assumed that the nitroxides are semi-randomly arranged with respect to the DNA.

These conclusions are consistent with the observed variation in peak intensity and extrema linewidth with humidity. The broadening and reduction in peak height of the lines from 98% to 33% indicate more

random distribution.

These changes occur mainly over the 66% to 75% humidity range. This is the region of the A to B-form DNA conformational transition. In the B-form the inter base-pair separation and the hydration conditions are known to favour intercalation of the ethidium bromide chromophore. The resultant increase in order would be consistent with the observations. The transition at lower humidities could be explained by the molecules moving to binding sites within the grooves. This would result in a semi-random distribution.

In view of the large population of ordered species at 98% an attempt was made to extract geometric information on the binding site. Computer lineshape simulations based on the fibre model were carried out. Both the variation in hyperfine splitting and g-value were reproduced by assuming the tilt of the nitroxide axis to the DNA was 15^{0} and the spin-labelled complex was rotated by 40^{0} about the nitroxide z-axis. This is consistent with the interpretation presented earlier. The exact geometry of the spin-label ethidium bromide link is not known neither is the amount of distortion to this geometry on binding. Likewise the possibility of restricted reorientation can not be eliminated. Consequently this information is at present unable to define the exact ethidium bromide DNA geometry.

A possible uncertainty in the nitroixde DNA geometry determined may be caused by limited mobility. This is most likely to be of the form of slow torsional oscillations about the DNA axis[5]. These may result in partial averaging and hence an uncertainty in tilt and twist. The quality of the fits obtained from the rigid limit simulations should, however, be noted.

7.4 Suggestions for Further Work

These studies could be readily extended by the use of synthetic

DNA. Fibres formed from poly (GC) have been shown to undergo a transition sequence. This would be of interest as the S-form is believed to be a left-handed form. Poly (AT) DNA shows a transition pathway D→B[6]. The D-form has been found to give high quality x-ray diffraction patterns. Complementary studies with EPR and x-ray diffraction may yield useful information on drug-DNA interactions in this form. The techniques may obviously be extended to any molecule showing interaction with DNA and that may be spin-labelled. The EPR studies have the advantage of being applicable over a wide range of P/D ratios down to P/D = 100.

EPR and computer lineshape simulations in concert have the potential to obtain geometric information on the ligand-DNA interaction. However, before this can be achieved the problems of nitroxide ligand orientation and of motion within the complexes must be overcome.

Spin-labelling through twin bonds onto the ligand would give the required rigidity. The geometry so defined must be known either through x-ray diffraction studies or steric hindrance arguments.

The problem of motion is more complex. In the particular case of spin-labelled ethidium bromide it would be of interest to determine the rate and type of motion involved. Ideally the semi-quantitative, ΔS[7] and two frequency[8] methods, should be applied in concert with lineshape simulation[10] and saturation transfer EPR[9]. The motion is likely to be anisotropic, Freed[10] discusses the theory for lineshape simulation for this situation. Marsh[11] and Robinson[12] discuss the influence of anisotropic motion on ST-EPR. Hurley et al.[6] have applied several of these methods to spin-labelled ethidium bromide complexes and have determined a rotational correlation time of approximately 40ns. Comparison of the maximum hyperfine splitting suggest a similar figure may be applicable for the complexes used in this study. The motion was

assumed to be due to torsional oscillations of the base pair drug complex about the DNA axis. The possibility of motion about the nitroxide drug bond was not considered. The chromophore was assumed to be rigidly bound and consequently the motion was due to flexing of the DNA. It would be of interest to confirm these results.

It may be useful to modify the transformation procedure of the FIBRE program to accommodate a forth axis system. This would be the ligand axis system, the first transformation would rotate the nitroxide into the ligand frame. For a rigid nitroxide drug complex the diffusion tensor would be coincident either with the ligand reference frame or the DNA frame dependent on the origin of the motion. Modification of the present program to take account of such motion would be simplified.

Currently there is interest in studying DNA conformational transitions under the influence of a number of different counterions. This could be of relevance to this study if ions from the transition or lanthanide series were used. It would then be possible to apply spin-probe-spin-label methods[13]. The magnetic interactions between a rapidly relaxing metal ion and a nitroxide result in predictable changes in lineshape and intensity in the EPR signal from the nitroxide. Leigh[14] has developed the theory for the rigid limit. The information that may be extracted from these studies is a radial distance between metal ion and spin-label. If the positions of the metal counter ion on the DNA could be defined it would be of interest to monitor this distance as a function of humidity.

REFERENCES

1. Feher, G., (1957), Bell Syst. Tech. J., 36, 449.
2. Strandberg, M.W.P., (1972), Rev. Sci. Inst., 43, 307.
3. Meijer, G.C.M., (1975), J. Appl. Sci. Eng.A, 1, 129.

4. Wilmshurst, T.H., (1967), Electron Spin Resonance Spectrometers, Adam Hilger

, London, p186.

5. Hurley, I., Osei-Gyiman, P., Archer, S., Scholes, C.P., and Lerman, L.S,

(1982), Biochemistry, 21, 4999.

6. Mahendrasingham, A., (1983), P.hd Thesis, University of Keele.

7. Mason, R.P, Freed, J.H, (1974), J. Phys. Chem., 78, 1321.

8. Hyde, J.S, Rao, K.V.S, (1980), J. Magn. Res., 38, 313.

9. Thomas, D.D, Dalton, L.R, and Dalton, L.A., (1976), J. Chem. Phys., 65,

3006.

10. Freed, J.H., (1976),in "Spin Labelling. Theory and Applications", Berliner,

L.J, ed., Voll, p55, Academic Press, New York.

11. Marsh, D., (1980), Biochemistry, 19, 1632.

12. Robinson, B.H., Dalton, L.R., (1980), J. Chem. Phys., 72, 1312.

13. Eaton, S.S, Eaton, G.K, (1978), Coordination Chem. Rev., 26, 207.

14. Leigh, J.S., Jr., (1970), J. Chem. Phys., 52, 2608.

APPENDIX A

A Study on the Effects of Static Electric Fields on DNA Fibre Orientation

Several methods exist for obtaining a degree of orientational order in DNA samples. The techniques developed by Rupprecht[1] and Fuller[2] produce long axis orientation of the DNA molecules in a ribbon or fibre and are, in general, preferred over sheer or flow ordered samples. However, even in these methods a proportion of material remains unordered and the distribution of molcular axes gaussian.

The work of Jennings and Rindler[3] on the electro-optical properties of nucleic acid-drug complexes has shown that a high degree of order may be imposed on DNA solutions exposed to electric field gradients. This has been implied from the degree of anisotropy observed in the polarised fluorescence components due to the drug. Pulsed electric fields up to 4 kV cm^{-1} and of millisecond duration were applied. The observations were consistent with DNA possessing an induced dipole moment directed along the helix axis and a negligible permanent dipole moment[4].

It was considered that application of similar fields during the drying phase of the Fuller method (see section 4.3) could improve the degree of order. Apparatus for the purpose was constructed in the departmental workshop it consisted of a perspex box holding the two field plates, the separation of which could be altered. The glass rods were mounted along the centre of the field plates and small adjustments in plate separation allowed the fibres to be pulled. A diagram of the arrangement is shown in Fig. A1. It was found field gradients up to 2 kV cm^{-1} were attainable with this arrangement.

Initial results showed that fibres dried under these fields were

conical in shape and this was attributed to a degree of solute motion. To overcome this problem it was decided to switch the field polarity. This was done using a period of the order of seconds to allow for relaxation effects. On the assumption that the dipole moment is induced polarity switching should not affect the degree of order. However, the x-ray diffraction patterns from fibres grown in this way showed no increase in order. The reasons for this failure to observe an improvement in order are unclear, however, it may be related to a concentration effect or a degree of misalignment between fibre axis and field axis.

Acknowledgement

I wish to thank Dr. V.T. Forsyth for taking the x-ray diffraction patterns.

REFERENCES

1. Grusband, A., Ehrenberg, A., Ruprecht, A. and Strom, G., (1971), Biochem. Biophys. Acta., 254, 172.

2. Fuller, W., Hutchinson, F., Spencer, M. and Wilkins, M.H.F. (1967), J. Mol. Biol., 27, 507.

3. Jennings, B.R. and Rindler, P.J. (1977), Chem. Phys. Letts., 45, 550.

4. Mahler, H.R., Kline, B. and Mehrotron, B.D., (1965), J. Mol. Biol., 9, 801.

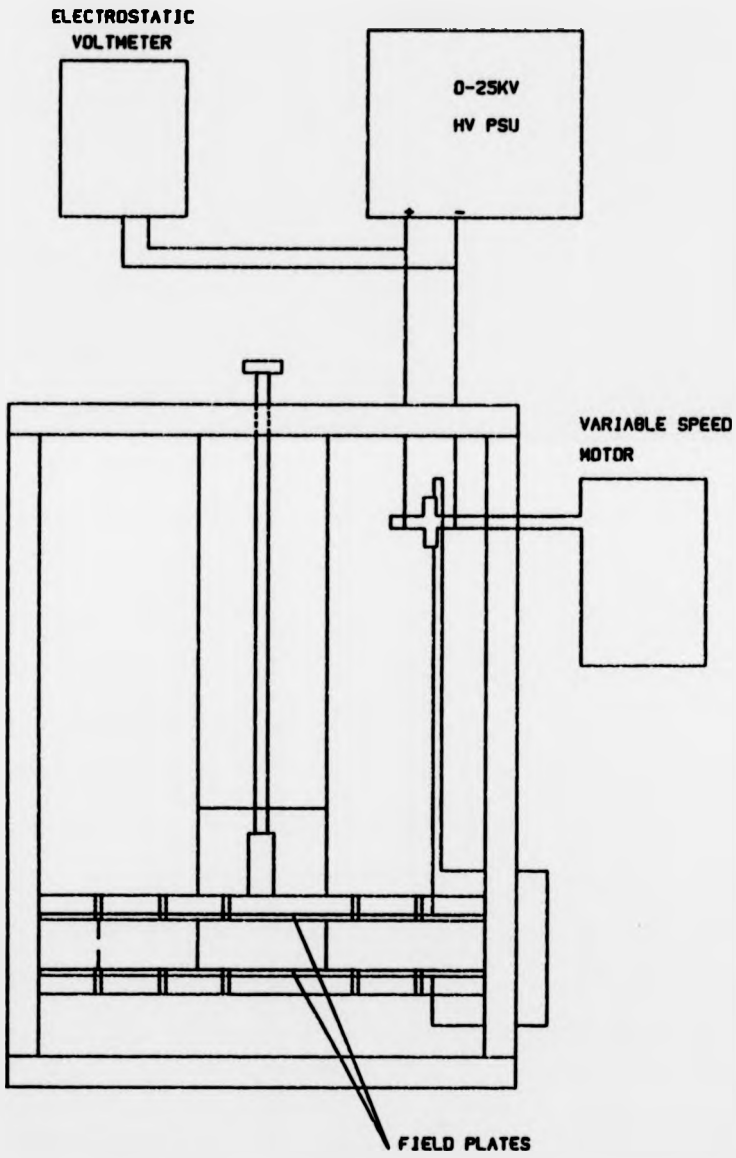

FIG. A1. APPARATUS FOR FIBRE PREPARATION UNDER CONSTANT OR POLARITY SWITCHED ELECTROSTATIC FIELDS.

APPENDIX B

Construction of a 10GHz-Band Loop-Gap Resonator

The potential advantages of a loop-gap resonator have been detailed in section 4.1.6. The method of construction initially was due to Froncisz and Hyde[1] in which a machinable glass ceramic hollow cylinder is slotted and the inner surfaces silvered. The approximate dimensions were a 10mm cylinder length an external diameter of 5mm with a 2mm internal diameter and a 0.1 mm longitudinal slot.

Due to the precision required for these sizes the exact resonant frequency is difficult to predict therefore a wide band swept frequency source is required for test purposes. The arrangement used in this study is given in Fig. B1. A ramp sweep was taken from a 8 to 11 GHz Hewlett Packard 686 sweep oscillator and connected to the time base of an oscilloscope the x-channel of which was fed from the microwave diodes via a low noise preamplifier. A 300 MHz range could be observed and manually swept from 8 to 11 GHz.

Microwave coupling was achieved using an inductive loop formed from semi-rigid coaxial cable. The loop-gap was held firmly in position by the holder shown in Fig. B2. This was designed to give mechanical support while allowing the loop-gap to coupler distance to be altered and samples positioned through a central hole. The inner surface of the outer cylinder was coated with silver aqua-dag to form a radiation shield.

It was attempted to construct a resonator similar to type 4 of the Froncisz paper, this had a 0.15 mm slot. No standard cutting wheels of this dimension are available, however, special diamond wheel was purchased from The Grinding Wheel Company, Stafford. After the ceramic cylinders had been slotted a chemically deposited silver coat

was applied. The layer was removed from unwanted surfaces before a further silver coat was electroplated. The final slot width was measured with a calibrated vernier attached to an optical microscope. This also revealed a slight taper. It should also be noted that difficulty was encountered in obtaining a high quality finish on the silver plated areas.

When tested no resonance could be observed further cylinders were constructed and slightly different dimensions used, however, without success. A second method was then tried that due to Bowman[2] in which thin copper foils were placed on the surfaces of quartz tubes to dimensions consistent with the Froncisz-Hyde formula. A gain, however, no resonance was observed.

Failure to observe resonance may be due to faulty construction or inadequate test facilities. In particular the output from the swept oscillator was not frequency independent and suffered from noise. A resonance dip from a wavemeter could be observed, however, the noise may make observation of low Q-factor dips difficult.

REFERENCES

1. Froncisz, W. and Hyde, J.S. (1982), J. Mag. Reson., 47, 515.
2. Dr. A.I. Vistnes (1984), Personal Communication.

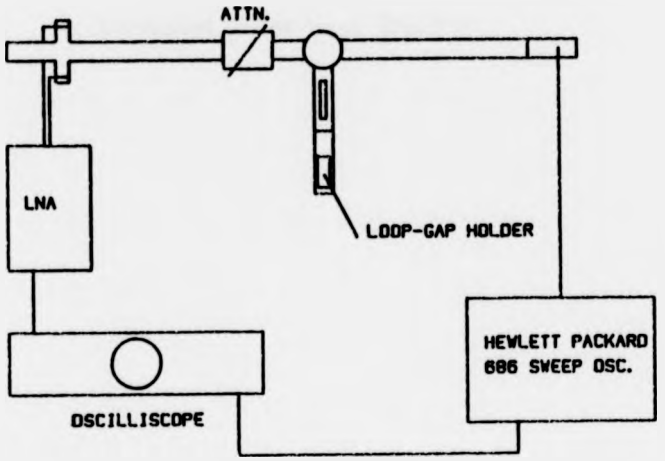

FIG. B1. LOOP-GAP RESONATOR TEST RIG.

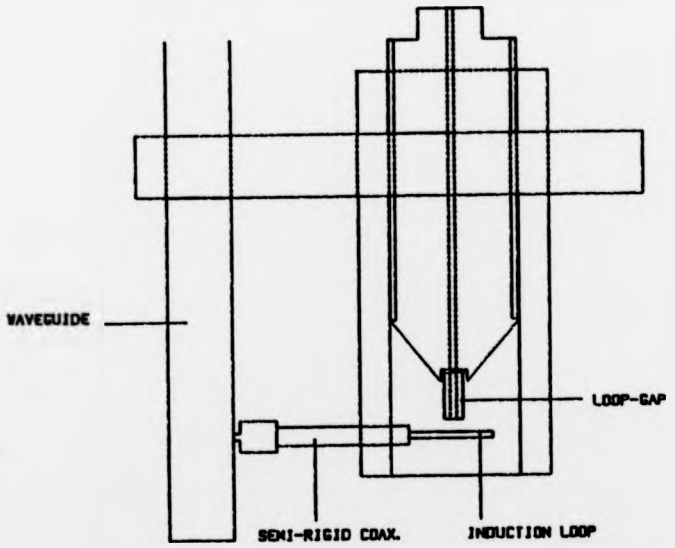

FIG. B2. LOOP-GAP RESONATOR HOLDER.

APPENDIX C

Simulated 35GHz-Band Spectra

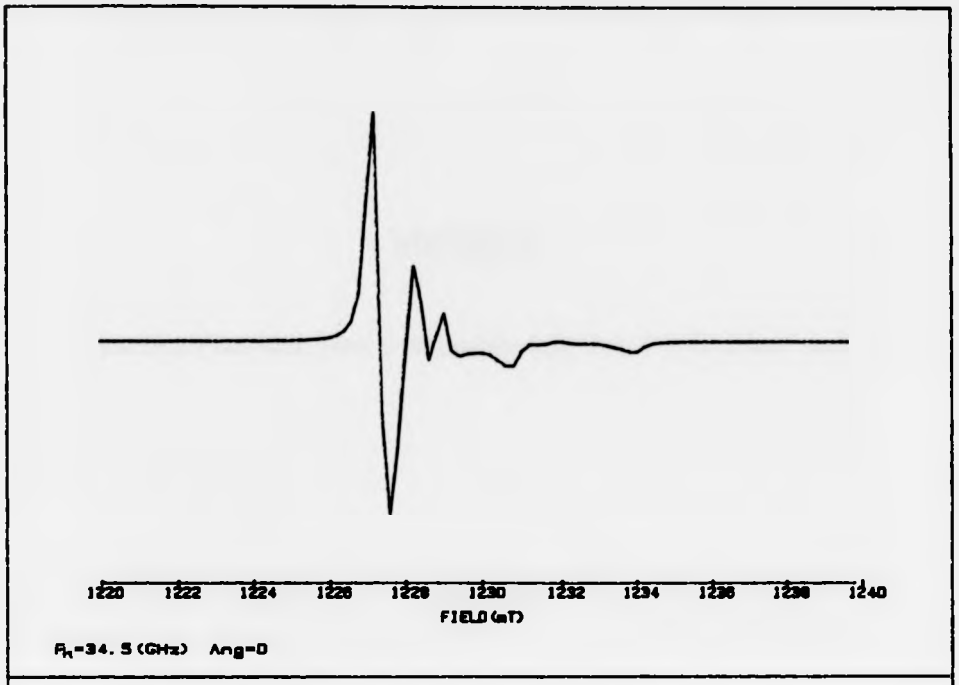
1220
1222
1224
1226
1228
1230
1232
1234
1236
1238
1240
FIELD (mT)
F_H=34.5 (GHz) Ang=0

FIG. C1

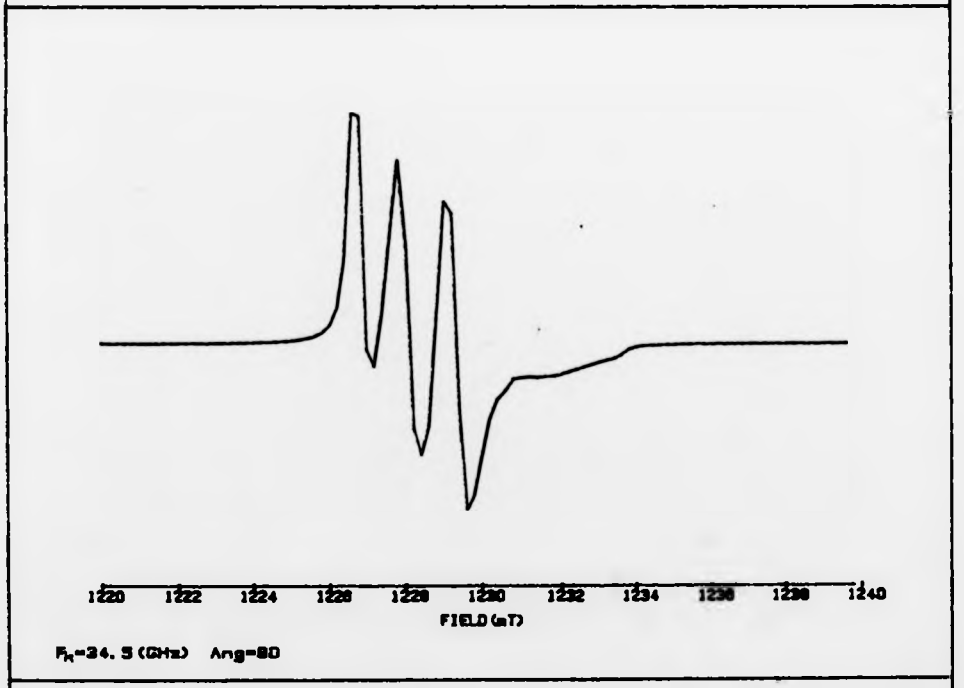
1220
1222
1224
1226
1228
1230
1232
1234
1236
1238
1240
FIELD (mT)
F_H=34.5 (GHz) Ang=80

FIG. C2

APPENDIX D

Spectra recorded from a SLEB-DNA P/D=100 Fibre 0.5mM NaCl

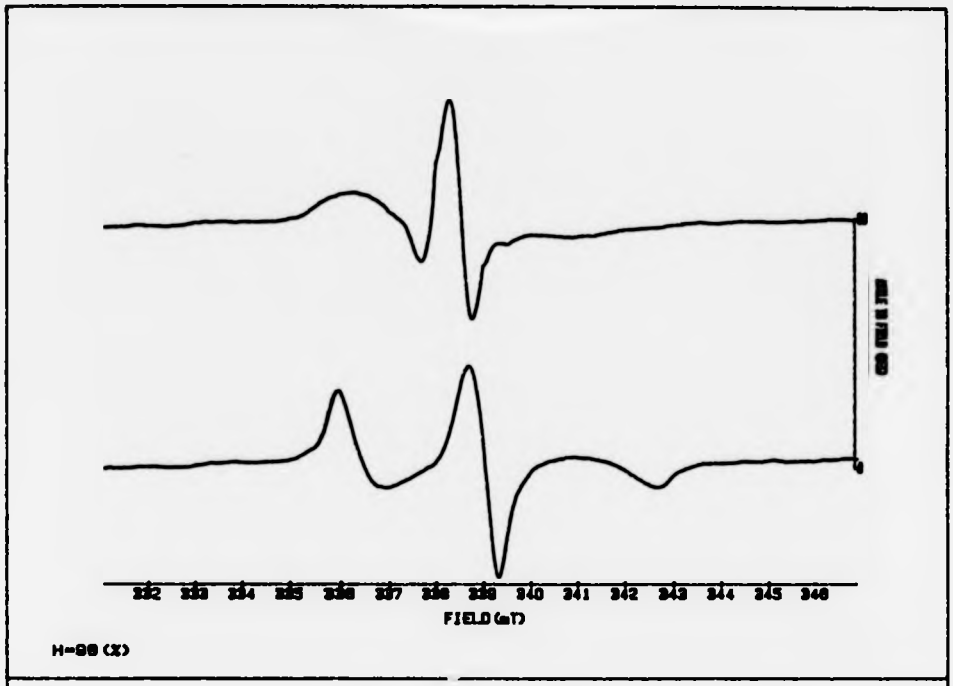

FIG. D1

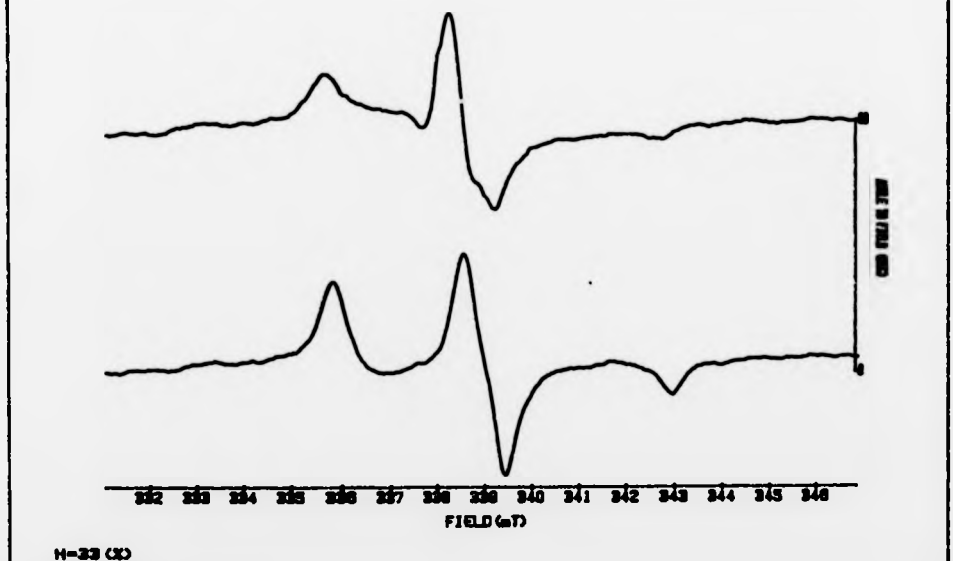

FIG. D2

APPENDIX E

Spectral Simulations for Comparsion with S.J. Hong and L.H Piette, Archv. Biochem. Biophys. (1978), 185, 307.

g_{xx}=2.0080, g_{yy}=2.0054, g_{zz}=2.0025, A_{xx}=A_{yy}=0.69mT A_{zz}=3.32mT
θ_2=45°, δ=5°, ϕ=0°

FIG. E1 ODEG TO THE FIELD.

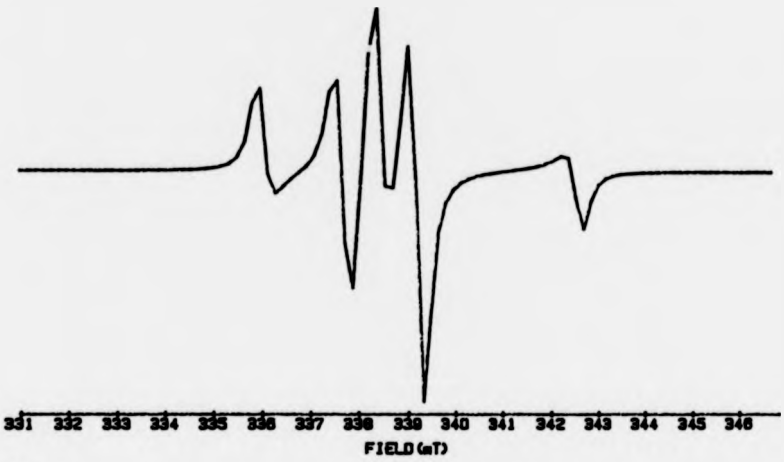

FIG. E2 45DEG TO THE FIELD.

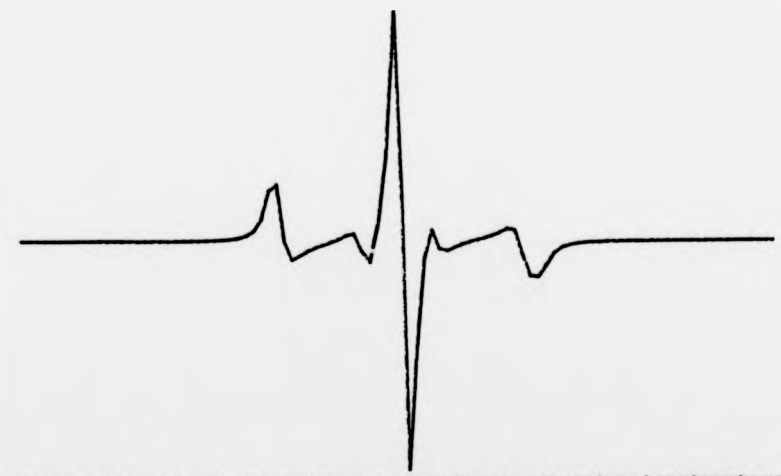

FIG. E3 90DEG TO THE FIELD.